NAS 1.60:1046

NASA Technical Paper 1046

Wind-Tunnel Tests of Wide-Chord Teetering Rotors With and Without Outboard Flapping Hinges

William H. Weller

Structures Laboratory
U.S. Army R&T Laboratories (AVRADCOM)

and

Bill L. Lee

Langley Research Center
Hampton, Virginia

National Aeronautics
and Space Administration

**Scientific and Technical
Information Office**

1977

SUMMARY

Wind-tunnel tests of aercelastically designed helicopter rotor models were conducted to obtain rotor aerodynamic performance and dynamic response data pertaining to two-bladed teetering rotors with a wider chord (1.47 m (58 in.)) and lower hover tip speed (195 m/s (640 ft/sec)) than currently employed on production helicopters. The effects of a flapping hinge at 62 percent radius were also studied. Finally, the effects of changing tip mass on operating characteristics of the rotor with the outboard flapping hinge were examined. The models were tested at several shaft angles of attack for five advance ratios, 0.15, 0.25, 0.35, 0.40, and 0.45. For each combination of shaft angle and advance ratio, the rotor lift was varied over a wide range to include simulated maneuver conditions.

At each test condition, rotor aerodynamic performance and dynamic response data were obtained. From these tests, it was found that wide-chord rotors may be subject to large control forces. An outboard flapping hinge may be used to reduce beamwise bending moments over a significant part of the blade radius without significantly affecting the chordwise bending moments. Increasing the tip mass was found to be an effective tool in restraining the flapping motions of the blade outboard of the hinge. The criteria for selecting outboard hinge location and tip mass must also include consideration of the effects of these parameters on rotor blade natural frequency.

INTRODUCTION

Two-bladed teetering rotors are widely employed in both military and civil applications which require light to moderate gross weight helicopters. The development and characteristics of two-bladed rotors are reviewed in references 1 to 3. As shown in reference 3, the diameter, chord, and operating tip speed of the two-bladed rotor have increased with greater gross weight and more stringent maneuver requirements. Because of considerations of handling and performance, continued increases in diameter or tip speed should be limited. However, significant growth in the chord dimension may still be possible. Reference 3 presents the results of conceptual studies pertaining to dynamic response of models of wide-chord rotors. Because the larger chord would result in higher rotor loads with potential fatigue problems, an outboard flapping hinge was incorporated on most of the models tested. Although the results reported in reference 3 are useful, some of the experimental measurements and conditions were limited.

An experimental study has been conducted to obtain rotor aerodynamic performance and dynamic response. Tests were made on aeroelastic models of a typical full-scale rotor with a wider chord (1.47 m (58 in.)) and a lower operat-

ing tip speed (195 m/s (640 ft/sec)) than currently employed on production helicopters. Because the outboard flapping hinge had been shown to be effective in reducing beamwise bending moments, two model rotors were used: one with outboard hinges and one without the hinges. The tip masses on the rotor with the hinges were changed to determine the effect of tip mass on measured rotor response. The model rotors were designed and built by Bell Helicopter Textron, and Bell personnel also participated in the tests.

Wind-tunnel tests of the model rotors were performed at the Langley transonic dynamics tunnel using the generalized rotor aeroelastic model (GRAM) described in reference 4. The models were tested at several shaft angles of attack for five advance ratios, 0.15, 0.25, 0.35, 0.40, and 0.45. For each combination of shaft angle and advance ratio, rotor lift was varied over a wide range to include simulated maneuver conditions. Aerodynamic performance and rotor response were obtained from the tests, and representative data are presented in this report.

SYMBOLS

Physical quantities defined in this report are given in the International System of Units (SI) and, where useful, in U.S. Customary Units. Conversion factors are presented in reference 5.

a_1 longitudinal flapping at hub about shaft axis (positive for aft flapping), deg

b number of blades

C_D rotor drag coefficient, $D/\pi R^2\rho(\Omega R)^2$

C_L rotor lift coefficient, $L/\pi R^2\rho(\Omega R)^2$

C_Q rotor torque coefficient, $Q/\pi R^3\rho(\Omega R)^2$

c blade chord, m

D rotor drag force, N

L rotor lift force, N

M_t rotor tip Mach number in hover

Q rotor torque, N-m

R blade radius, m

r radial blade station measured from center of rotation, m

V forward velocity, m/s

x nondimensional blade station measured from center of rotation, r/R

α_s rotor shaft angle of attack (positive with fuselage nose up), deg

$\theta_{0.75R}$ blade collective pitch angle at 0.75R, deg

μ advance ratio, $V/\Omega R$

ρ density of air, kg/m^3

σ rotor solidity, $bc/\pi R$

Ω rotational speed, rad/s

ω rotating natural frequency of rotor blade, rad/s

EXPERIMENTAL APPARATUS AND PROCEDURES

Test Facility

The experimental program was conducted in the Langley transonic dynamics tunnel (TDT). The TDT is a continuous-flow tunnel with a slotted test section which is capable of operation over a Mach number range from 0 to 1.20 at pressures ranging from near 1376 N/m^2 (0.2 psia) to atmospheric pressure. Either air or Freon-12 may be used as a test medium. The tunnel test section is 4.9 m (16 ft) square with cropped corners and has a cross-sectional area of 23 m^2 (248 ft^2). The present investigation was conducted in Freon-12 at a density of 4.12 kg/m^3 (0.008 $slug/ft^3$).

During testing, use was made of the TDT computerized data acquisition system. The data system includes a digital computer, transducer signal conditioners, amplifiers, and calibration signal sources sufficient to handle 60 channels of data. From the amplifiers, data are routed to a direct-record FM tape recorder and through a multiplexer system onto a frequency multiplexed FM tape. The direct-record tape can accept up to 12 channels of data. The multiplex system can record 60 channels of data by multiplexing 5 channels onto a single track. Data from the signal amplifiers are also routed to a 60-channel analog-to-digital system and then to the system computer for processing. The computer is controlled by a graphics display unit and associated keyboard.

Generalized Rotor Aeroelastic Model

The generalized rotor aeroelastic model (GRAM) is shown in figures 1 and 2 and described in reference 4. This model serves as a powered test stand for research related to helicopter dynamics. The GRAM rotor shaft is driven by two variable frequency synchronous motors, each rated at 35 kW at a rotational speed of 1256 rad/s. The motors are connected to the rotor shaft through a two-stage speed reduction of 17.47:1. Rotor speed is controlled by varying the electric line frequency to the synchronous motors. The pitch attitude of the model can be remotely changed by electromechanical actuators over a range from 20° nose down to 8° nose up. The model features a complete main rotor control system. The swashplate, shown in figure 2, is mounted on the rotor shaft below

the rotor shaft adapter and is raised or lowered by three assemblies combining a hydraulic actuator and an electric servo to achieve collective pitch, lateral, and longitudinal cyclic swashplate motions.

The GRAM is instrumented to provide continuous displays of all model control settings and selected rotor loads. Rotor shaft speed is determined by a magnetic sensor. Rotating blade data are transferred to the fixed system through a 60-ring, horizontal-disk, slip-ring assembly. The combined rotor and fuselage forces and moments are measured by using a six-component strain-gage balance mounted below the baseplate and covered by a shroud. The balance is post mounted and does not rotate with the fuselage.

Model Rotor Systems

The wide-chord model rotors are shown in figures 3 and 4 mounted on the GRAM. The rotor without the outboard hinges (fig. 3) is referred to as the baseline rotor, and the other (fig. 4) as the hinged rotor. Both models were aeroelastically designed but did not represent any full-scale production rotor. The hub and yokes used on both rotors were 1/4-scale models of those of the AH-1G rotor and are described in reference 6. The hub had a built-in precone angle of 2.75° inboard of the feathering mechanism. Both rotors had a 3.26-m (10.7-ft) diameter and solidity of 0.0992. The blades had rectangular planforms with a chord of 25.4 cm (10 in.), NACA 0012 airfoils, and linear twist distributions of -10.3° extending from 15 percent radius to the tip. The rotors were scaled for operation at full-scale Mach numbers (M_t = 0.58) in a Freon-12 test medium with a rotational speed of 54.04 rad/s (516 rpm). Aeroelastic simulation was achieved by matching model and full-scale advance ratios and ratios of blade natural frequency to rotor rotational speed. Scale factors relating full-scale values to model values are listed in table I.

The blade consisted of a stainless steel spar embedded in an aluminum honeycomb core. The spar widened at the inboard end to form the blade grip and extended to the tip where the tip masses were attached. Fiber glass cloth was bonded to the honeycomb core to form a closed blade skin. The hinged rotor had a flapping hinge at 62 percent radius, which is shown in figure 5. Ball bearings and a steel pin that allowed the blade to flap were bolted to the main spar sections. Stops restricted flapping to between 10° up and 6° down. The glass skin on the outboard portion of the blade was extended inboard over the hinge, and the remaining break in the skin was sealed with adhesive tape to provide a continuous aerodynamic surface. Two sets of tip masses 0.104 kg (0.23 lb) and 0.626 kg (1.38 lb) per blade, were tested on the hinged rotor. The baseline rotor and the hinged rotor with the lighter tip masses had Lock numbers of 9.3. The Lock number for the hinged rotor with heavy tip masses was 7.2.

The spanwise distributions of structural properties for the baseline and hinged rotors were supplied by Bell Helicopter Textron and are tabulated in table II. These data were used with a coupled (beamwise, chordwise, and torsional) lumped-mass analysis described in reference 7 to estimate rotating natural frequencies and bending mode shapes of the rotor. For the analysis, the outboard flapping hinge was approximated by a zero value of the beamwise

structural stiffness at that station. The beamwise and chordwise mode shapes and the corresponding moment distributions for both rotor systems are plotted in figures 6 to 9. Only the principal components (the direction having the largest deflection) are shown. The collective beamwise modes and the cyclic chordwise modes are the clamped symmetric rotor modes in the out-of-plane and in-plane directions, respectively. The cyclic beamwise modes are the pinned, antisymmetric out-of-plane modes. The coupled rotating natural frequencies are presented in tables III and IV for the baseline and hinged rotors, respectively.

The rotors were instrumented with four-arm strain gage bridges. Shaft torque, pitch-link axial load, and hub beamwise ($x = 0.05$) and chordwise ($x = 0.03$) bending moments were measured. Beamwise and chordwise bending moments at 24, 36, 53, and 63 percent radius and torsion at 24 and 53 percent radius were measured on the baseline rotor. Beamwise and chordwise bending moments at 24, 36, 54, 69, and 81 percent radius and torsion at 24, 54, and 69 percent radius were measured on the hinged rotor. Rotor flapping relative to the shaft was measured by an angular potentiometer mounted to the shaft and geared to the hub. Relative flapping of the outer portion of the blade relative to the inner portion was sensed with a gaged leaf spring extending across the hinge.

Experimental Procedure and Data Reduction

Rotor aerodynamic performance and dynamic response were measured on both rotor systems over wide ranges of shaft angle of attack, collective pitch angle, and advance ratio. Each test was initiated by setting the collective pitch to a low value, bringing the rotor speed up to 54.04 rad/s (516 rpm), and pitching the model to the first shaft angle of attack. The free-stream speed was established to yield the first advance ratio. Collective pitch was increased, generally by 2° increments, until excessive blade loads were encountered. At each test point, rotor first harmonic flapping relative to the shaft was eliminated, or the rotor was maintained at a trimmed-to-shaft condition. Then, the collective pitch was returned to the original setting, the shaft angle was increased by 2°, and the procedure was repeated. After data were recorded at each shaft angle, the tunnel speed was increased to produce the next desired advance ratio, and the process was repeated for each remaining advance ratio.

The maximum and minimum values of lift coefficient achieved during tests of the baseline rotor are identified in figure 10 for each combination of shaft angle and advance ratio. The associated full-scale load factors are also shown based on a helicopter with mass of 8255 kg (18 200 lb). The maximum test advance ratio, 0.45, simulates a full-scale velocity of 87.5 m/s (170 knots). To study the effects of rotor flapping on blade response, a limited number of tests were made by varying rotor longitudinal flapping by 0.5° increments about the initial trimmed-to-shaft setting while maintaining relatively constant lift.

Rotor performance and dynamic response were recorded at each combination of collective pitch, rotor flapping, shaft angle, and tunnel speed. The tunnel operating conditions, balance data, and model control settings were recorded on

punched cards. The rotor response data and the 1/rev rotor pulse signal were recorded on tape.

Rotor aerodynamic performance measurements were processed by a special purpose digital computer program using the TDT data acquisition system in an off-line mode. Corrections were made for weight tares, fuselage aerodynamic effects, and balance interactions, but the aerodynamic contributions of the hub are included in the data. The measurements were transferred from the balance centroid to the hub, and the lift and drag coefficients, normalized by rotor solidity, were then computed in the wind-axis system. The normalized thrust and shaft torque coefficients and power were determined by rotating the transferred measurements into the shaft-axis system.

Rotor response was determined by using another special purpose digital computer program. The data recorded on magnetic tape were input to the TDT data acquisition system computer. From each channel, 2 seconds were digitized at a rate of 1000 samples per second. The resulting digitized data were processed to yield mean and oscillatory response. The oscillatory response is equal to one-half of the peak-to-peak dynamic response. A discrete Fourier analysis was carried out to produce response harmonics, which are the total amplitudes of the components of response at integral multiples of the rotor rotational speed. Shunt calibration signals recorded on tape enabled all data to be converted to engineering units.

RESULTS AND DISCUSSION

The baseline rotor was tested over the operating envelope in figure 10. Originally, the hinged rotor was to be tested over the same range of operating conditions as the baseline rotor. However, because a near resonance occurred between a cyclic beamwise bending mode and the fifth harmonic of the rotor speed, excessive loads resulted and limited the rotor lift that could be achieved at the higher advance ratios. The use of existing hardware designed for the different operating conditions of previous tests was the cause of the resonance problem. However, sufficient data were collected with the hinged rotor to meet test objectives. The near resonance condition does not reflect upon the merits of the concepts under study, because structural design changes can usually eliminate the resonance problem. Additional discussion of the resonance problem is given subsequently.

The following discussion is organized into three sections, each dealing with rotor performance and dynamic response. In the first section, the characteristics of the baseline rotor are presented. In the second section, measurements on the baseline rotor and hinged rotor are compared. In the third section, the effect of tip mass on the response of the hinged rotor is discussed.

Baseline Rotor Characteristics

Figures 11 and 12 illustrate the measured aerodynamic performance characteristics of the baseline rotor from hover to an advance ratio of 0.45. The data are plotted in terms of torque and lift coefficients normalized by rotor

solidity (fig. 11) or as normalized lift and drag coefficients (fig. 12). The performance data are plotted for three shaft angles of attack at each advance ratio. The values of shaft angle were selected to encompass the operating attitudes of a typical full-scale helicopter. The performance data exhibit smooth, uniform trends with variations in shaft angle and advance ratio. The data in figure 12 can be interpolated to approximate shaft attitudes for various gross weights, maneuver conditions, and fuselage drag areas. From the lift and interpolated shaft angle, the data in figure 11 can then be employed to determine power requirements.

Spanwise distributions of blade oscillatory bending moments and the first five harmonic components of these bending moments are plotted in figures 13 and 14. In these figures the designation P denotes harmonic orders of the rotor rotational speed. The data in figure 13 pertain to a low lift condition, simulating a full-scale load factor of 0.79. Figure 14 presents response measured at high lift, simulating a full-scale load factor of 1.34. For both figures, the advance ratio is 0.35 and the shaft angle is -6°.

At the lower lift, the oscillatory beamwise moment (fig. 13(a)) exhibits a peak near 50 percent radius primarily resulting from the higher harmonic moment distributions and the fact that the first harmonic is relatively flat through this area of the blade. However, this peak does not occur on the distribution for the higher lift (fig. 14(a)) because of the change in character of the first harmonic moment distribution and its increased dominance. At the inboard measurement station, the first harmonic represents 85 percent of the oscillatory response in figure 14(a). In both figures, an increase in oscillatory and first harmonic moments inboard of 35 percent radius occurs because of increased stiffness associated with the widening of the spar structure at the inboard end of the blade. The third harmonic moment is influenced by the first cyclic beamwise mode. This mode is in near resonance with the 3/rev air loads at low lift conditions, with increased frequency separation as the collective pitch angle is increased (table III). The result is a large decrease in the third harmonic amplitude between figures 13(a) and 14(a). Although the measured beamwise response was greatest at 24 percent radius, the oscillatory and odd harmonic moments decrease for stations further inboard with all odd harmonics becoming zero at the center line. (See fig. 8(b).)

The distributions of chordwise bending moments are presented in figures 13(b) and 14(b). The character of the oscillatory distribution along the inboard portion of the blade varies with lift, or collective pitch. At the lower lift, a peak occurs in the oscillatory distribution near 36 percent radius, where the second and third harmonics are large relative to the first harmonic. The third harmonic decreases in magnitude with increases in lift (collective pitch angle), because the first cyclic chordwise mode frequency becomes more separated from that of the 3/rev air loads (table III). The amplitudes of the second and fourth harmonics do not vary significantly with collective pitch because the first collective chordwise mode is above 7/rev. However, the first harmonic increases significantly with lift until it is the dominant component of the oscillatory moment in general. At the higher lift, the first harmonic and, therefore, the oscillatory distributions are similar to the first cyclic chordwise mode (fig. 8(c)).

The torsional response is shown in figures 13(c) and 14(c). Shown for comparison is an equivalent root (x = 0) moment, derived from the pitch-link force and the offset between the feathering axis and the pitch horn (0.061 m). Both the torsional moment and pitch-link force are responses mostly to the 1/rev air loads. The dominance of the first harmonic increases with lift, and the higher harmonic moments on the blade are all approximately equal at the higher lift condition. The first harmonic of the equivalent root moment is significantly higher than the blade torsional amplitudes, because of contributions from the inertial forces generated by driving the hub feathering mechanism at 1/rev. The second harmonic of the root moment is also higher than the corresponding values on the blade because of structural coupling in the hub hardware which causes the pitch-link response to be influenced by the blade beamwise moment and shear. This coupling effect may also contribute to the large first harmonic component of the pitch-link force.

Variations of the dynamic response of the baseline rotor with lift and advance ratio are presented in figures 15 and 16, respectively. Both oscillatory and the more significant harmonic amplitudes are shown for beamwise, chordwise, and torsional moments (x = 0.24) and for the pitch-link force. The dominance of the first harmonic of the beamwise moment increases with both lift and advance ratio (figs. 15(a) and 16(a)), particularly for the latter parameter. The higher harmonics do not show as significant a variation with either lift or advance ratio. The third harmonic of the beamwise response peaks at moderate lift conditions as a result of the near resonance of the first cyclic beamwise mode and the 3/rev air loads.

Chordwise bending trends (figs. 15(b) and 16(b)) are very similar to those for beamwise bending. The first harmonic becomes more dominant at the higher values of lift and advance ratio, and the third harmonic has a peak with variations in lift because of the characteristics of the first cyclic chordwise mode. In addition, a significant amount of the fifth harmonic of the chordwise moment occurs at the higher lift and advance ratios.

The trends of torsional moment and pitch-link force in figures 15(c), 15(d), and 16(c) further demonstrate the significance of the first harmonic component at conditions of high lift and/or advance ratio. The second and third harmonic components are always less than the first and, in general, do not change as significantly as the first with variations in operating conditions. The variations with lift of the second and third harmonics of the torsional moment and pitch-link force are dissimilar. For the torsional moment (fig. 15(c)), the second harmonic peaks in the midrange of the lift conditions shown. The third harmonic of the torsional moment consistently increases with lift, except for the lowest lift condition. The pitch-link force trend with lift (fig. 15(d)), however, more closely resembles the trends of beamwise bending moment (fig. 15(a)) in that the third harmonic peaks at moderate lift values while the second harmonic continually increases with lift. The trends of beamwise moment and pitch-link force with advance ratio are also similar, as shown in figures 16(a) and 16(c). This further demonstrates that beamwise shears and moments induced pitch-link responses through structural coupling in the hub area.

Variations in beamwise and chordwise bending with rotor longitudinal flapping are presented in figure 17. The first and third harmonics of the beamwise bending moments at $x = 0.24$ (fig. 17(a)) vary most with longitudinal flapping. For 1° of flapping, the variations are 8 and 11 percent for first and third harmonics, respectively. In the chordwise direction (fig. 17(b)), the third harmonic shows the greatest variation with flapping, up to 94 percent per degree of flapping change. The oscillatory chordwise moment changes only 11 percent over the same range, mostly because of the effects of the third harmonic.

Hinged Rotor Characteristics

Criteria for selecting the outboard hinge location were reviewed in reference 3 where it was suggested that 57.5 percent radius was an optimum location. The blades for the hinged rotor were designed and built on the basis of this hinge location. However, the tests of reference 3 were limited by excessive dynamic response due to improper blade tuning. For the present investigation the same hinged blades were used but with the larger AH-1G model hub to accommodate the larger dynamic response and, perhaps, alter the rotor natural frequencies. This design change resulted in a hinge location of 62 percent radius. From figure 11 of reference 3, movement of the outboard hinge from 57.5 to 62 percent radius should result in lower beamwise response on the outboard portion of the blade without significantly increasing the maximum beamwise response on the inboard section.

Figure 18 presents a comparison of the aerodynamic performance measured on the baseline rotor and on the hinged rotor. The hinged rotor requires more power in hover than the baseline rotor (fig. 18(a)). As mentioned previously, the break in the skin in the hinge area was aerodynamically sealed with adhesive tape which may have degraded performance because of surface irregularities. As shown in figure 18(b), the hinged rotor seems to require more power at very low lift but less at higher values of lift for nonzero values of advance ratio. The difference in slope of the curves in figure 18(b) is associated with the flapping of the outboard portion of the blade relative to the inboard portion. The comparison of figure 18(b) is made for equal values of collective pitch, shaft angle, and advance ratio with the first harmonic flapping at the hub trimmed out. In the presence of a free stream, however, the rotor tip-path plane still tilts back relative to the shaft because of blade deflections. The blades on the hinged rotor deflect more, resulting in smaller rotor tip-path-plane angles than on the baseline rotor. The relative aft tilt, which increases with thrust, reduces the propulsive force (fig. 19) and the torque on the hinged rotor. When the shaft angle is changed to correct for this condition, the slopes of the performance curves should become nearly identical. The differences in power requirements between the baseline and hinged rotors at various advance ratios would be similar to the difference observed for the hover condition (fig. 18(a)).

Comparisons of the bending moments measured on the baseline and hinged rotors are shown in figures 20 and 21 for beamwise and chordwise bending, respectively. Only the more significant harmonics and the oscillatory values are illustrated. The first and third harmonics of the beamwise moments are

lower on the hinged rotor along most of the blade radius. Although figure 20(b) suggests that the third harmonic on the hinged rotor may exceed that on the baseline rotor for stations inboard of 24 percent radius, the difference should not be too great because the third harmonic amplitude should peak near 15 percent radius and drop to zero at the center line (figs. 8(b) and 9(b)). It is evident that the outboard hinge can be very effective in reducing beamwise moments on the wide-chord blade and thereby in improving its fatigue life. However, the fifth harmonic of the beamwise moment incurred on the hinged rotor is amplified because of the frequency of the second cyclic beamwise mode (table IV). The result is illustrated in figure 20(c). Although the fifth harmonic moment on the hinged rotor is less than that on the baseline rotor in the vicinity of the hinge, large magnitudes occur at other radial stations, particularly toward the blade root. The total effect can be seen in figure 20(d) which presents the spanwise distribution of the oscillatory beamwise moments on both rotors. On the hinged rotor, the oscillatory moment is less for stations between 45 and 75 percent radius but is significantly higher for inboard stations. From the preceding discussion, it is obvious that the benefits of using the outboard hinge will be realized only if the hinged rotor is designed to preclude near resonance conditions within its operating envelope.

The first and third harmonic components of the chordwise moment (figs. 21(a) and 21(b)) are higher on the hinged rotor. The difference in the third harmonic is more significant and increases for stations toward the blade root. The fifth harmonic moment (fig. 21(c)) is less on the hinged rotor for stations outboard of 50 percent radius. Inboard of this point, the fifth harmonic on the hinged rotor increases abruptly until it is higher than the measured values on the baseline rotor. Because the second cyclic chordwise mode has a frequency ratio above 7/rev, the significant magnitudes of the fifth harmonic of the chordwise moment may be due to dynamic coupling effects which cause the large beamwise vibrations at this frequency to influence the measured chordwise moments. The chordwise moment oscillatory distribution is presented in figure 21(d). Because of the combined effects of the third and fifth harmonic components, the oscillatory moment at 24 percent radius is 50 percent higher on the hinged rotor. For comparably tuned rotors, the presence of the hinge would probably reduce the oscillatory and harmonic components of the beamwise moment over more than half of the blade radius without significantly affecting the chordwise moments.

With regard to tuning, the radial location of the outboard hinge is an important parameter. Table V illustrates the changes in blade natural frequencies which result from moving the hinge from 62 to 47 percent radius. For the inboard location, the frequency of the two cyclic beamwise modes has been significantly improved. Movement of the hinge toward midspan should also decrease the beamwise moment at the blade root where the maximum value occurs.

Figure 22 presents trends of the dynamic responses of the baseline and hinged rotors with advance ratio. The selected responses include beamwise bending at 24 and 54 percent radius, chordwise bending at 24 percent radius, and pitch-link force. At 24 percent radius, the first and second harmonics of the beamwise moment are nearly equal except at the higher advance ratios (fig. 22(a)). The difference in the oscillatory magnitudes is attributed to the much larger fifth harmonic on the hinged rotor due to the frequency of the

second cyclic beamwise mode. At 54 percent radius (fig. 22(b)), the components of the beamwise moment on the hinged rotor are approximately one-half those on the baseline rotor throughout the test range of advance ratio. The trends of the oscillatory and first harmonic chordwise moments with advance ratio (fig. 22(c)) are the same for both rotors, but the magnitudes on the hinged rotor are over 20 percent higher at an advance ratio of 0.45. The second harmonic of the pitch-link force on the hinged rotor (fig. 22(d)) is higher with a sharp increase in magnitude at the higher advance ratios. This trend is similar to that of the beamwise moment shown in figure 22(a). At the lower advance ratios, the first harmonic component of the pitch-link force is approximately the same for both rotors, but at the higher advance ratios, the component on the hinged rotor is significantly less, causing the oscillatory amplitude to be less on the hinged rotor at an advance ratio of 0.45.

Effect of Tip Mass on Rotor Response

Tip mass and the location of the outboard hinge are design parameters which can significantly affect the rotor natural frequencies and, therefore, the magnitudes of the dynamic response. Table IV and figures 20 and 21 illustrate the effects of changing the tip mass. The natural frequency ratios of the hinged rotor vary with tip mass by almost 0.2 for some of the modes listed in table IV. As a result of the relative frequencies of the second cyclic beamwise mode, the fifth harmonics of the beamwise and chordwise moments at 24 percent radius are higher for the light tip mass than for the heavy tip mass; the difference is 35 and 83 percent for the beamwise and chordwise moments, respectively (figs. 20(c) and 21(c)). Similarly, the frequencies of the first cyclic beamwise mode result in a 17-percent increase in the third harmonic of the chordwise moment at 24 percent radius for the heavy tip mass (fig. 21(b)). The combined effect is that the heavy tip mass decreased the oscillatory beamwise and chordwise moments at 24 percent radius by 14 and 2 percent, respectively. Clearly, the criteria used for selecting tip mass and location of the outboard hinge must include consideration of the effects of these parameters on rotor natural frequencies.

The tip mass also significantly affects the flapping motion of the section of the blade outboard of the hinge. The variation of the mean droop angle (outboard blade section down relative to the inboard section) with lift coefficient is shown in figure 23. The droop angle decreases linearly with lift as the outboard blade cones up. Because of increased centrifugal stiffening, the heavy tip mass reduces the change in droop angle from about 2° to less than 0.5° over a range of C_L/σ between 0.015 and 0.104. The dynamic flapping response of the outboard blade is also greatly reduced by the addition of tip mass (fig. 24). The reductions in oscillatory and first, second, and third harmonic amplitudes are approximately 40, 35, 55, and 50 percent, respectively. The second harmonic, which is the largest component for the light tip mass, is reduced the greatest amount until it becomes less than the first harmonic of the response.

The variation of mean droop angle with advance ratio (fig. 25(a)) may be greater for the rotor with the heavy tip mass, but it is still less than 0.5° over the test range of advance ratio. The most significant effect of using the

heavy tip mass is an increase in droop by 0.5° at all advance ratios. The trends of dynamic flapping response with advance ratio (fig. 25(b)) point out that the heavy tip mass is most effective in reducing the second harmonic component which becomes less than the first harmonic at the higher values of advance ratio. At an advance ratio of 0.4, the second harmonic and oscillatory responses are both reduced by about one-half. This is important because the oscillatory amplitude is almost 7° for the rotor with light tip mass.

The outboard blade flapping variations around the azimuth are illustrated for both tip masses at a high lift (fig. 26(a)) and a moderate value of advance ratio (fig. 26(b)). In figure 26(a), the major differences in the waveforms associated with each tip mass are the shift in the mean droop angle and the change in the amplitude of the peak occurring at approximately 300° azimuth. As illustrated in figure 23, the shift in the mean value is due to the relative stiffening effects of the tip masses at the higher C_L/σ values. Because the outboard hinge is located outside the region of reversed flow for the conditions of figure 26(a), stall effects may be the contributing factor to the occurrence of the large peak on the retreating side of the tip-path plane. This peak contributes mostly to the 2/rev component of response which is the largest harmonic on the rotor with the light tip mass. At a higher advance ratio (fig. 26(b)), a large peak has formed on the advancing side causing the flapping excursion to come close to the 6° down stop. The condition of approaching the lower stop was another factor which restricted the test envelope of the hinged rotor with the light tip mass. The outboard blade did not flap near to the upper stop. As shown in figure 27, longitudinal flapping at the rotor center line does not significantly affect the flapping response of the outboard blade.

CONCLUDING REMARKS

Wind-tunnel tests of aeroelastically designed helicopter rotor models were conducted to obtain rotor aerodynamic performance and dynamic response pertaining to two-bladed teetering rotors with a wider chord (1.47 m (58 in.)) and lower hover tip speed (195 m/s (640 ft/sec)) than currently employed on production helicopters. The effects on performance and response of incorporating an outboard flapping hinge at 62 percent radius were also studied. Finally, the effects of changing tip mass on the measured characteristics of the rotor with an outboard hinge were examined. The models were tested at several shaft angles of attack for five advance ratios, 0.15, 0.25, 0.35, 0.40, and 0.45. For each combination of shaft angle and advance ratio, the rotor lift was varied over a wide range to include simulated maneuver conditions.

Data were acquired for the wide-chord model without the outboard hinge (baseline rotor). The measured aerodynamic performance curves exhibited smooth trends with variations in shaft angle and advance ratio. The pitch-link forces were high due in part to significant contributions from inertial loads resulting from feathering of the hub and inboard blade structure, as well as from structural coupling with beamwise shears. These trends were also observed for the hinged rotor. The results indicate that the use of outboard flapping hinges could reduce the beamwise moments over more than half of the blade radius without significantly affecting the chordwise moments for comparably

tuned rotors. Movement of the hinge location toward 50 percent radius would improve the blade natural frequencies for this configuration and lower the beamwise moments at the blade root and in the hub area. The outboard blade flapping excursions were large at the higher advance ratios but were reduced by about one-half through addition of tip mass. Of the two outboard flapping stops, 6° down and 10° up, only the lower stop was closely approached during the tests. The criteria for selecting outboard hinge location and tip mass must include consideration of the effects of these parameters on blade natural frequencies. Otherwise, the benefits may be more than offset by the large dynamic response arising from a resonance condition.

Langley Research Center
National Aeronautics and Space Administration
Hampton, VA 23665
September 23, 1977

REFERENCES

1. Kelley, Bartram: Contributions of Bell Helicopter Company to Helicopter Development. Aeronaut. J., vol. 76, no. 735, Mar. 1972, pp. 157-165.

2. Sonneborn, Walter G. O.: Current Developments in Main Rotors at Bell Helicopter Company. AIAA Paper No. 73-1160, Oct. 1973.

3. Kidd, David L.; Brogdon, V. H.; and White, James A.: Advanced Two-Bladed Rotor Systems at Bell Helicopter Textron. Proceedings of Symposium on Rotor Technology, American Helicopter Soc., 1976.

4. Weller, William H.: Load and Stability Measurements on a Soft-Inplane Rotor System Incorporating Elastomeric Lead-Lag Dampers. NASA TN D-8437, 1977.

5. Mechtly, E. A.: The International System of Units - Physical Constants and Conversion Factors (Second Revision). NASA SP-7012, 1973.

6. Lee, Charles; Charles, Bruce; and Kidd, David: Wind-Tunnel Investigation of a Quarter-Scale Two-Bladed High-Performance Rotor in a Freon Atmosphere. USAAVLABS Tech. Rep. 70-58, U.S. Army, Feb. 1971. (Available from DDC as AD 721 660.)

7. Bennett, R. L.: Digital Computer Program DF1758 Fully Coupled Natural Frequencies and Mode Shapes of a Helicopter Rotor Blade. NASA CR-132662, [1975].

TABLE I.- MODEL SCALE FACTORS

Parameter	Scale factor
Mach number	1.0
Structural frequency ratio	1.0
Advance ratio	1.0
Lock number	1.0
Froude number	.85
Reynolds number	2.46
Length, m	5.8
Structural stiffness, $N\text{-}m^2$	1552.9
Angular velocity, rad/s	.382
Linear velocity, m/s	2.214
Force, N	46.16
Moment, N-m	267.7
Power, W	102.2

TABLE II.- STRUCTURAL PROPERTIES OF BASELINE AND HINGED ROTOR MODELS

Inboard station of segment, r, m	Mass, kg/m	Structural stiffness, N-m^2			Radius of gyration, m	Chordwise shear center offset,[a] m	Chordwise center of gravity offset,[b] m
		Beamwise	Chordwise	Torsional			
0	27.50	120 819	176 781	1435	0.0090	0	0
.033	7.30	89	83 225	1435	.0175	0	0
.091	19.47	5 137	91 547	1435	.0107	0	0
.142	14.02	1 607	20 978	1435	.0126	0	0
.244	17.23	16 100	53 953	1435	.0114	0	0
.310	9.46	8 466	972 867	1435	.0876	.0823	-.0823
.387	4.11	2 927	99 296	1291	.0492	.0333	-.0333
.460	2.30	861	107 618	1033	.0618	-.0135	.0135
.533	2.30	861	107 618	1033	.0618	-.0135	.0135
.607	2.30	861	107 618	1033	.0618	-.0135	.0135
.753	2.30	861	107 618	1033	.0618	-.0135	.0135
.826	2.30	861	107 618	1033	.0618	-.0135	.0135
.899	6.63	861	107 618	1033	.0618	-.0135	.0135
.999	8.63	[c]861	107 618	1033	.0618	-.0135	.0135
1.018	6.63	861	107 618	1033	.0618	-.0135	.0135
1.119	2.30	861	107 618	1033	.0618	-.0135	.0135
1.265	2.30	861	107 618	1033	.0618	-.0135	.0135
1.338	2.30	861	107 618	1033	.0618	-.0135	.0135
1.484	2.30	861	107 618	1033	.0618	-.0135	.0135
1.558	[d]2.30	861	107 618	1033	[e].0618	-.0135	.0135

[a]Positive for offset aft of pitch axis (0.25c).

[b]Positive for offset forward of pitch axis (0.25c).

[c]For hinged rotor the beamwise stiffness of this segment is zero.

[d]For hinged rotor with heavy tip mass the mass of this segment is 9.41 kg/m.

[e]For hinged rotor with heavy tip mass the radius of gyration of this segment is 0.0376 m.

TABLE III.- COUPLED NATURAL FREQUENCY RATIOS FOR BASELINE ROTOR

ω/Ω^a for $\theta_{0.75R}$ of -		Principal mode identity
6°	11°	
1.08	1.08	Collective beamwise
2.60	2.37	Cyclic chordwise
3.19	3.17	Collective beamwise
3.69	3.83	Cyclic beamwise[b]
5.81	5.86	Cyclic beamwise
6.48	6.47	Collective beamwise
7.14	7.13	Blade torsional

[a]Ω = 54.0 rad/s.
[b]This mode also contains significant chordwise deflections.

TABLE IV.- COUPLED NATURAL FREQUENCY RATIOS FOR HINGED ROTOR

ω/Ω^a for rotor with -		Principal mode identity
Light tip mass	Heavy tip mass	
1.08	1.07	Collective beamwise
2.16	2.07	Cyclic chordwise
2.46	2.54	Collective beamwise
3.16	2.99	Cyclic beamwise[b]
5.14	5.21	Cyclic beamwise
5.49	5.67	Collective beamwise
6.97	6.84	Blade torsional

[a]Ω = 54.0 rad/s; $\theta_{0.75R}$ = 11°.
[b]This mode also contains significant chordwise deflections.

TABLE V.- VARIATION OF COUPLED NATURAL FREQUENCY RATIOS

WITH LOCATION OF OUTBOARD HINGE

ω/Ω^a for hinge location of -		Principal mode identity
47 percent radius	62 percent radius	
1.07	1.07	Collective beamwise
2.04	2.07	Cyclic chordwise
2.68	2.54	Collective beamwise
3.25	2.99	Cyclic beamwise
5.75	5.21	Cyclic beamwise
6.30	5.67	Collective beamwise
6.96	6.84	Blade torsional

$^a\Omega$ = 54.0 rad/s; $\theta_{0.75R}$ = 11°; heavy tip mass.

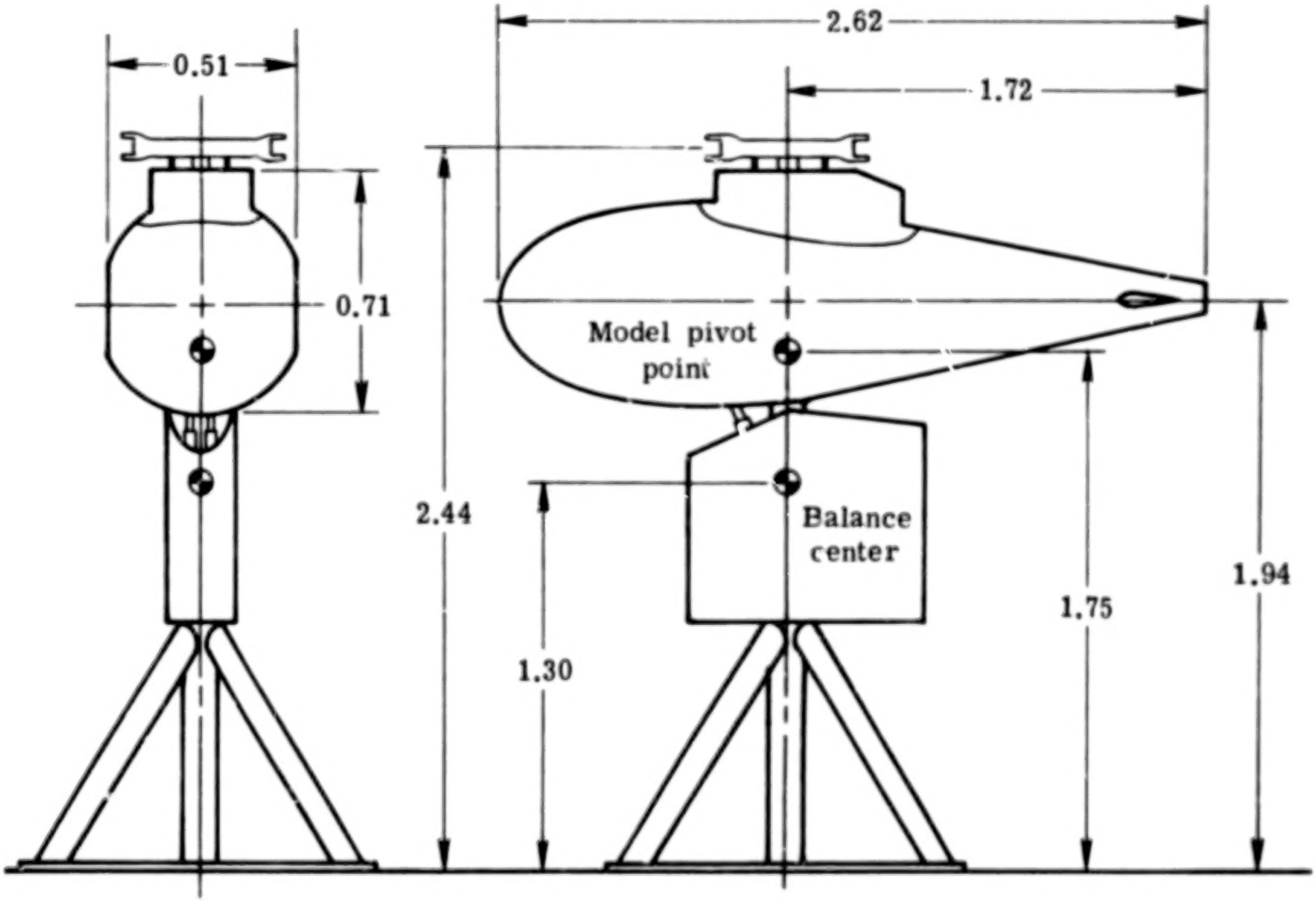

Figure 1.- Schematic diagram of generalized rotor aeroelastic model.
All dimensions are given in meters.

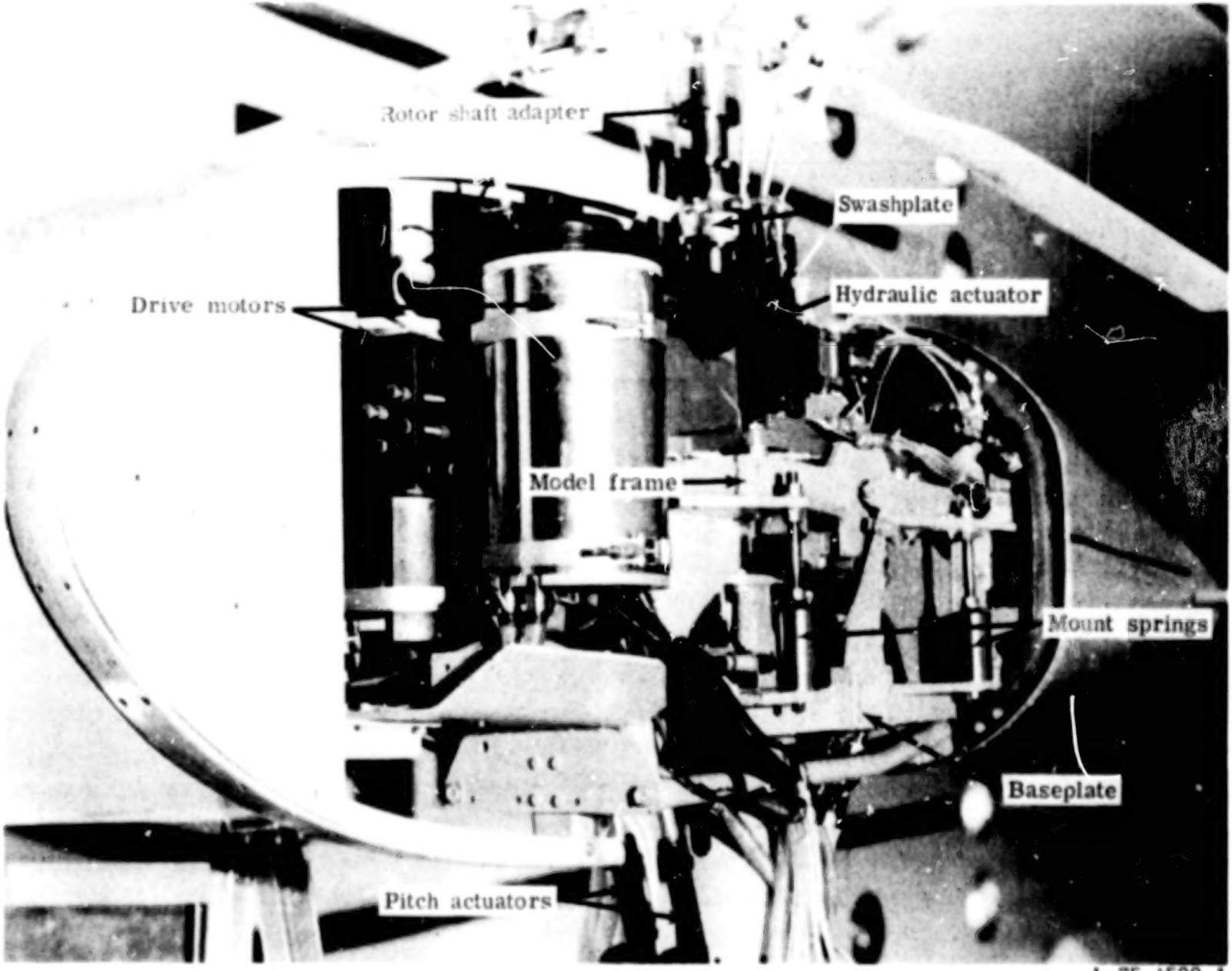

L-75-1500.1

Figure 2.- Detailed view of generalized rotor aeroelastic model.

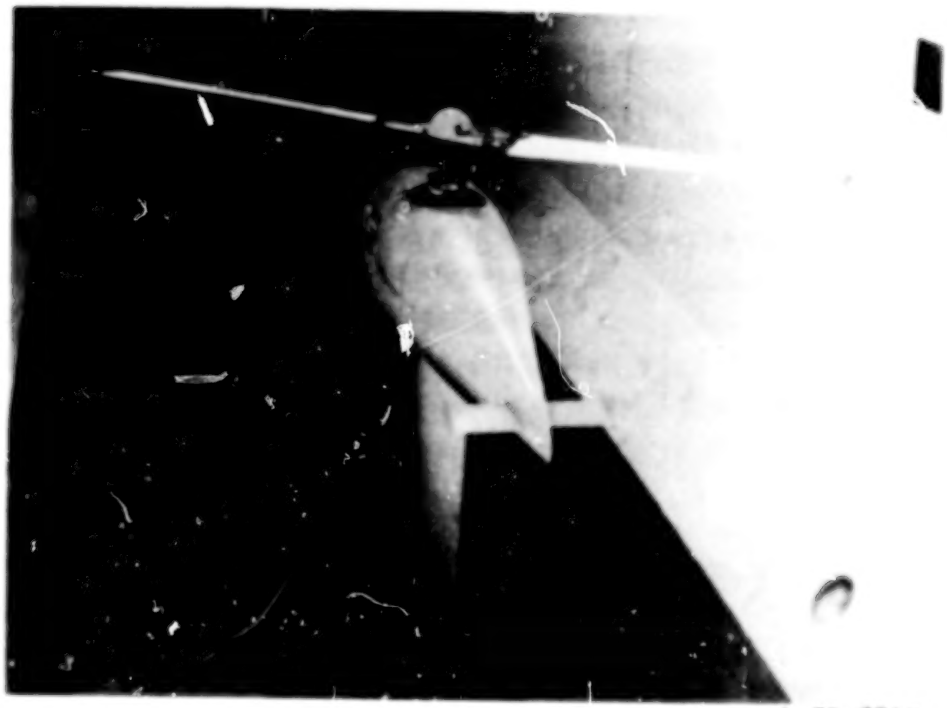

L-75-8845

Figure 3.- Baseline rotor mounted on generalized rotor aeroelastic model.

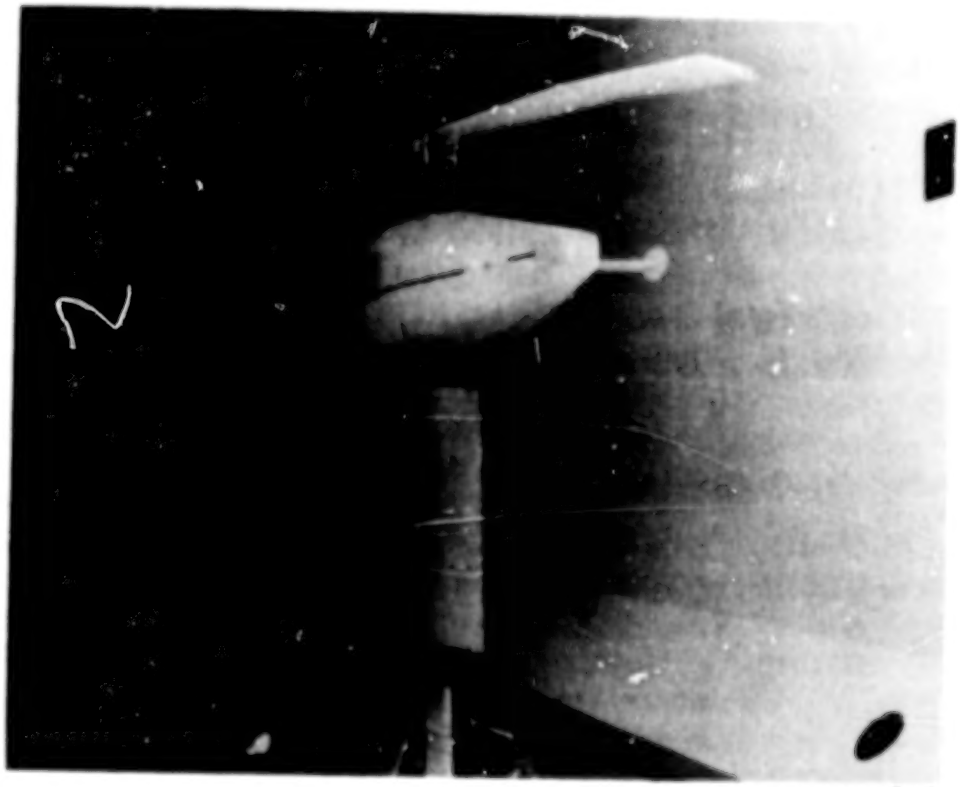

L-75-1836

Figure 4.- Hinged rotor mounted on generalized rotor aeroelastic model.

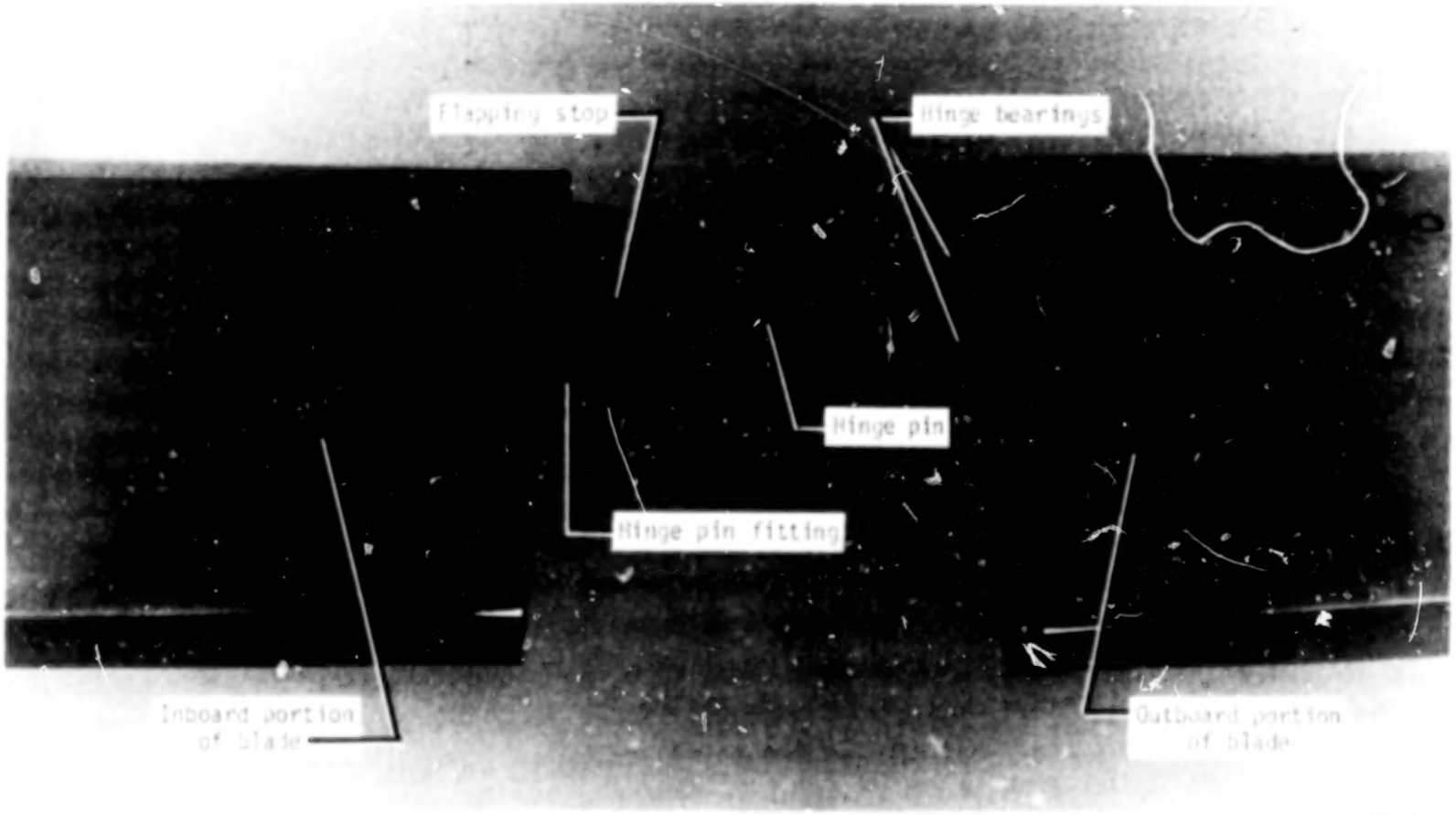

L-76-4904.1

Figure 5.- Details of outboard flapping hinge.

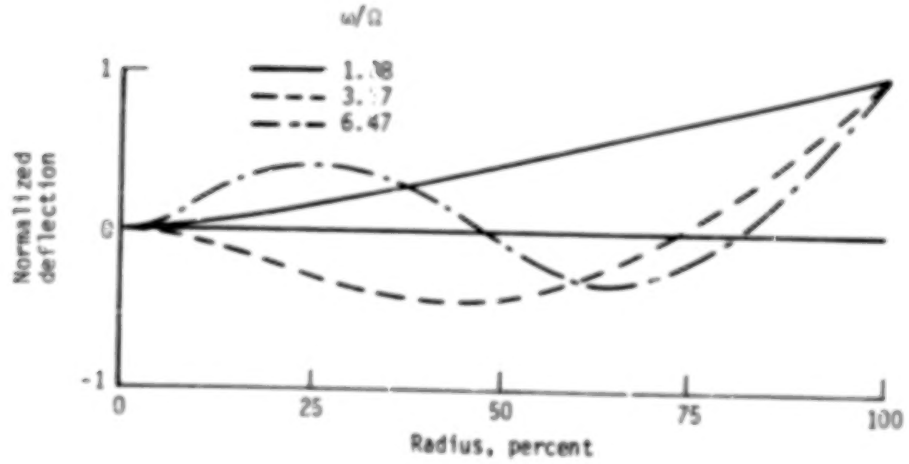

(a) Collective beamwise modes.

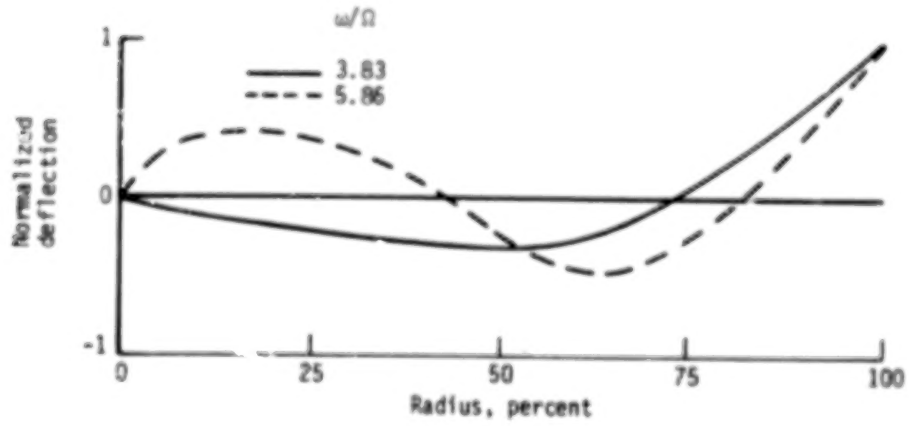

(b) Cyclic beamwise modes.

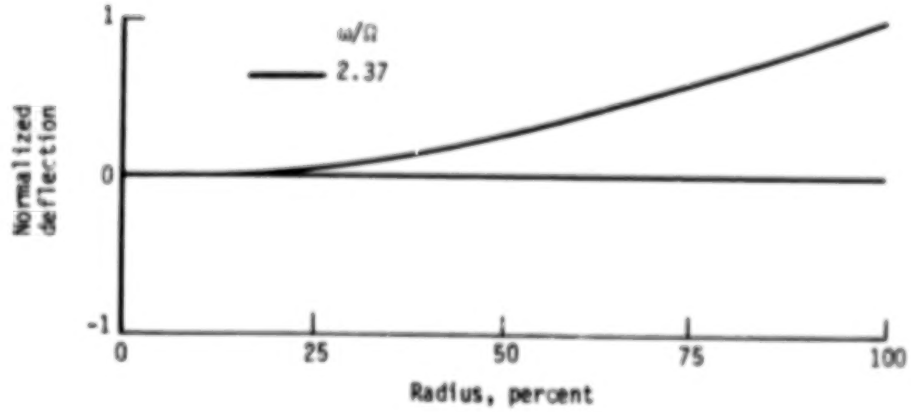

(c) Cyclic chordwise mode.

Figure 6.- Calculated principal deflection shapes of baseline rotor modes. Ω = 54.0 rad/s; $\theta_{0.75R}$ = 11°.

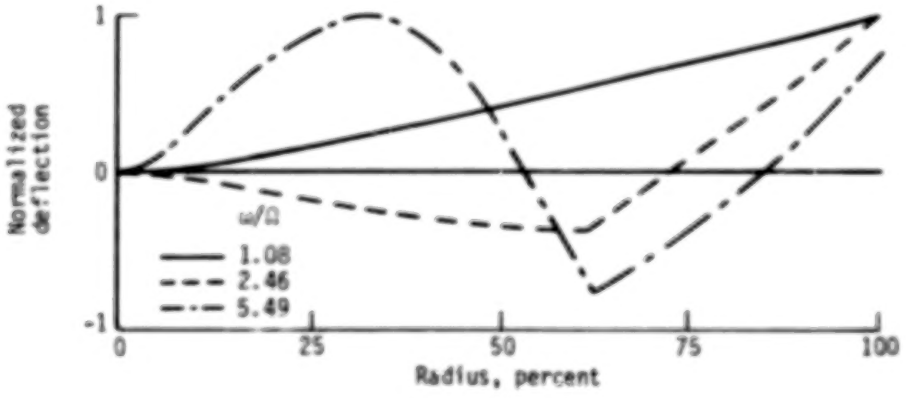

(a) Collective beamwise modes.

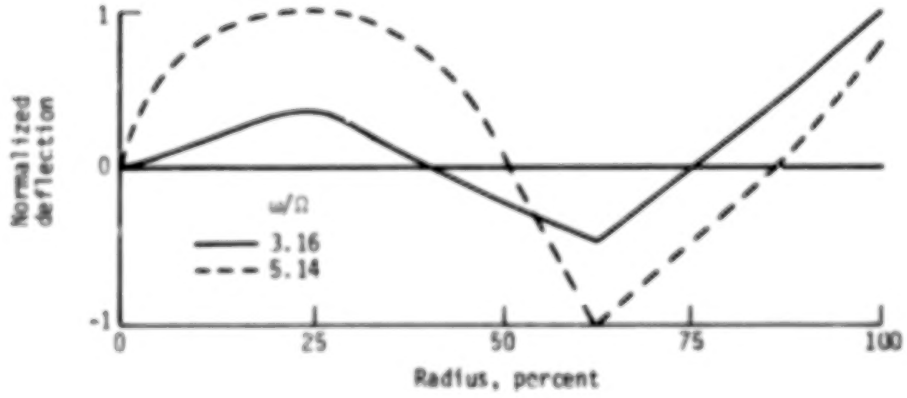

(b) Cyclic beamwise modes.

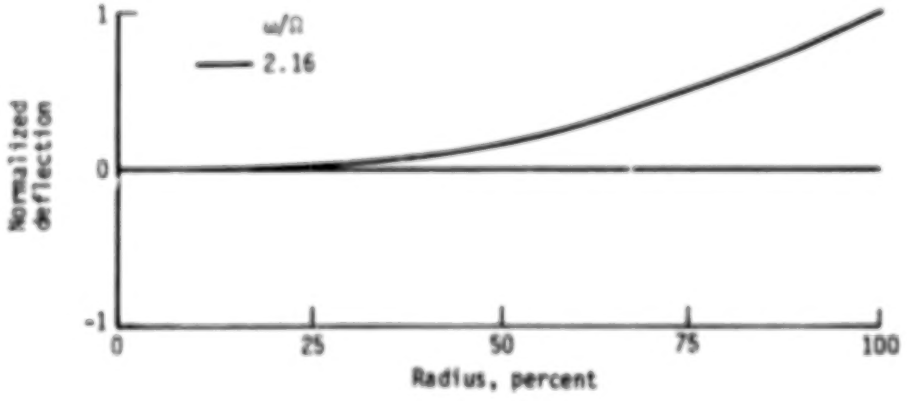

(c) Cyclic chordwise mode.

Figure 7.- Calculated principal deflection shapes of modes of hinged rotor with light tip mass. Ω = 54.0 rad/s; $\theta_{0.75R}$ = 11°.

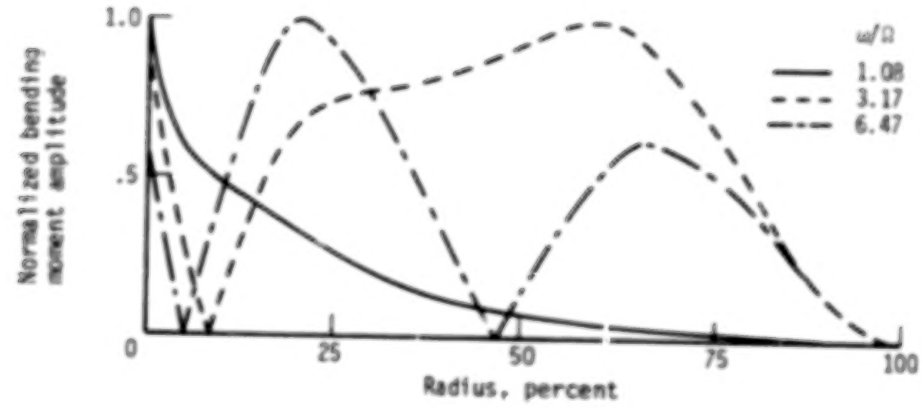

(a) Collective beamwise modes.

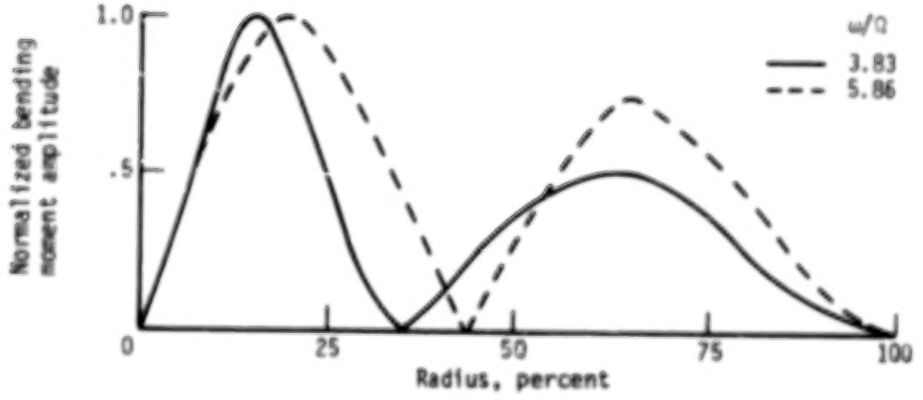

(b) Cyclic beamwise modes.

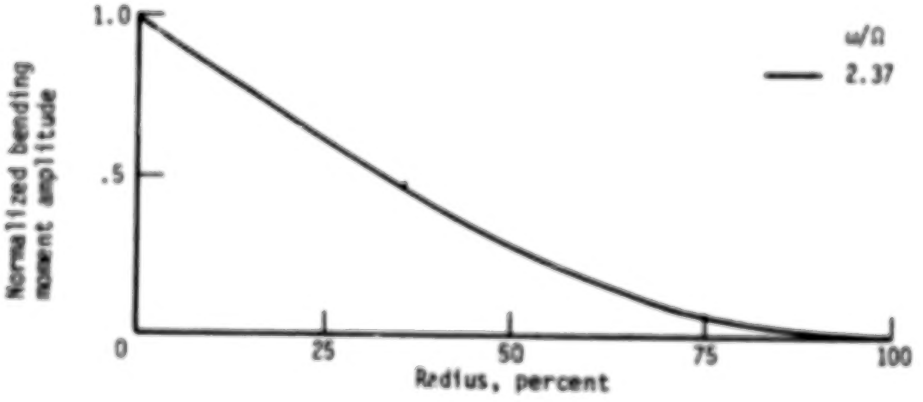

(c) Cyclic chordwise mode.

Figure 8.- Calculated principal moment distributions of baseline rotor modes. Ω = 54.0 rad/s; $\theta_{0.75R}$ = 11°.

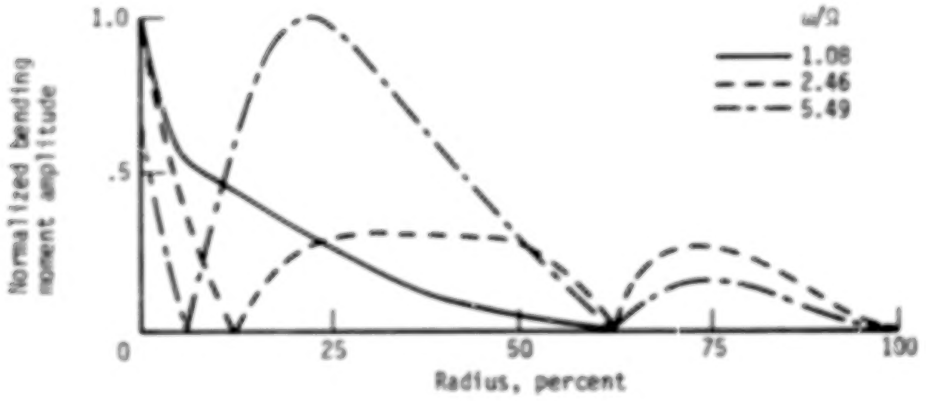

(a) Collective beamwise modes.

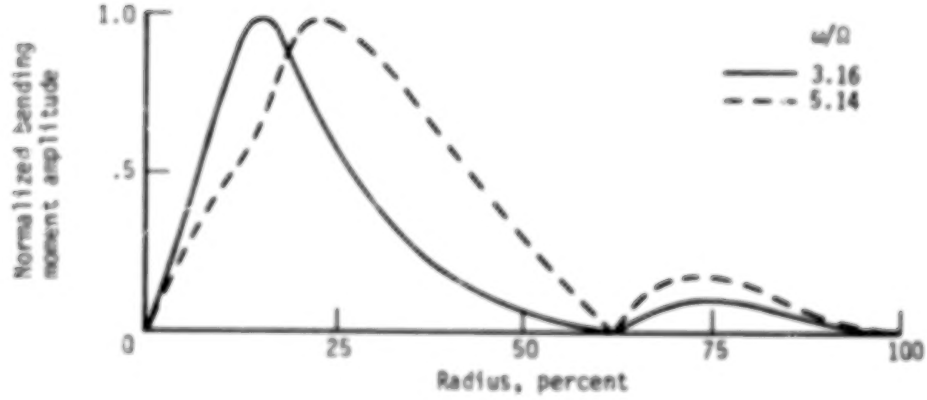

(b) Cyclic beamwise modes.

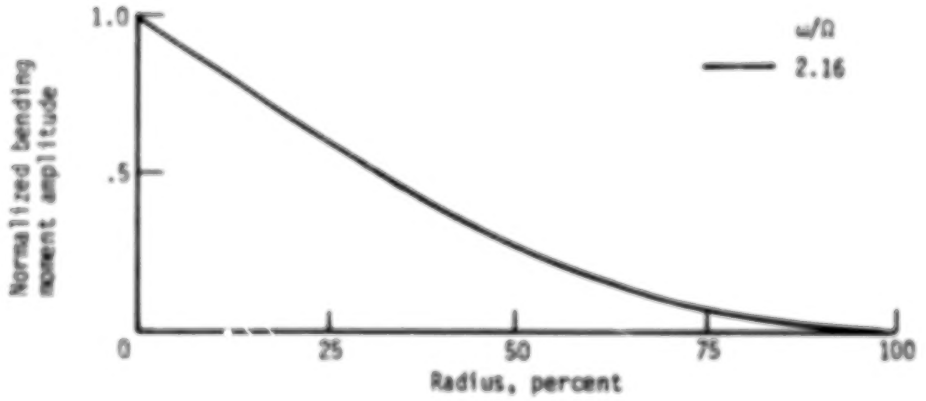

(c) Cyclic chordwise mode.

Figure 9.- Calculated principal moment distributions of modes of hinged rotor with light tip mass. Ω = 54.0 rad/s; $\theta_{0.75R}$ = 11°.

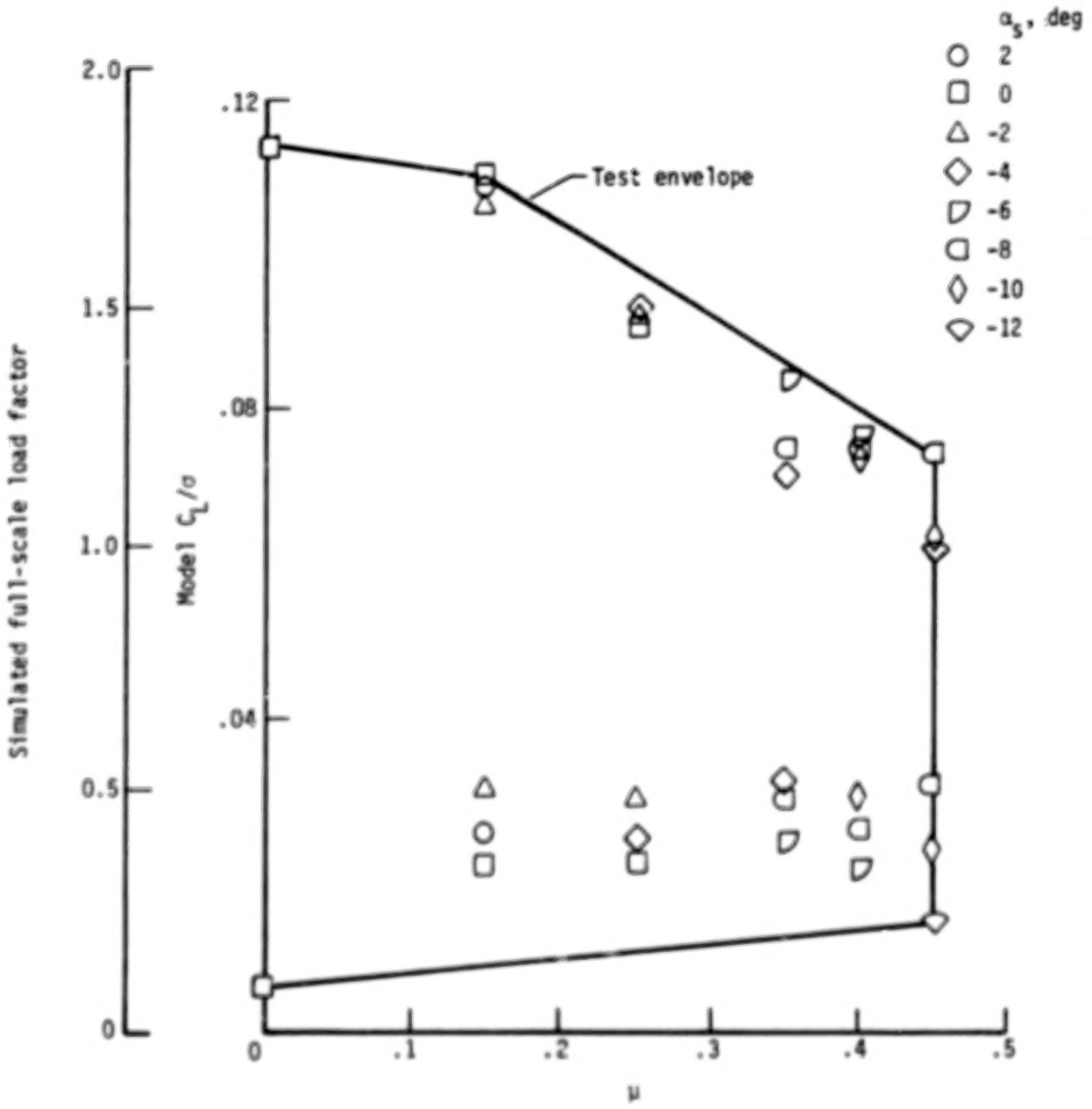

Figure 10.- Maximum and minimum values of C_L/σ achieved during tests for baseline rotor.

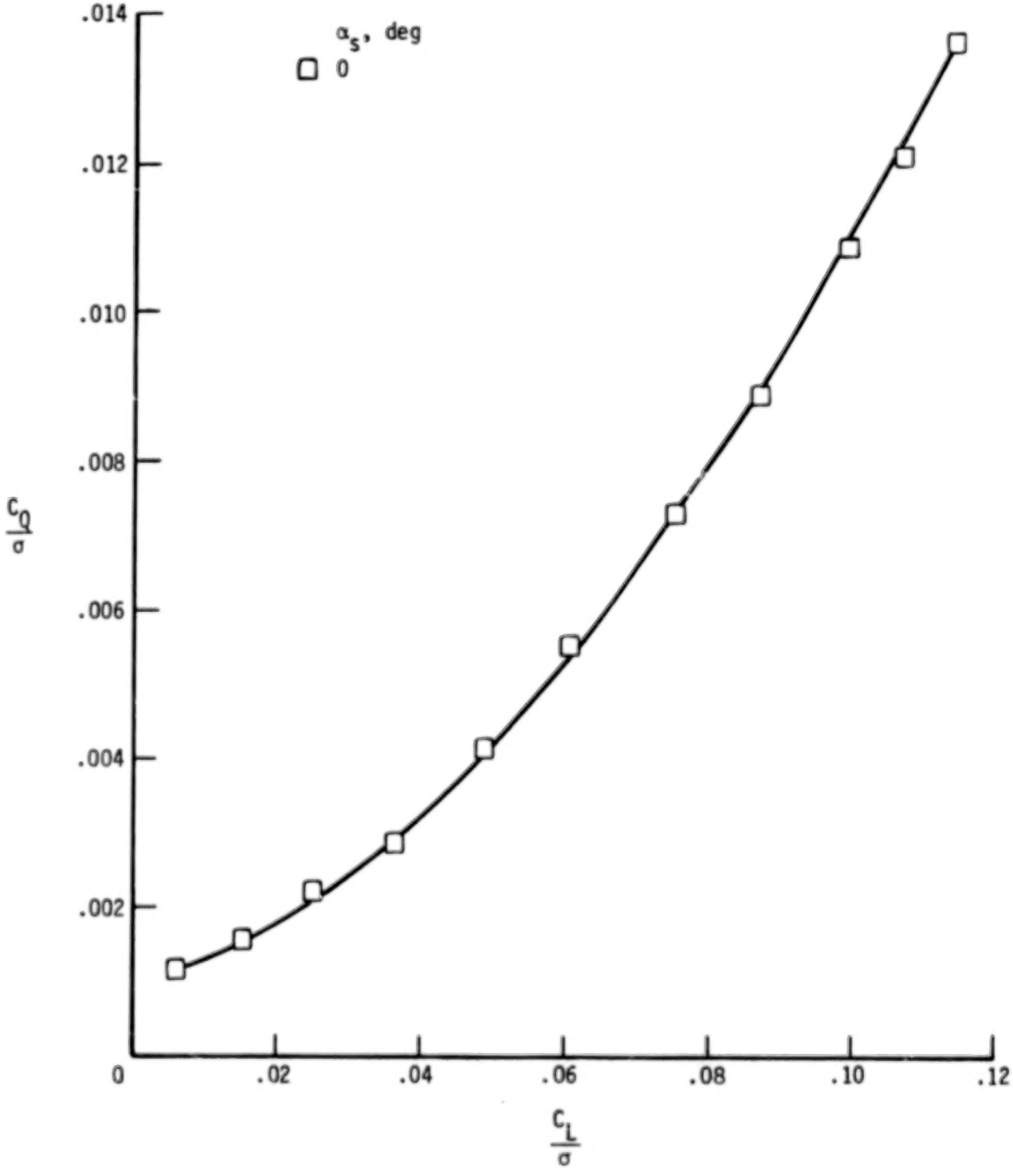

(a) $\mu = 0.$

Figure 11.- Variation of rotor torque with lift for baseline rotor at six advance ratios.

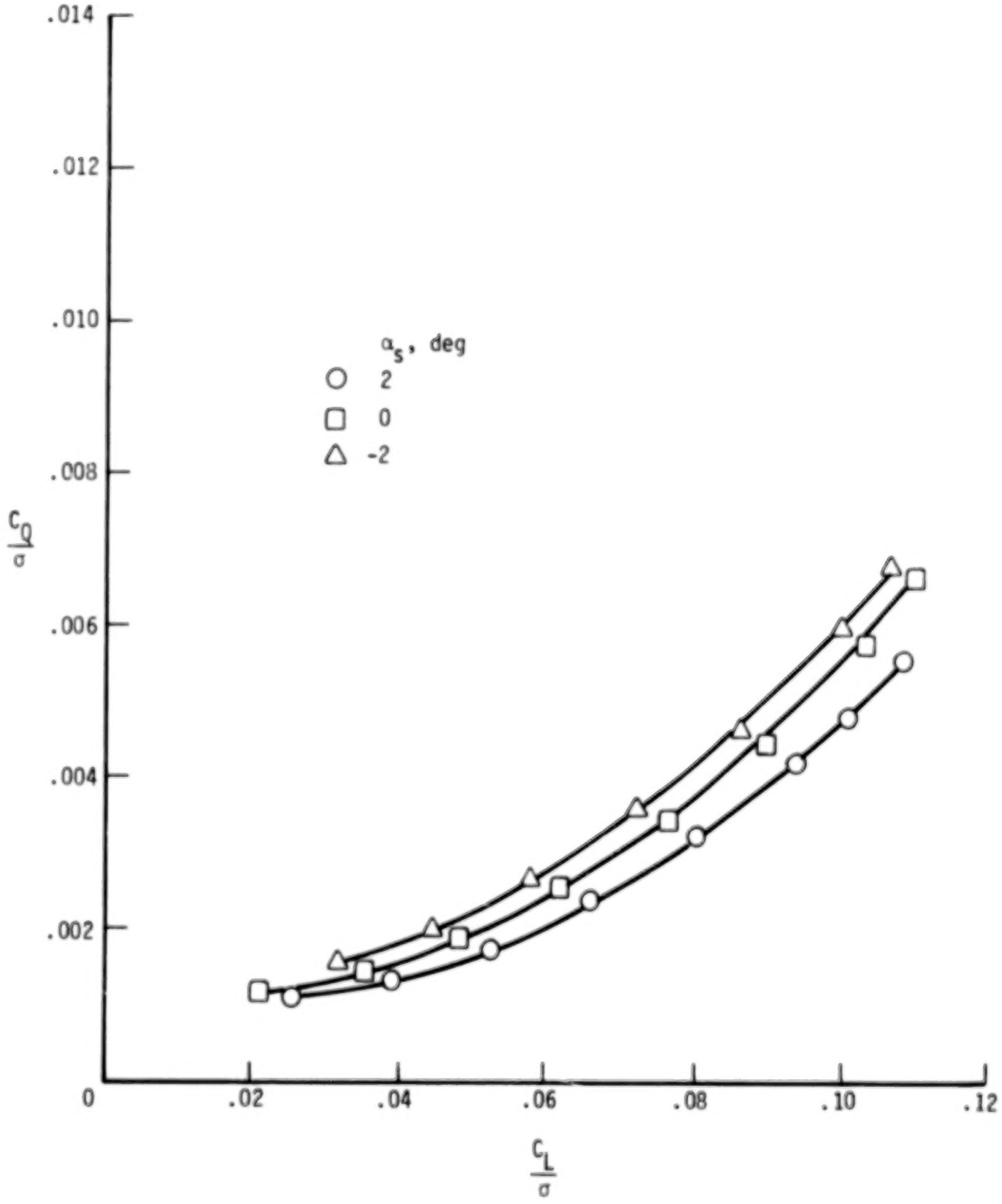

(b) $\mu = 0.15$.

Figure 11.- Continued.

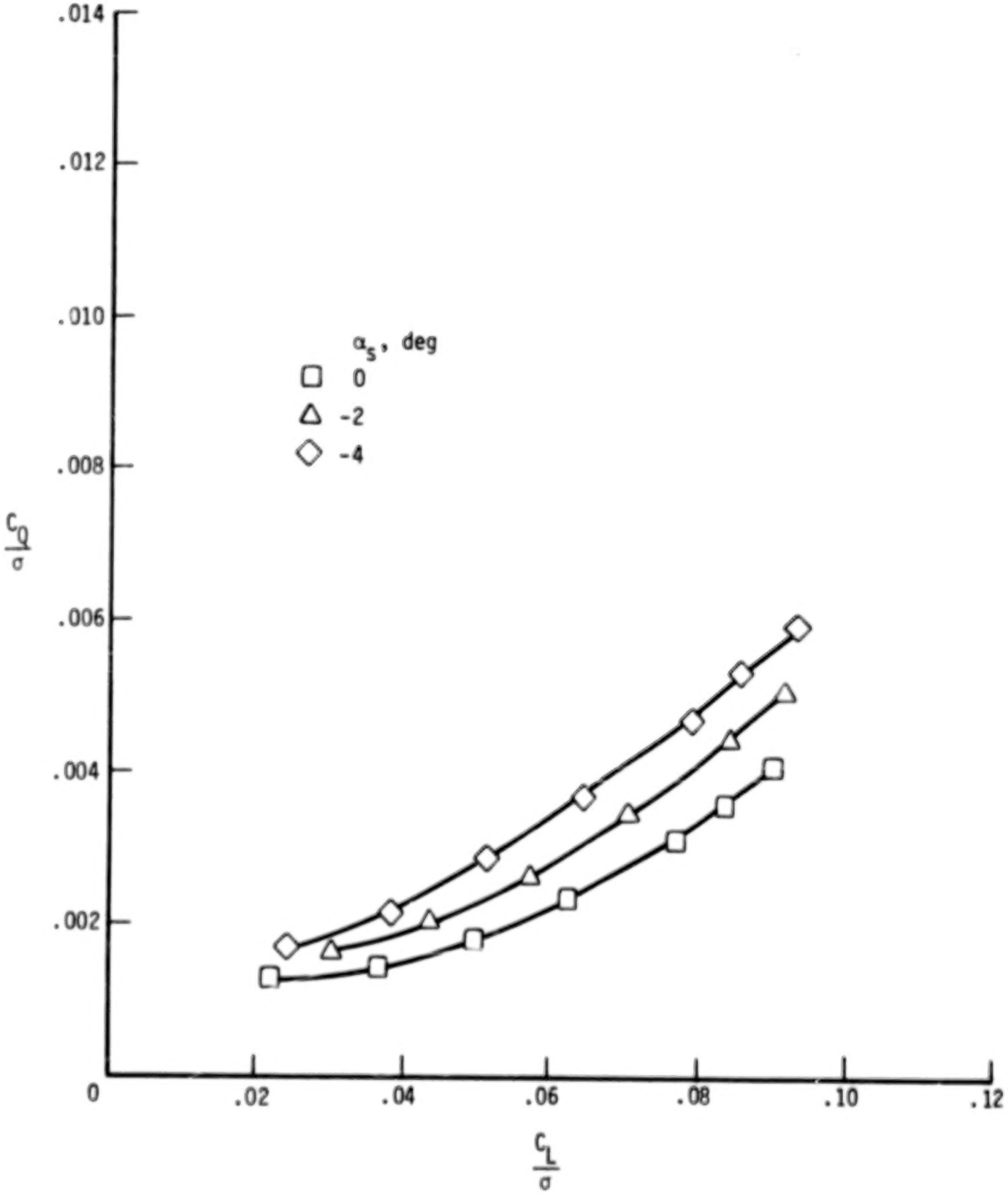

(c) $\mu = 0.25$.

Figure 11.- Continued.

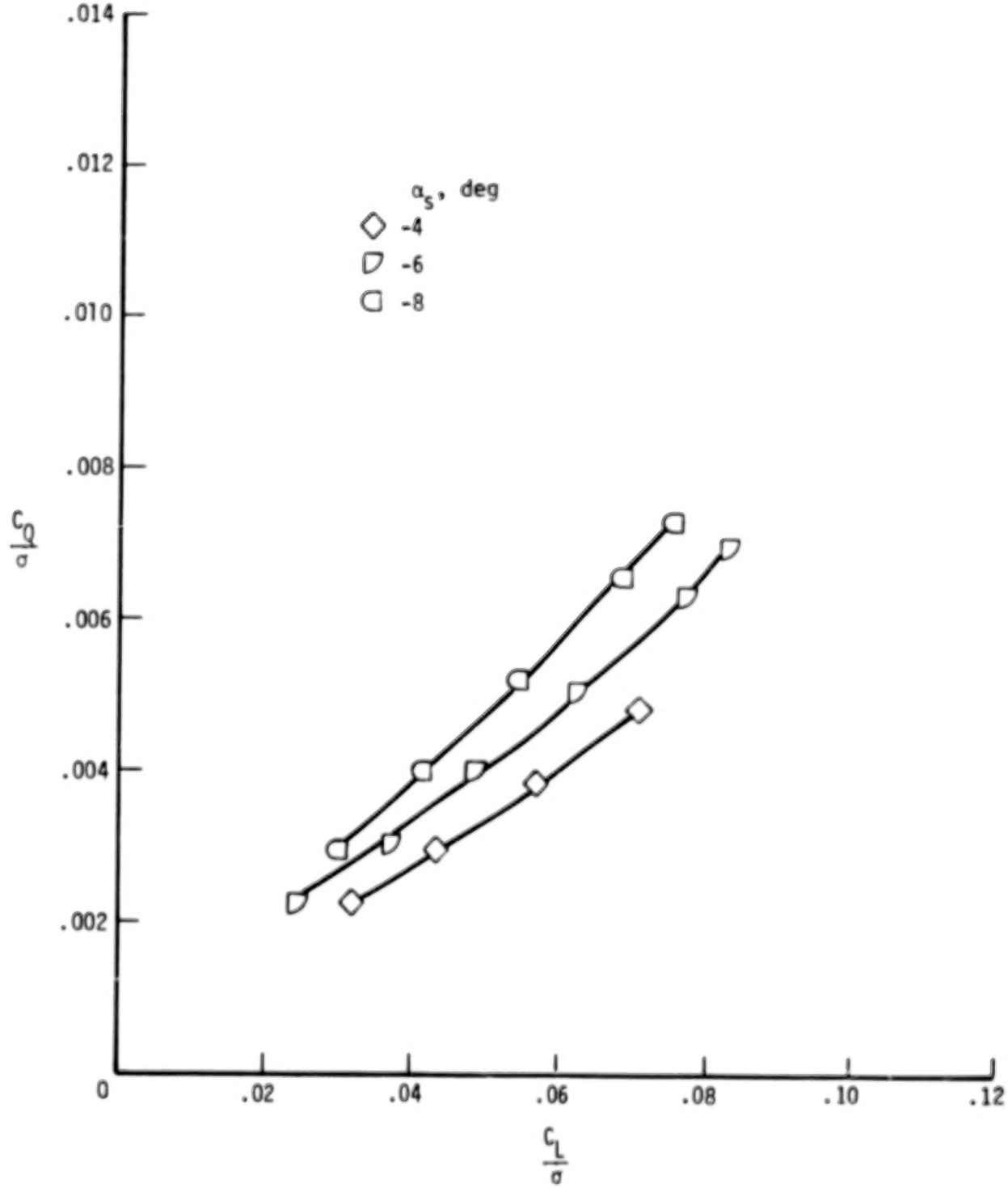

(d) $\mu = 0.35$.

Figure 11.- Continued.

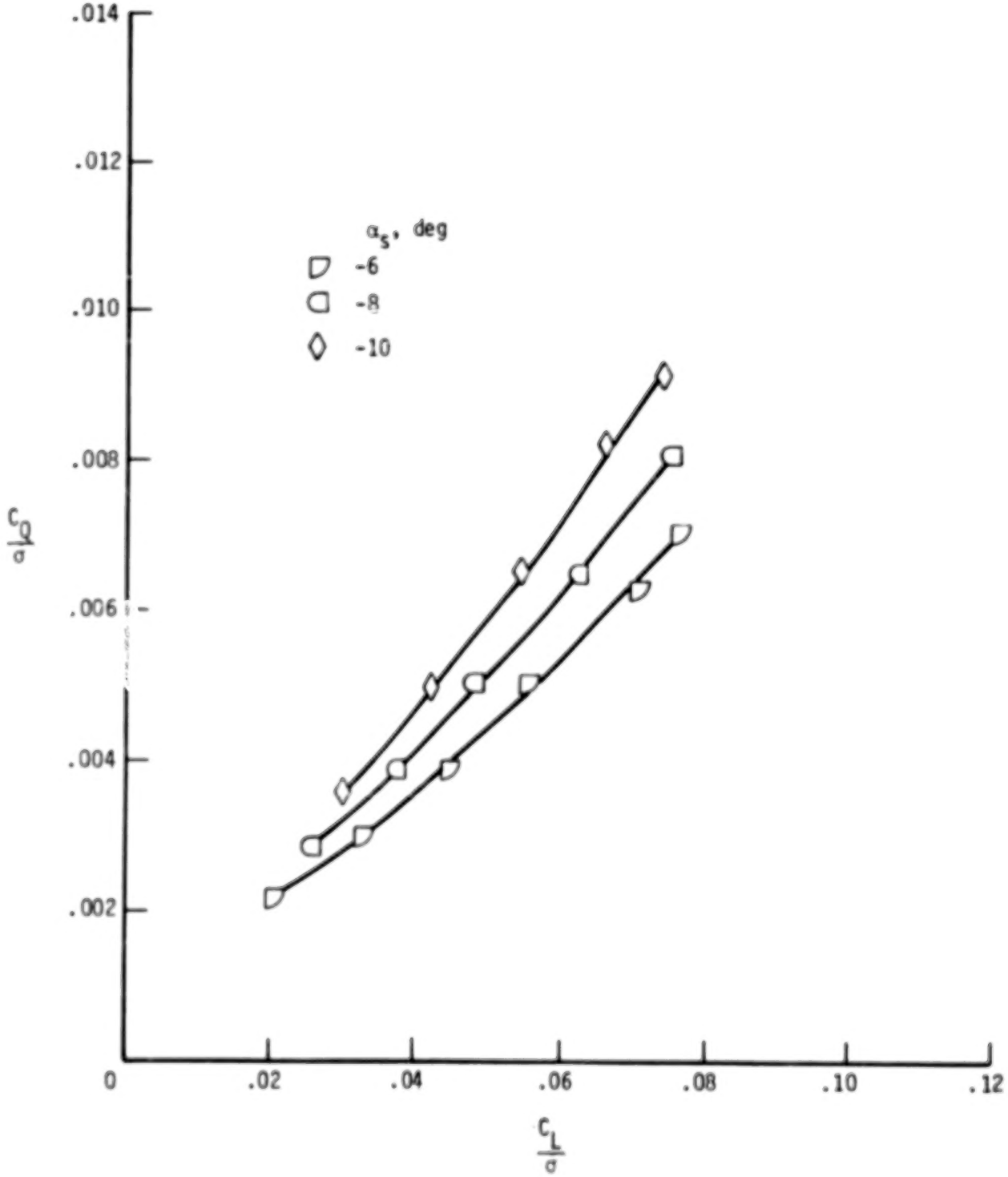

(e) $\mu = 0.40$.

Figure 11.- Continued.

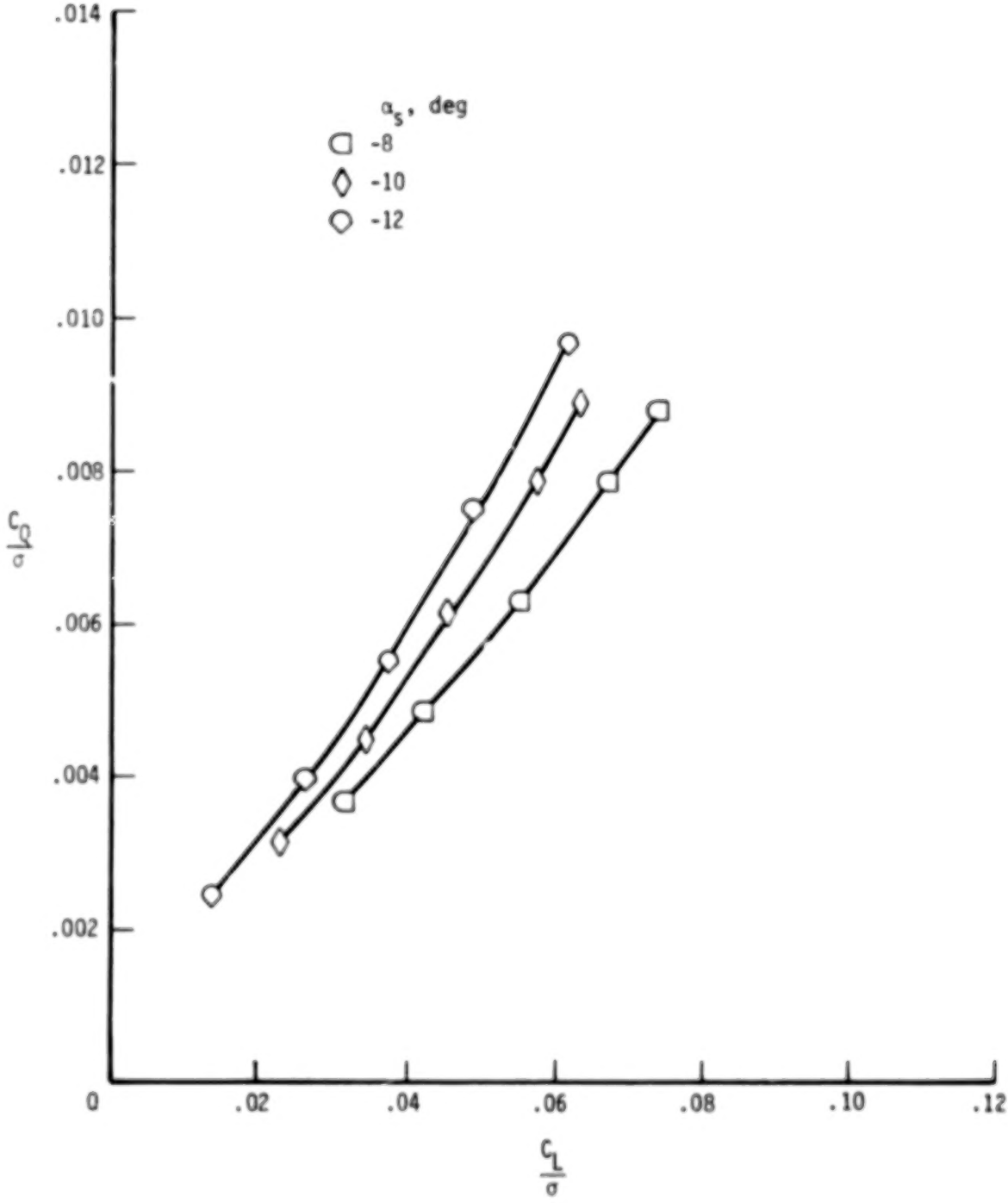

(f) $\mu = 0.45$.

Figure 11.- Concluded.

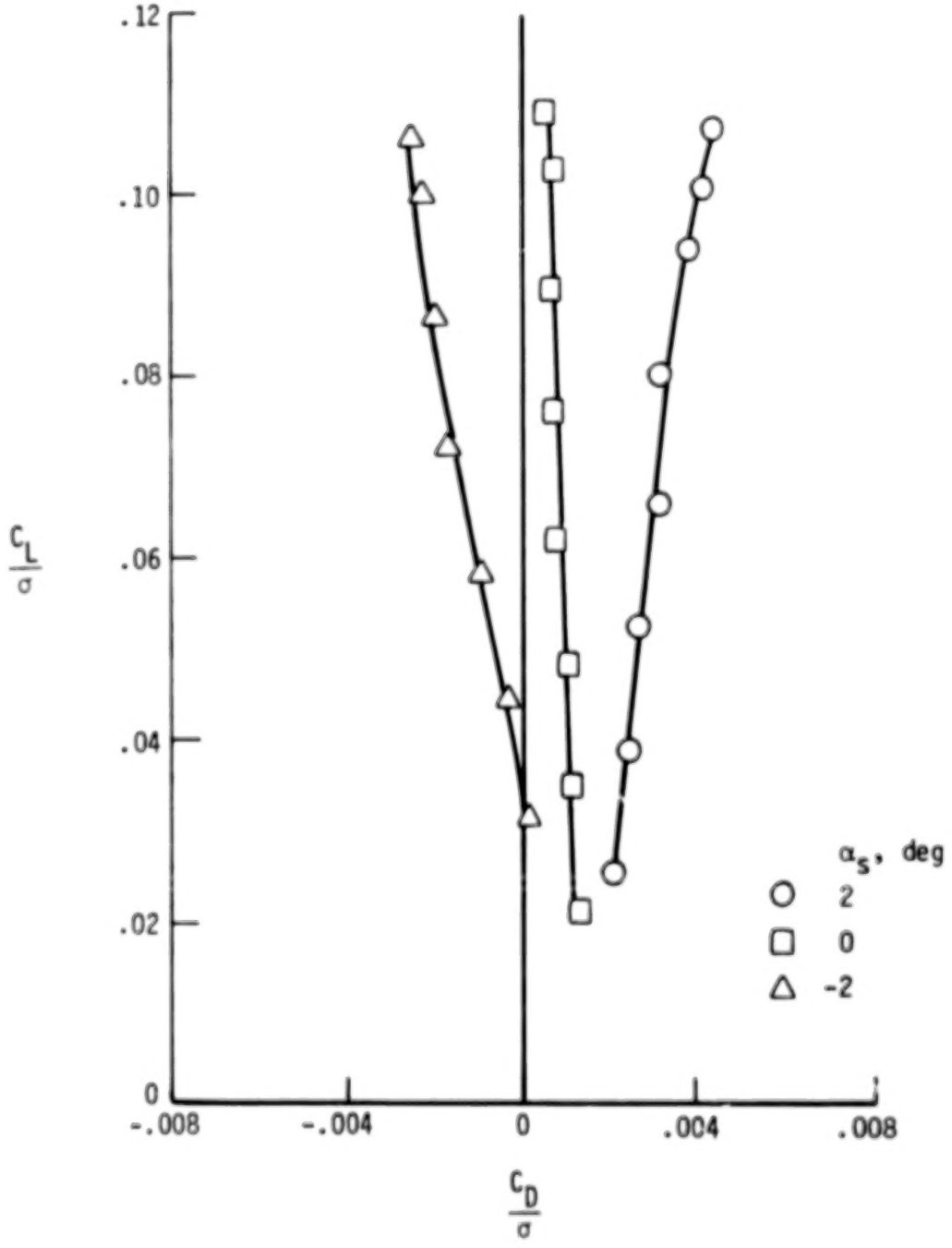

(a) $\mu = 0.15$.

Figure 12.- Variation of rotor lift with drag for baseline rotor at five advance ratios.

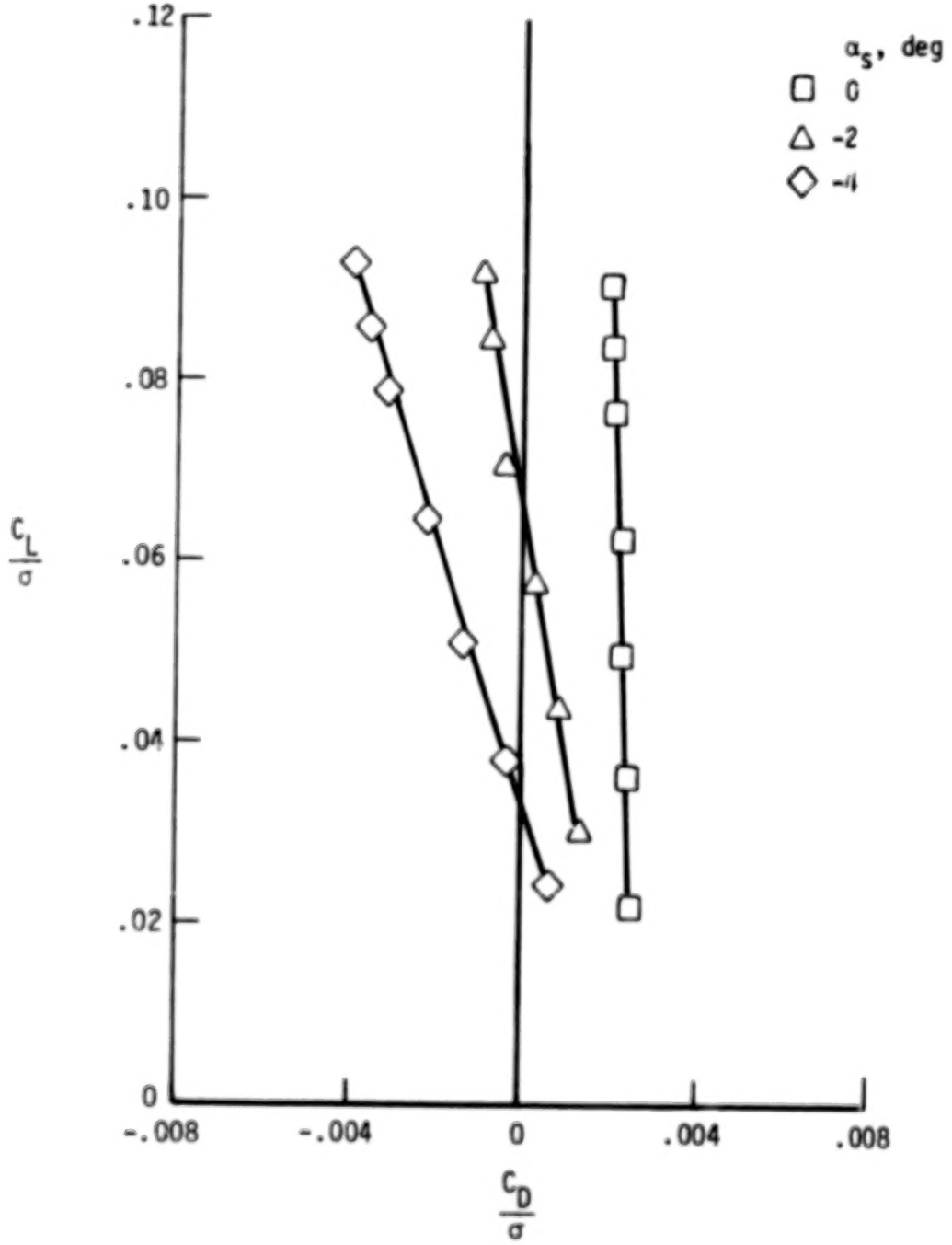

(b) $\mu = 0.25$.

Figure 12.- Continued.

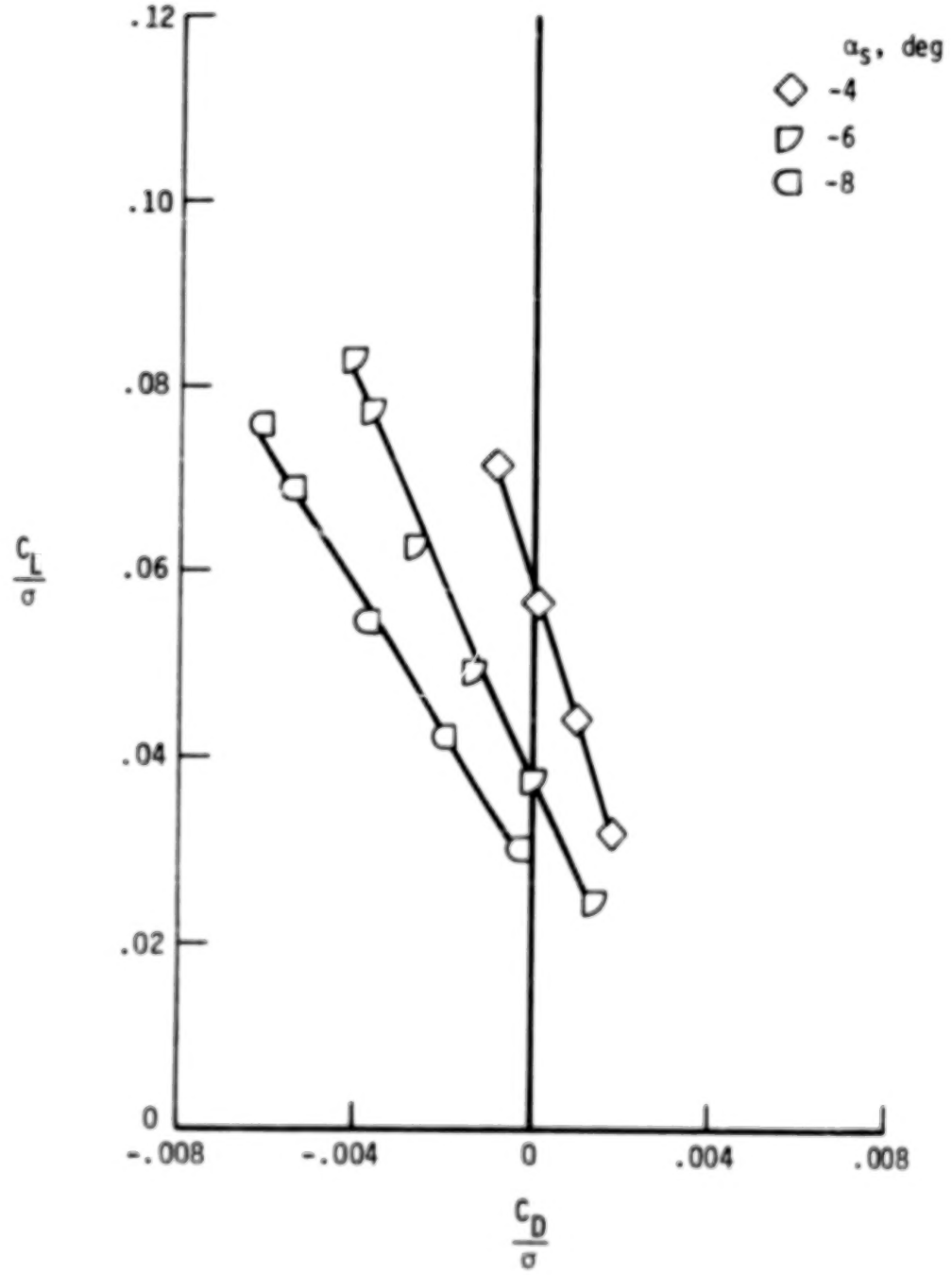

(c) $\mu = 0.35$.

Figure 12.- Continued.

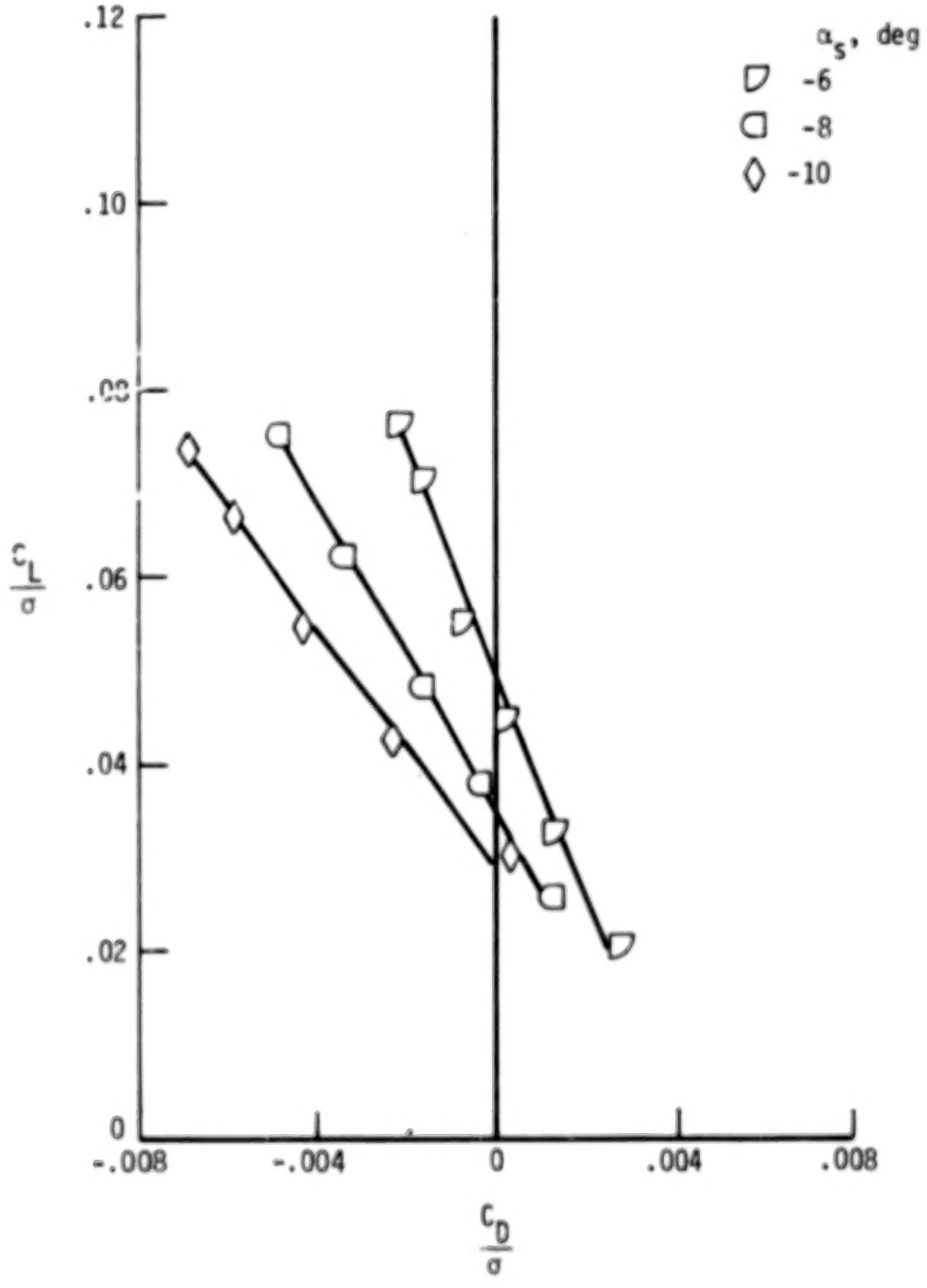

(d) $\mu = 0.40$.

Figure 12.- Continued.

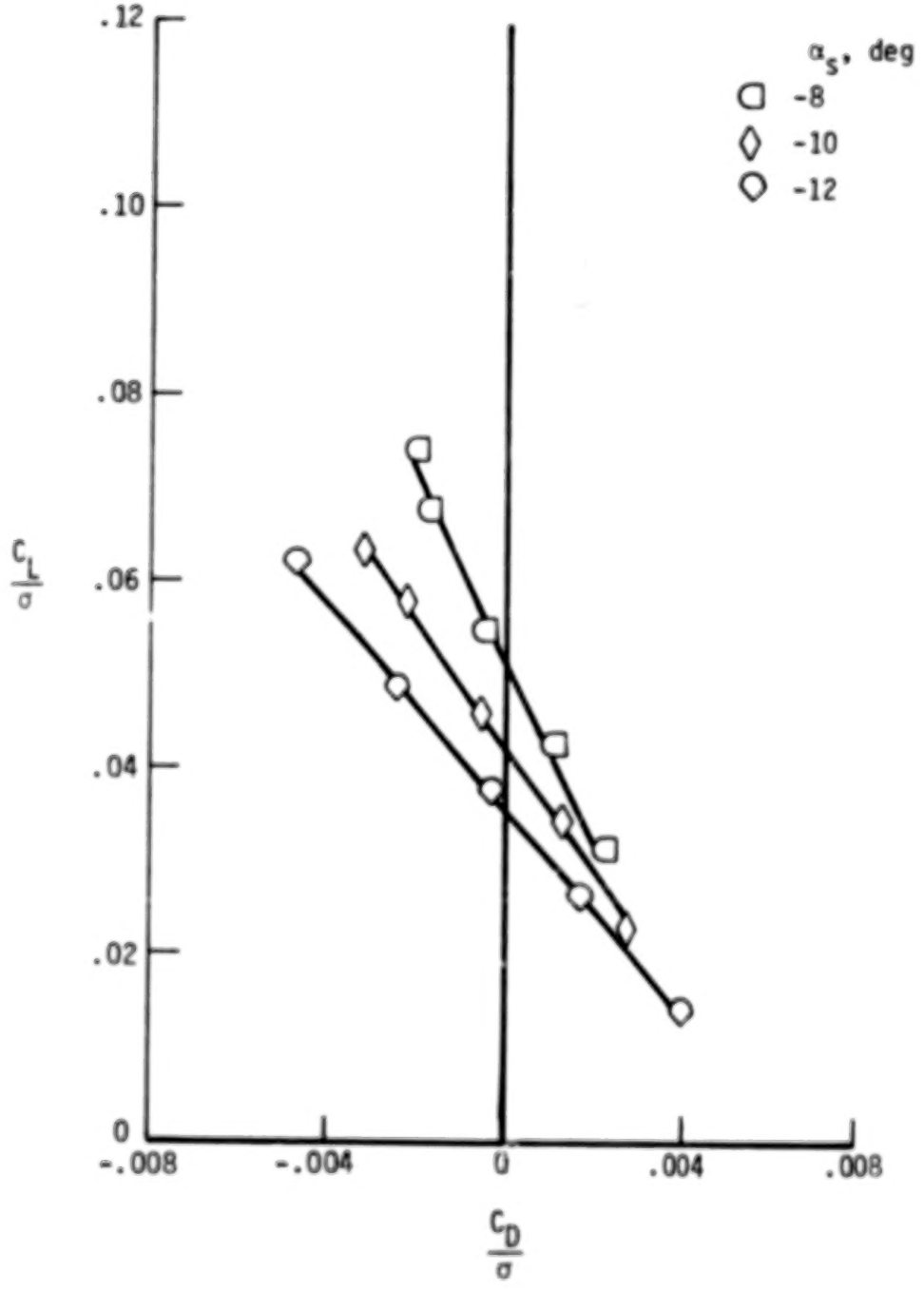

(e) $\mu = 0.45$.

Figure 12.- Concluded.

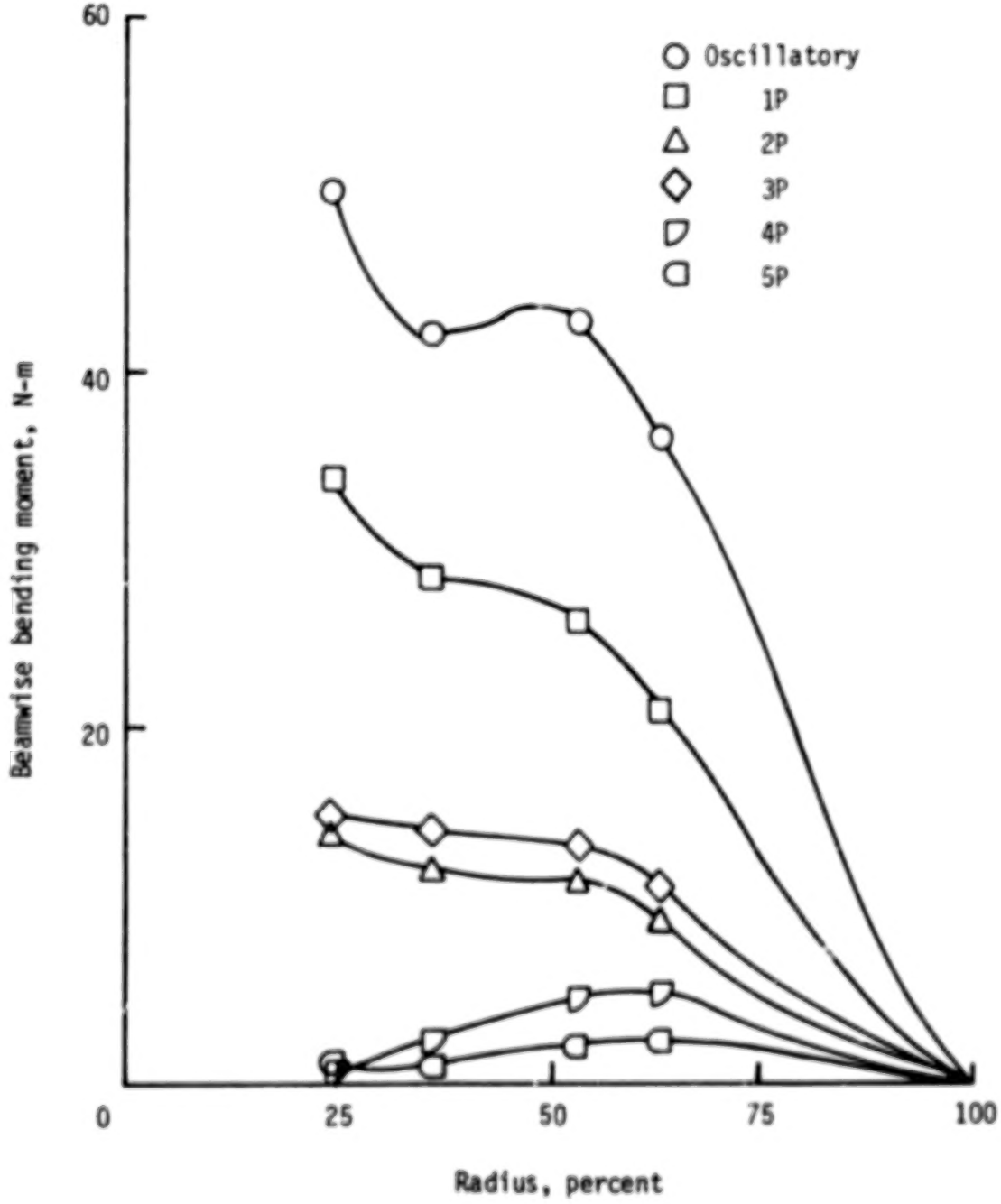

(a) Beamwise bending.

Figure 13.- Spanwise moment distributions measured on baseline rotor for low value of rotor lift. $\mu = 0.35$; $C_L/\sigma = 0.049$; $C_D/\sigma = -0.001$; $\alpha_s = -6^\circ$.

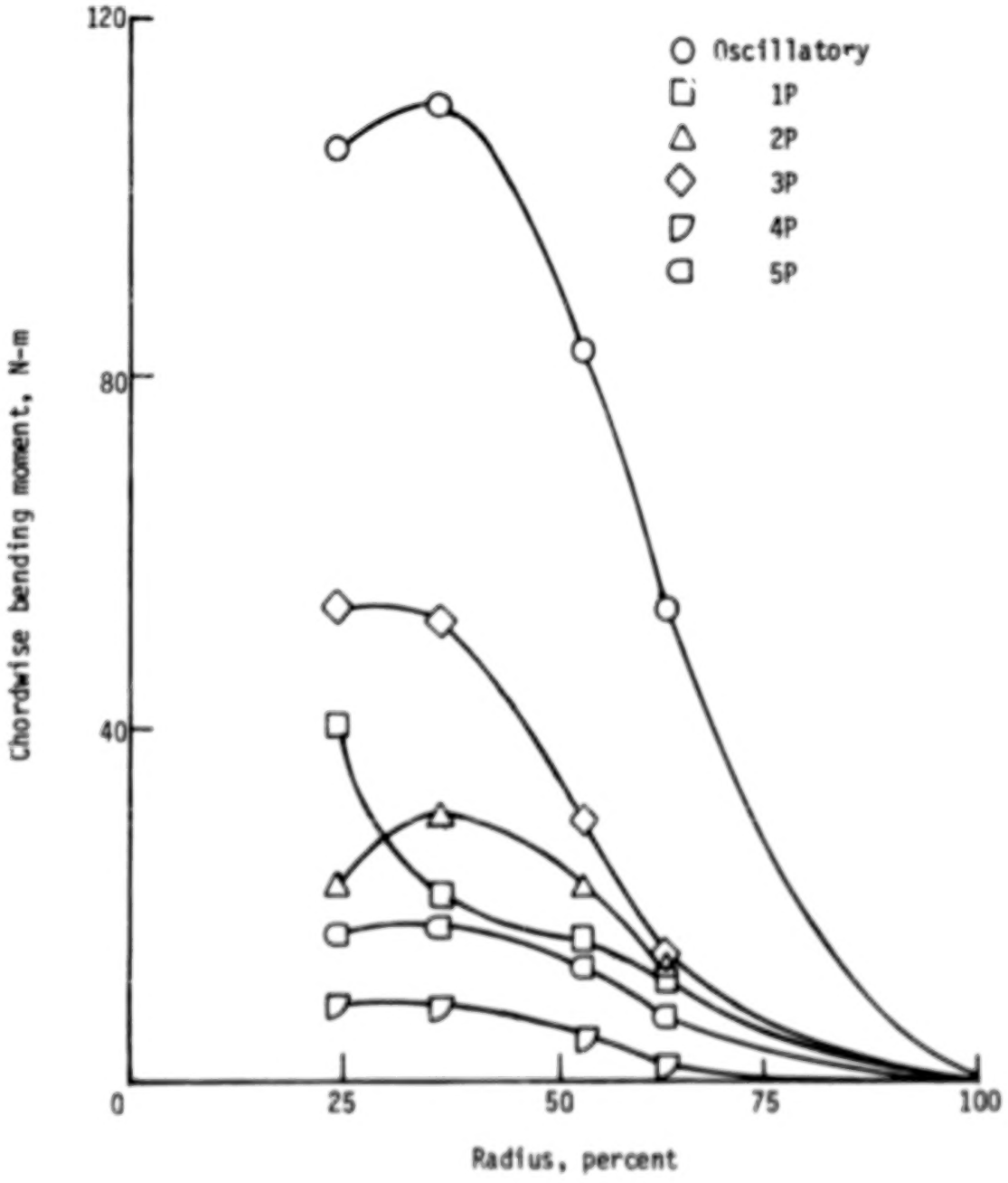

(b) Chordwise bending.

Figure 13.- Continued.

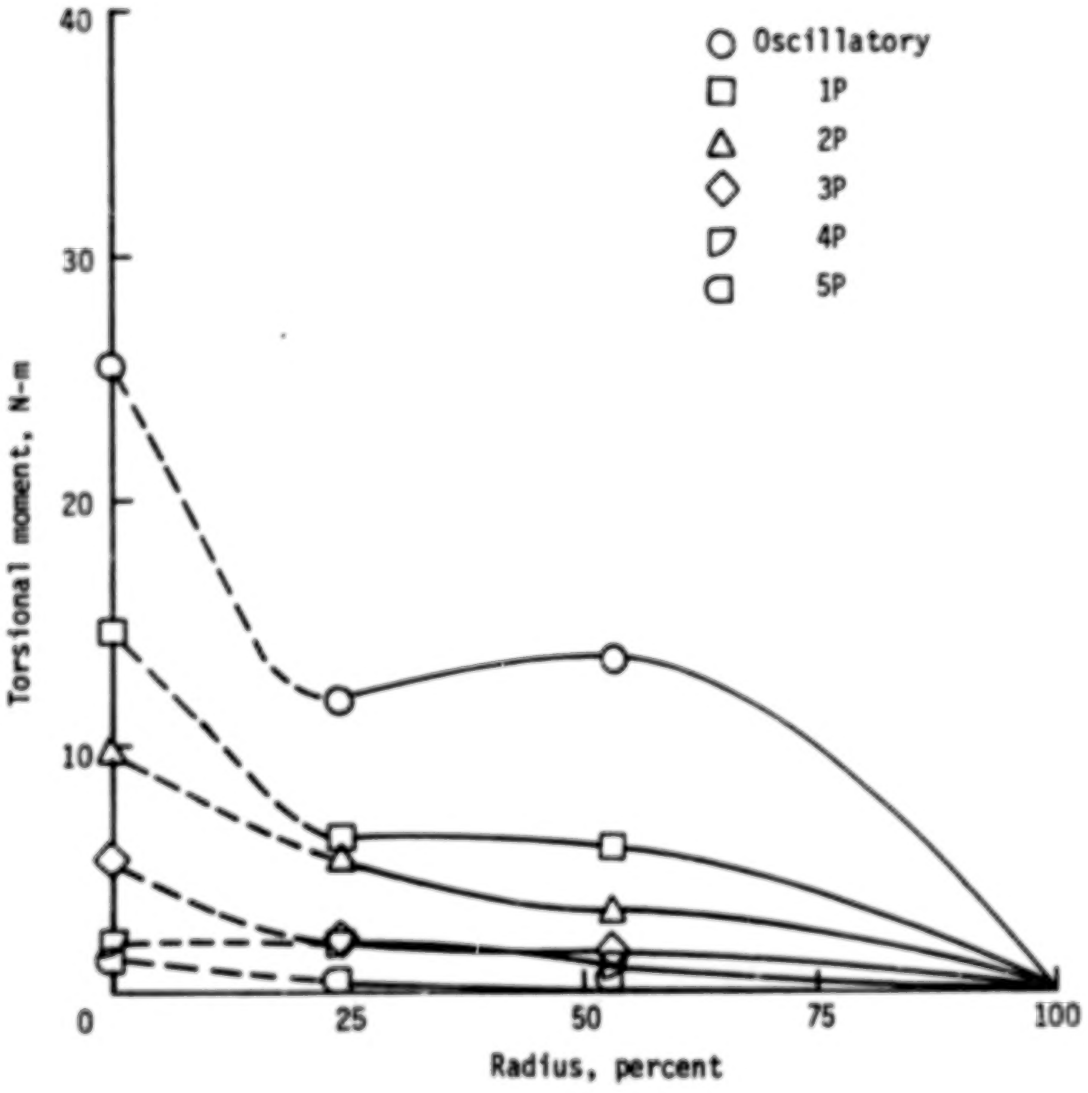

(c) Torsional moment.

Figure 13.- Concluded.

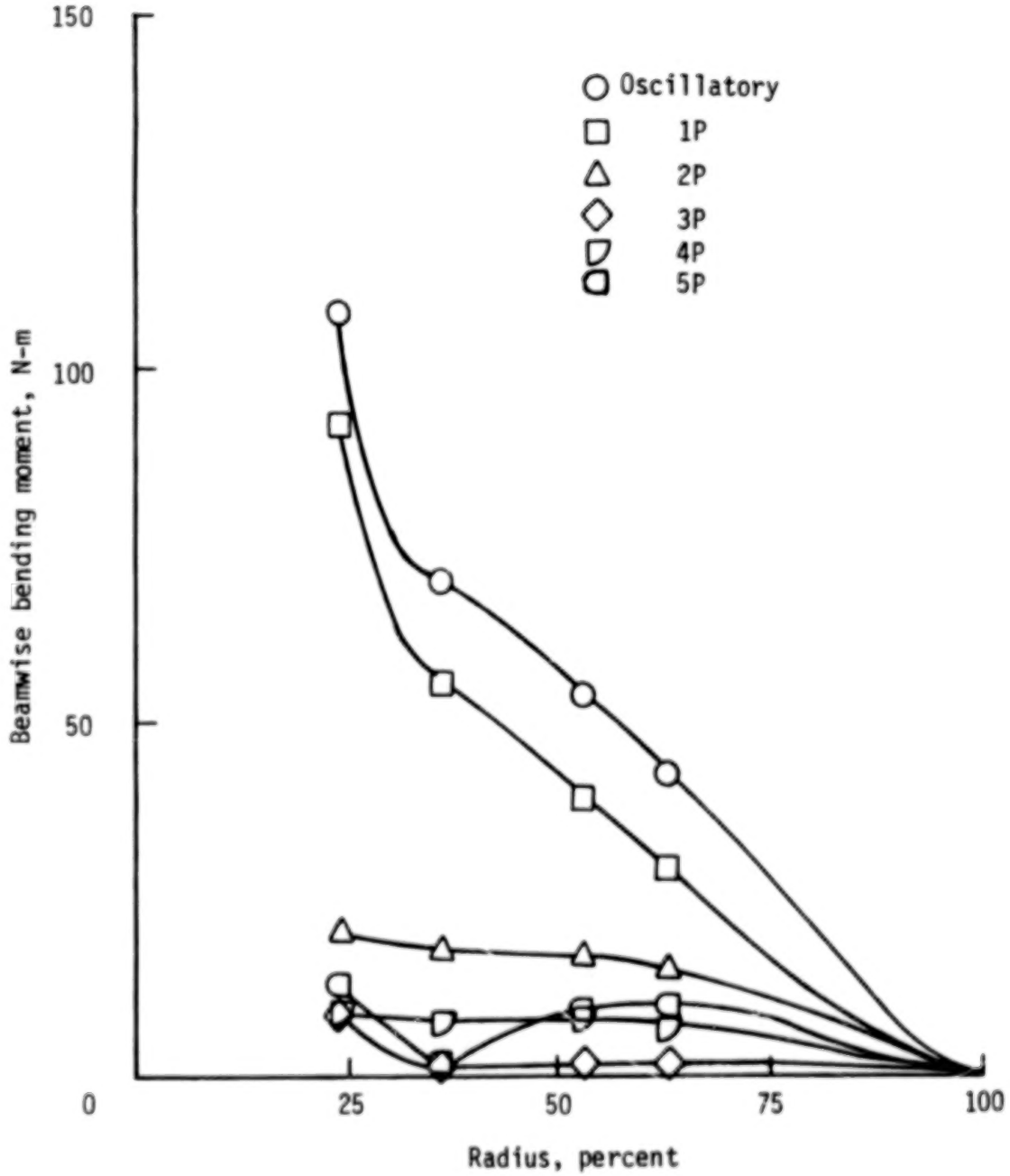

(a) Beamwise bending.

Figure 14.- Spanwise moment distributions measured on baseline rotor for high value of rotor lift. $\mu = 0.35$; $C_L/\sigma = 0.083$; $C_D/\sigma = -0.004$; $\alpha_s = -6^\circ$.

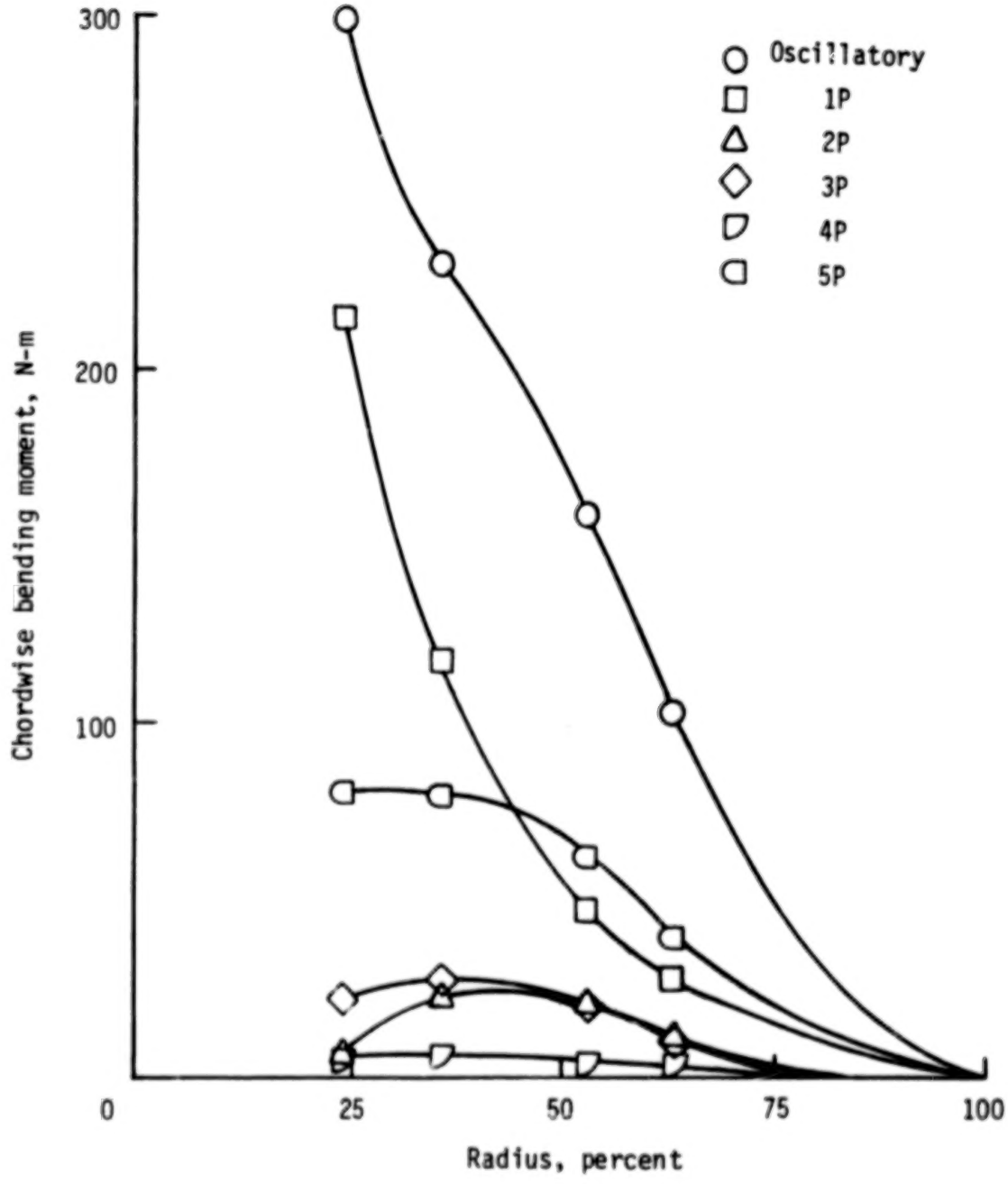

(b) Chordwise bending.

Figure 14.- Continued.

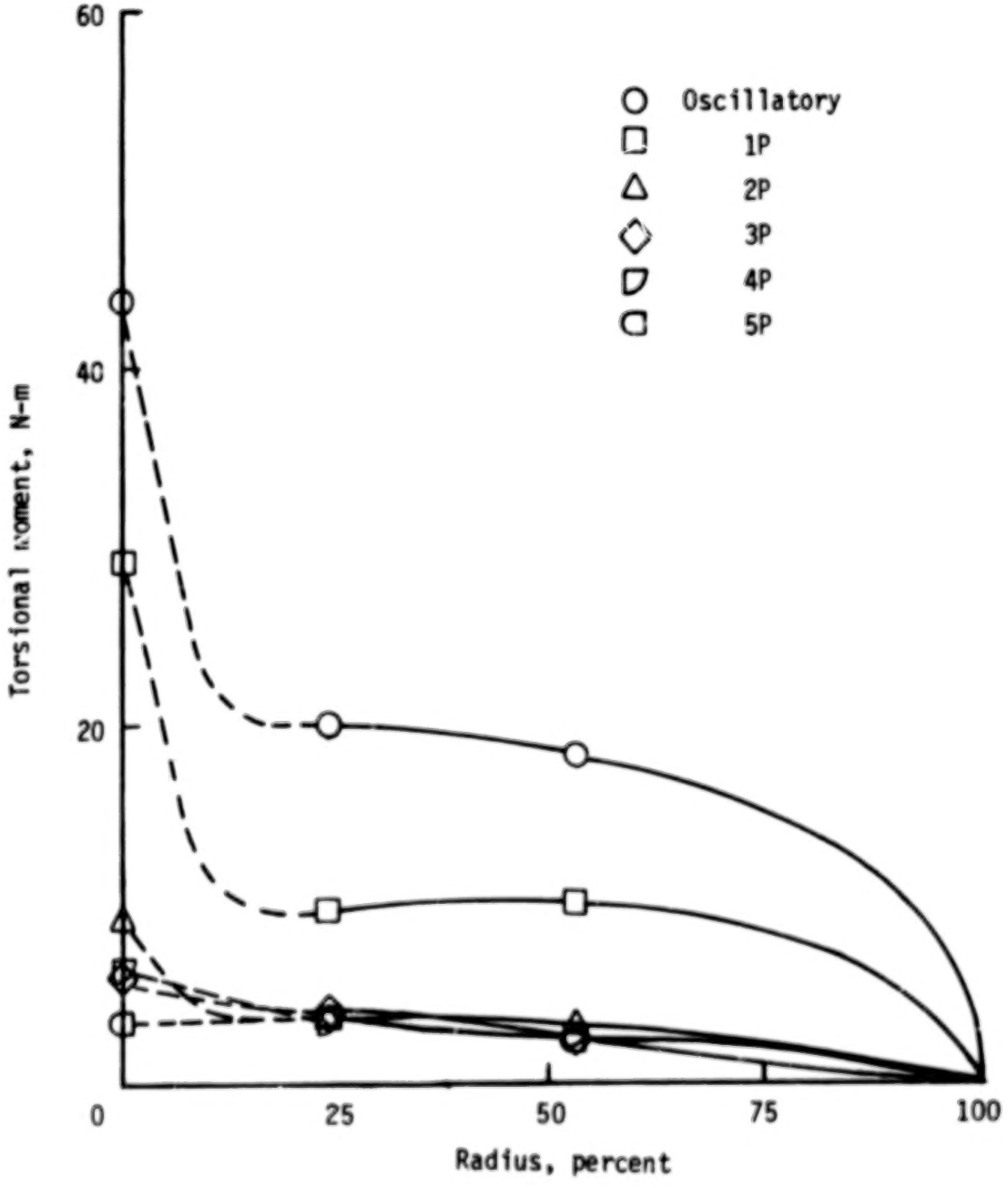

(c) Torsional moment.

Figure 14.- Concluded.

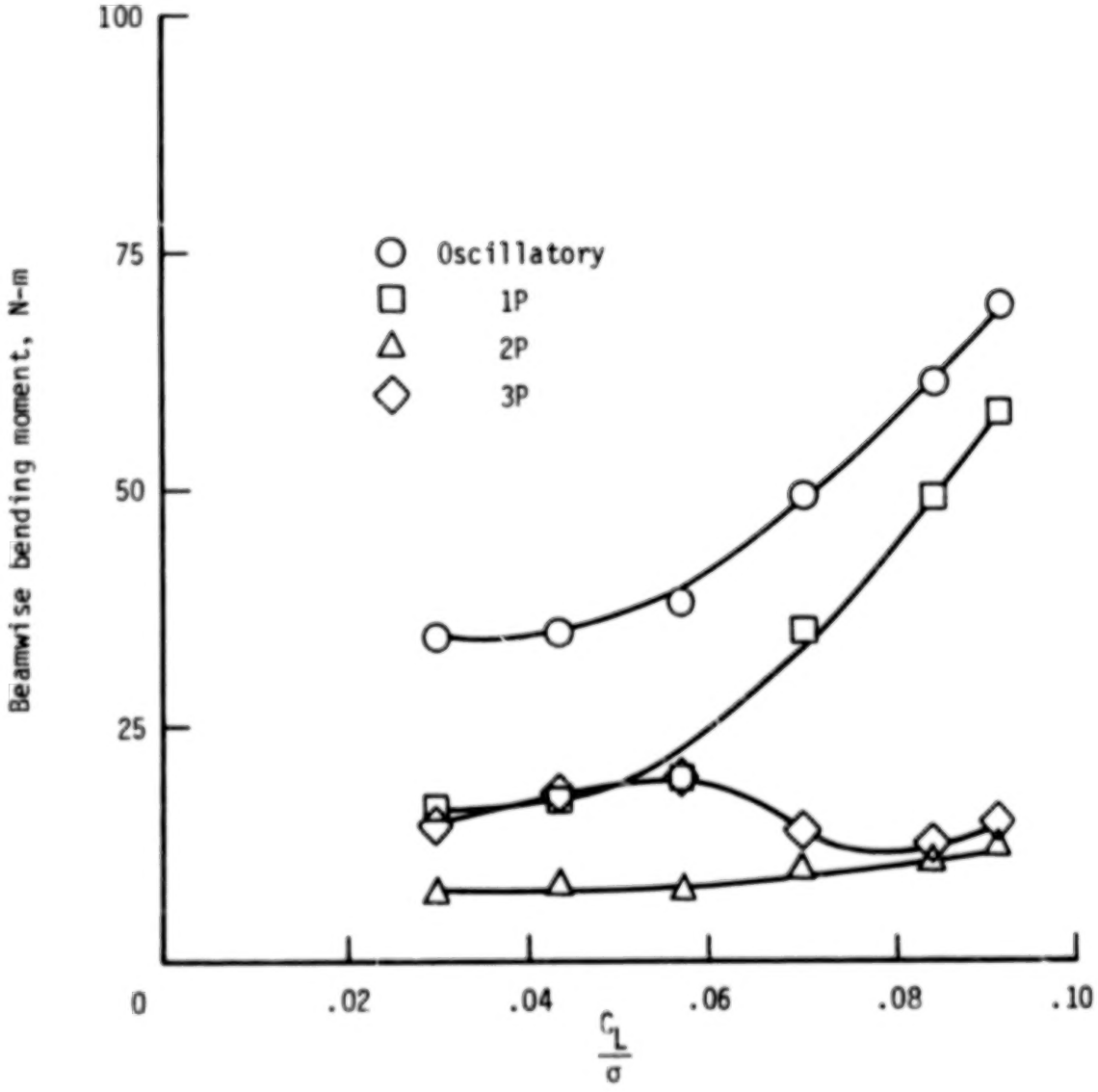

(a) Beamwise bending at x = 0.24.

Figure 15.- Variation of baseline rotor dynamic response with lift. $\mu = 0.25$; $\alpha_s = -2^o$.

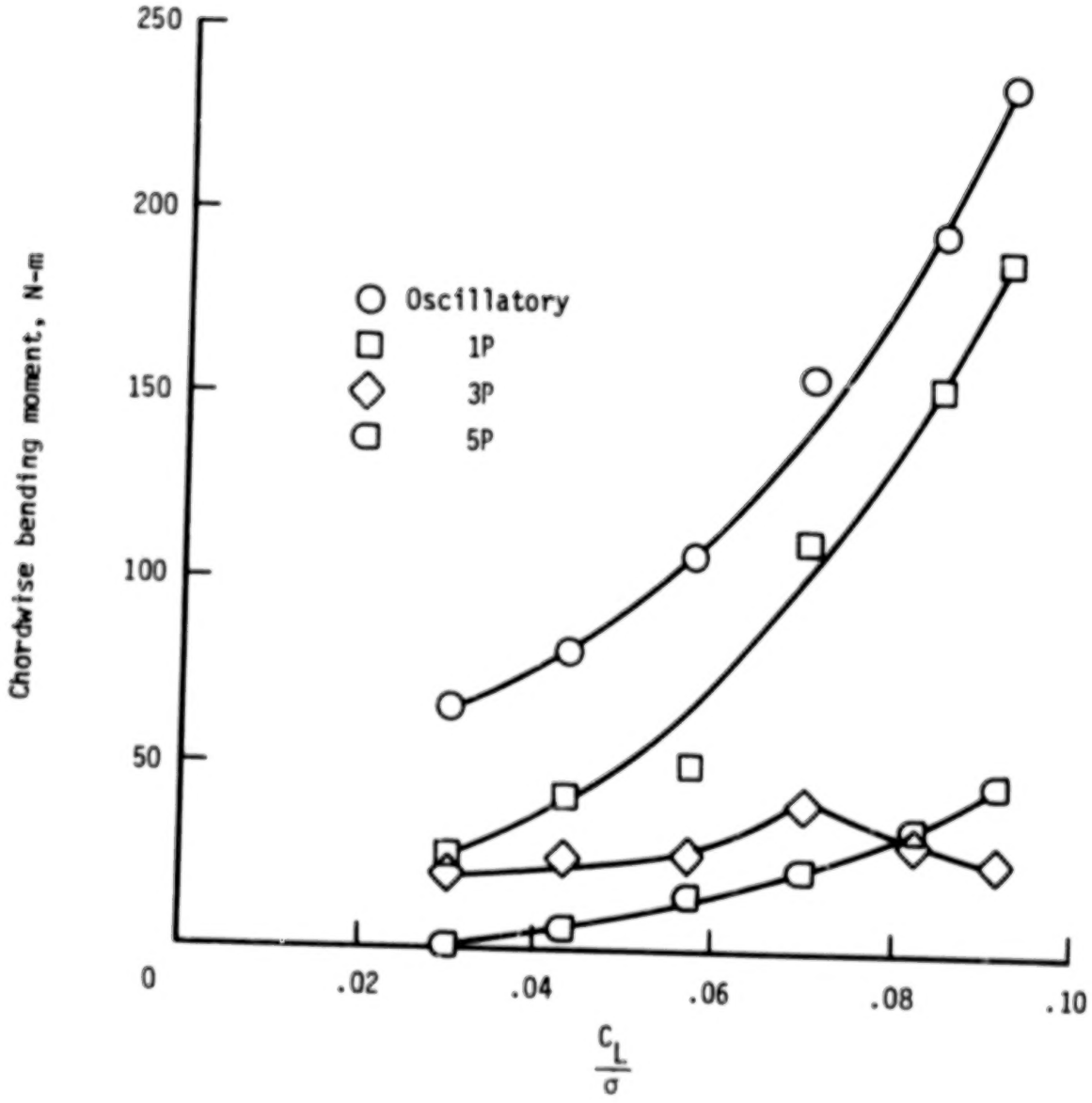

(b) Chordwise bending at $\lambda = 0.24$.

Figure 15.- Continued.

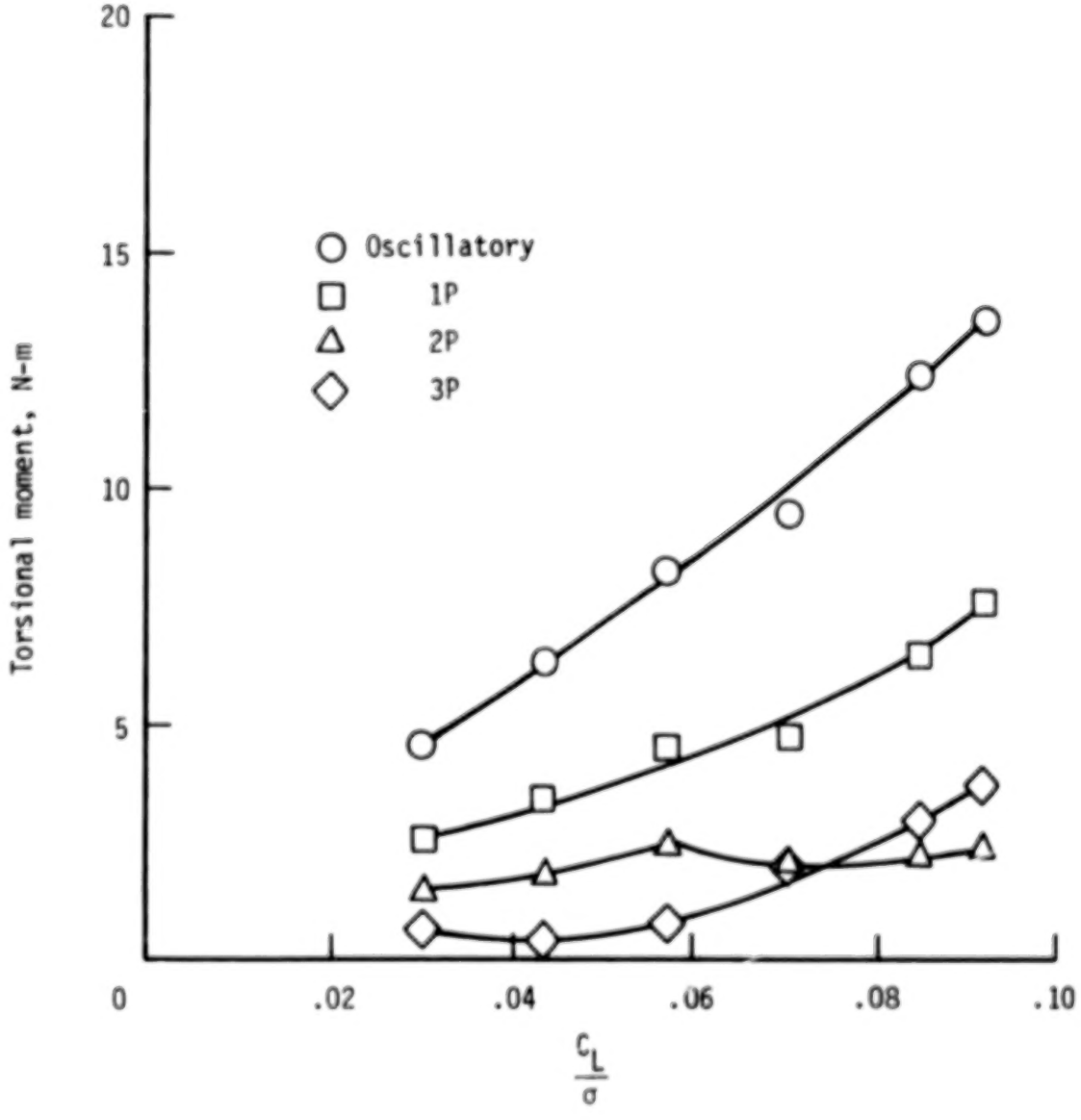

(c) Torsional moment at x = 0.24.

Figure 15.- Continued.

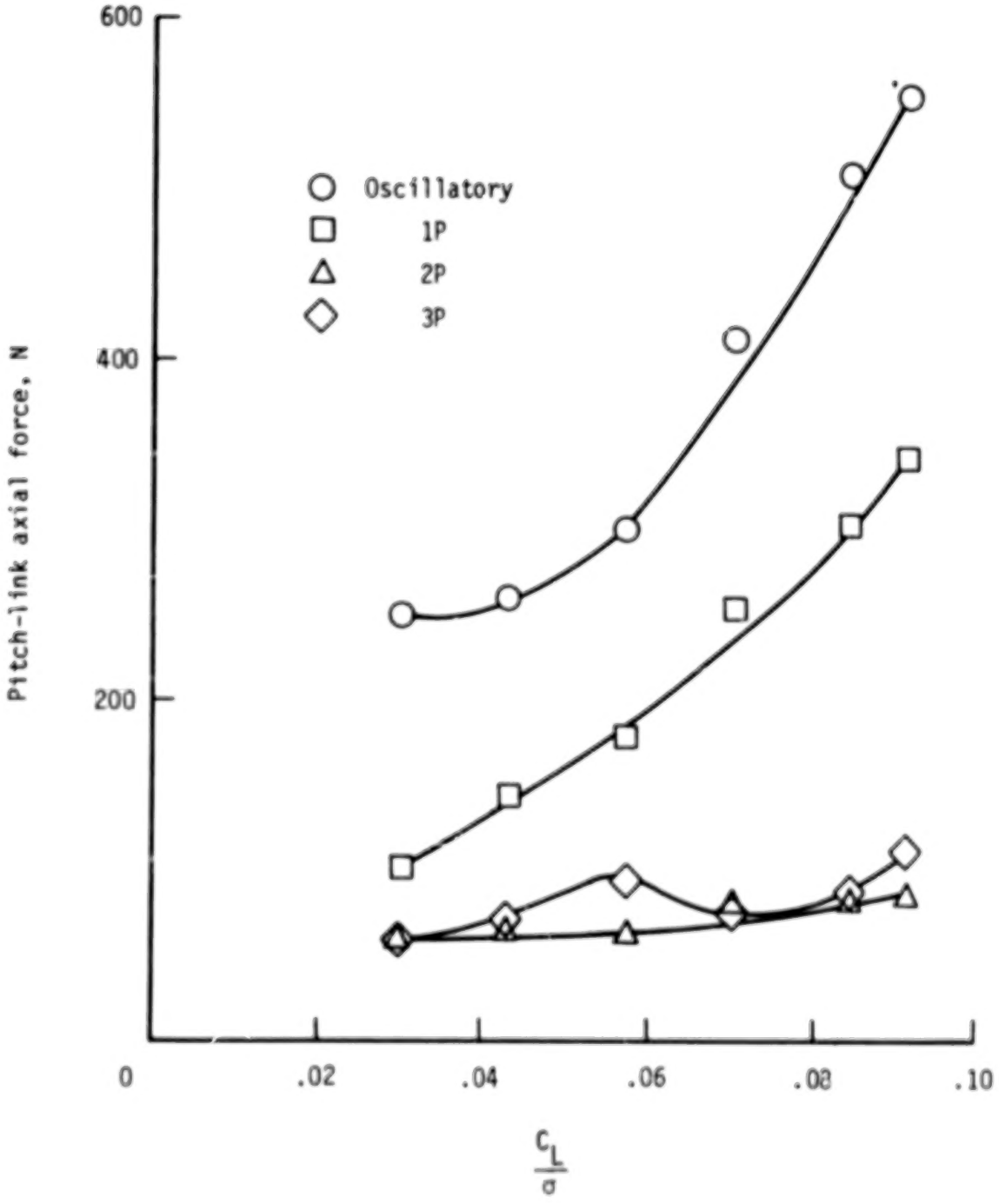

(d) Pitch-link force.

Figure 15.- Concluded.

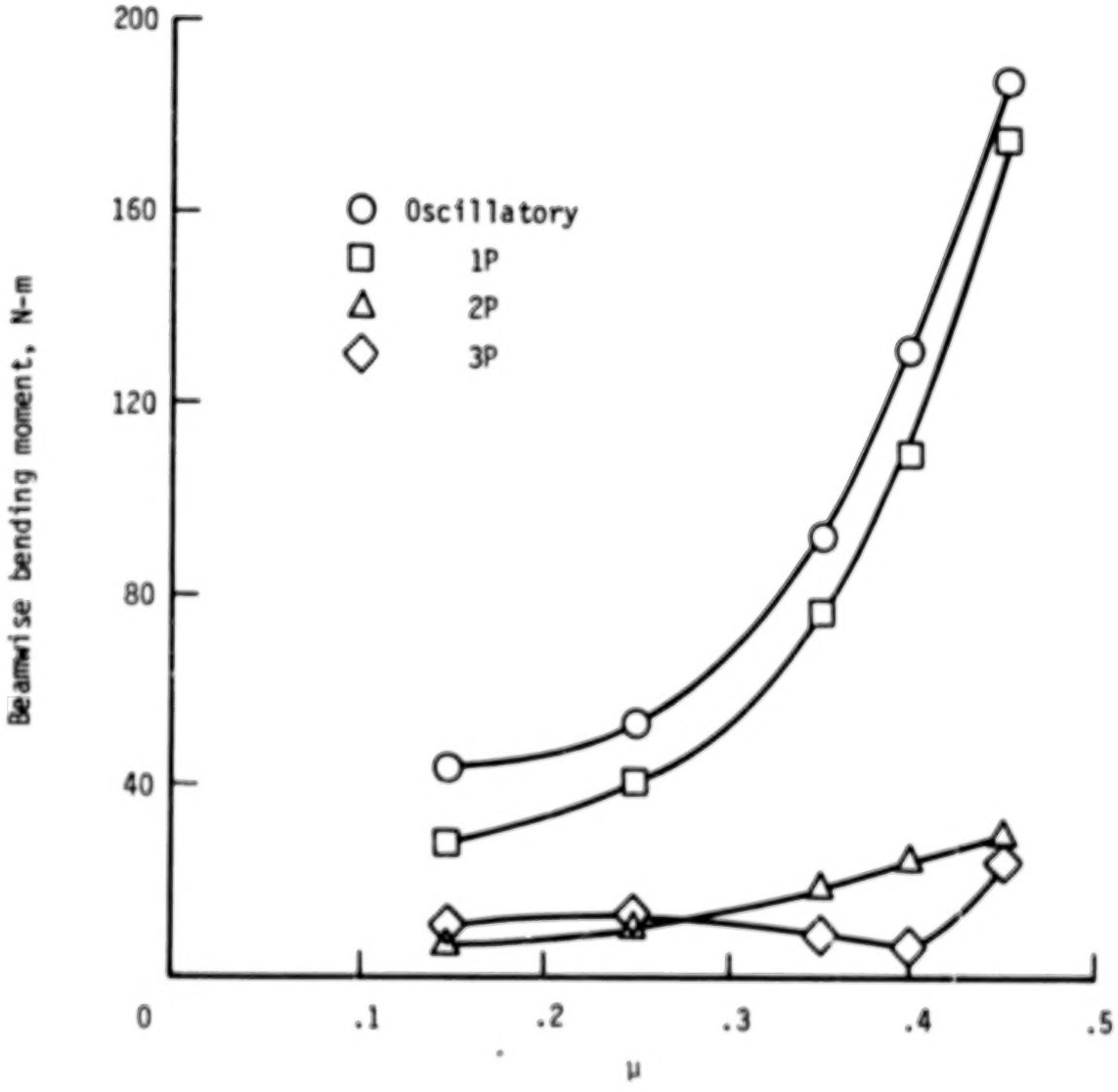

(a) Beamwise bending at x = 0.24.

Figure 16.- Variation of baseline rotor dynamic response with advance ratio. $C_L/\sigma = 0.075$.

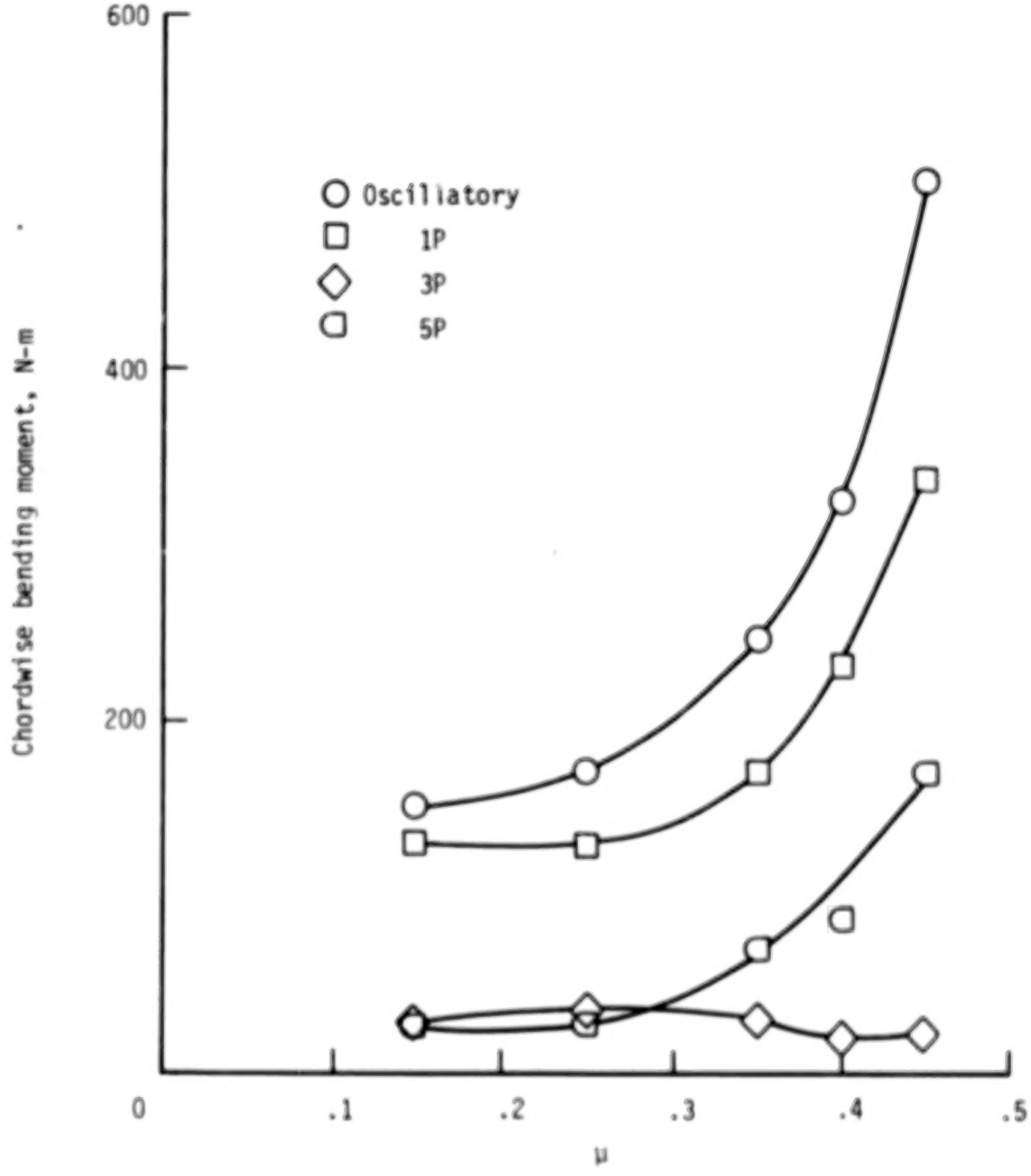

(b) Chordwise bending at x = 0.24.

Figure 16.- Continued.

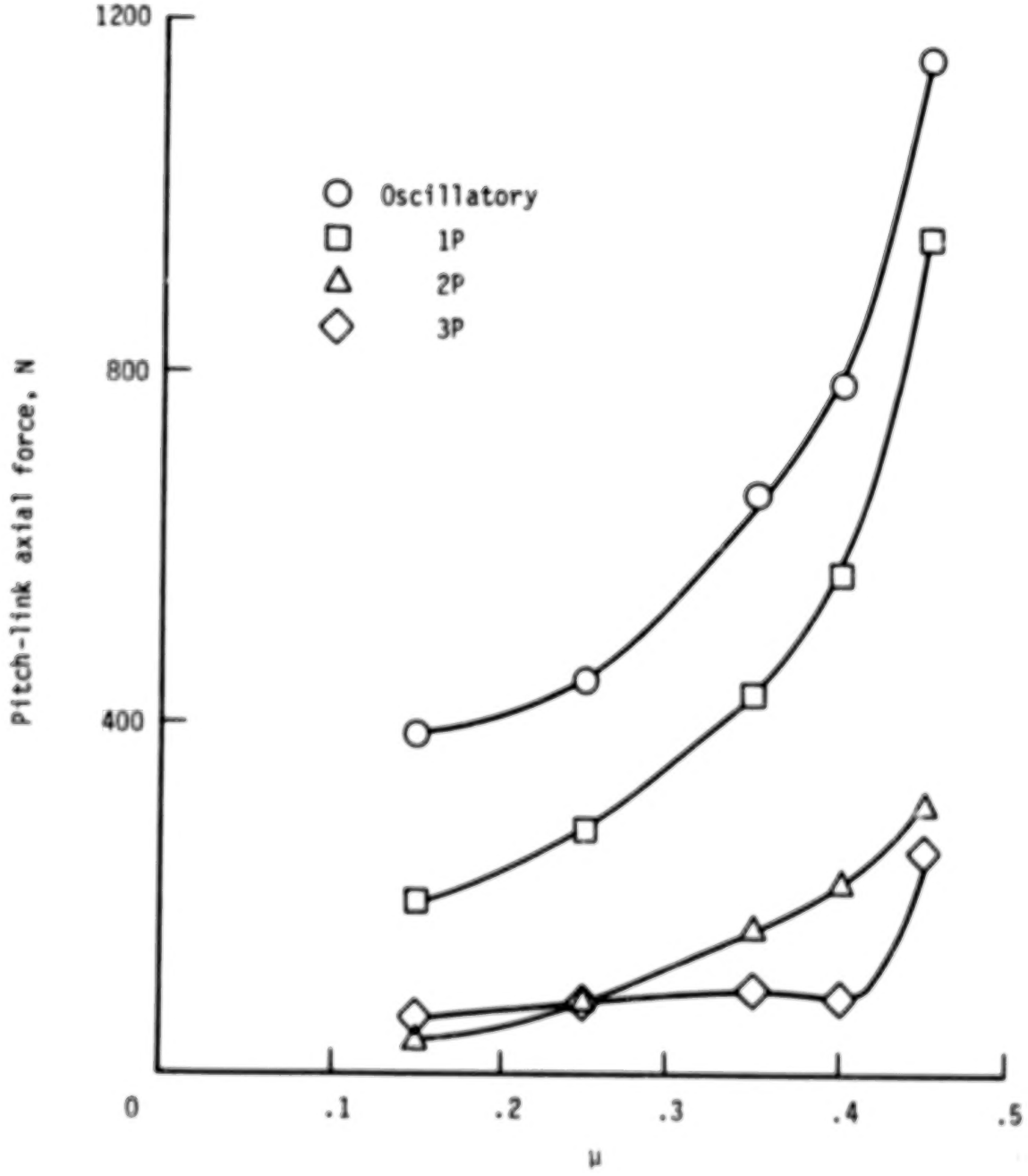

(c) Pitch-link force.

Figure 16.- Concluded.

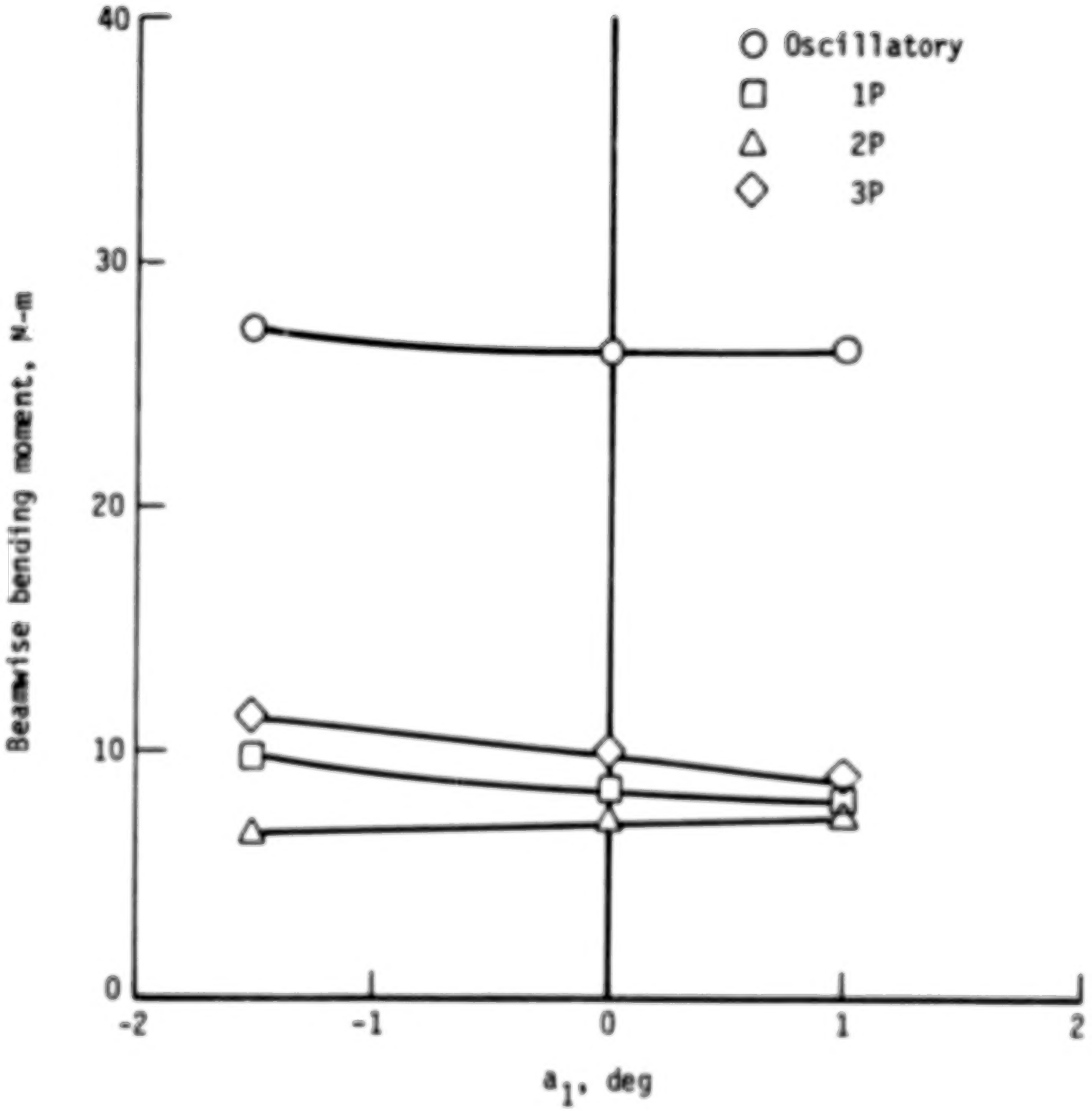

(a) Beamwise bending at x = 0.24.

Figure 17.- Variation of baseline rotor dynamic response with rotor longitudinal flapping. $\mu = 0.15$; $C_L/\sigma = 0.051$; $\alpha_s = -0.4^\circ$.

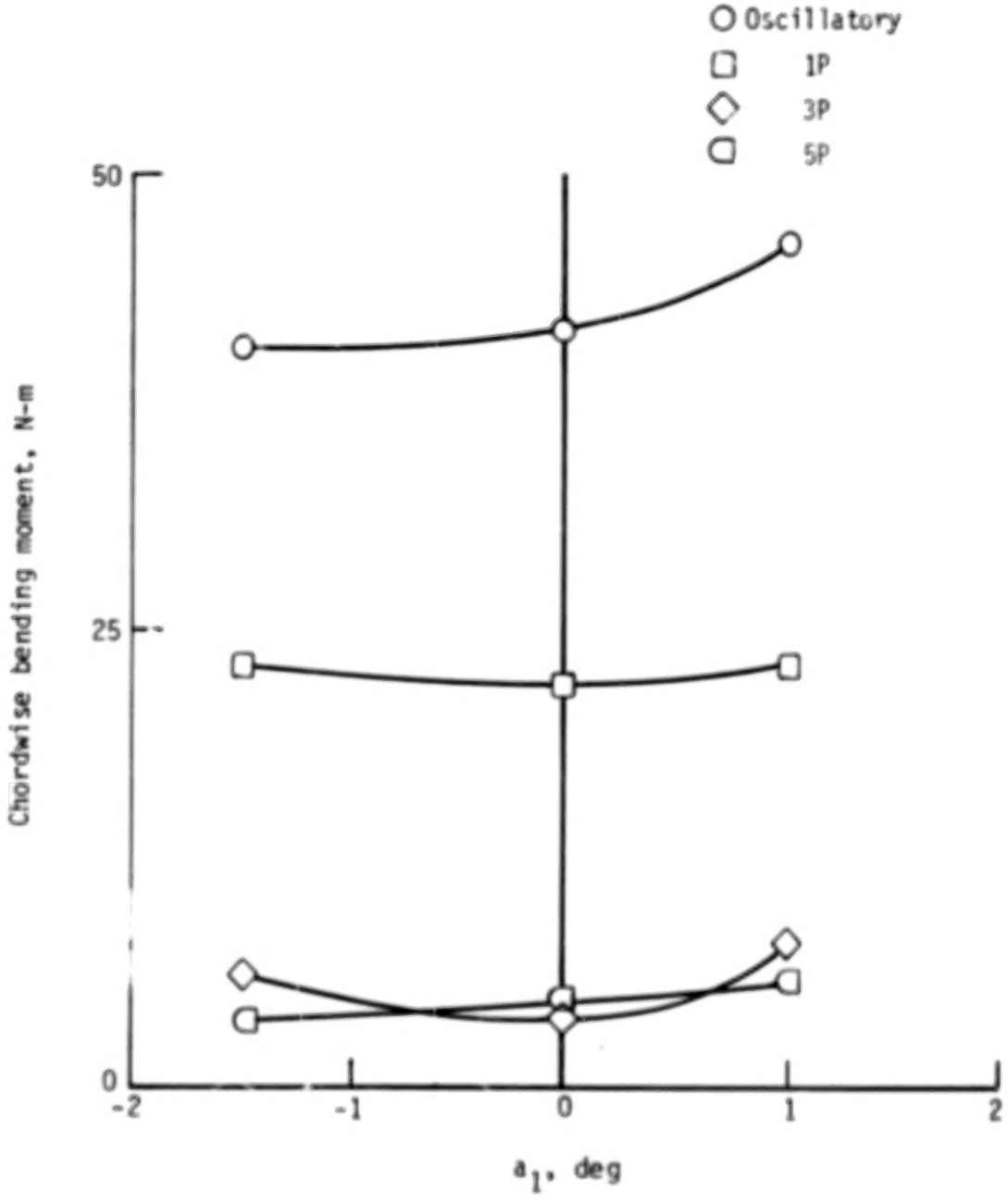

(b) Chordwise bending at x = 0.24.

Figure 17.- Concluded.

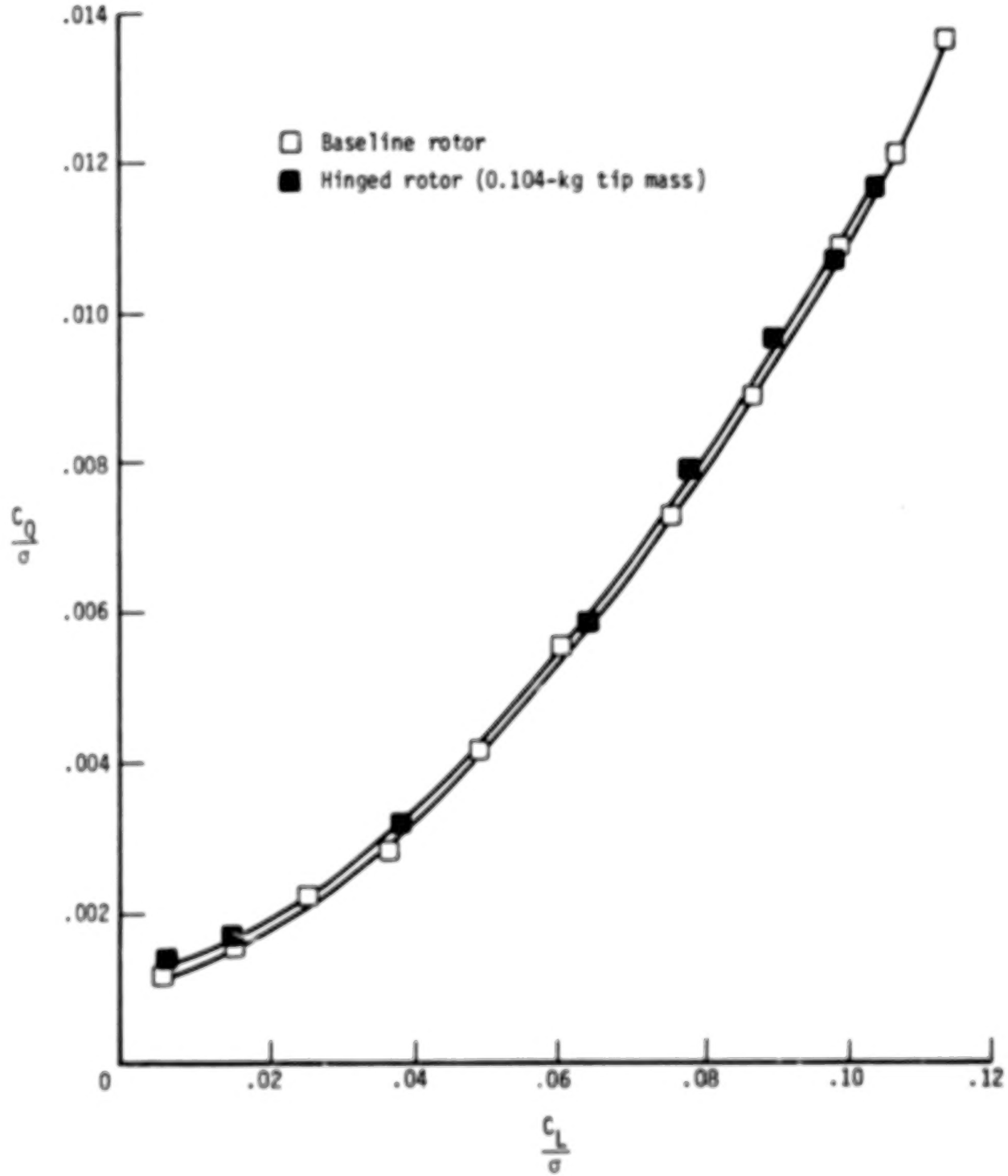

(a) $\mu = 0$; $\alpha_s = 0^o$.

Figure 18.- Variation of rotor torque with lift for baseline and hinged rotors.

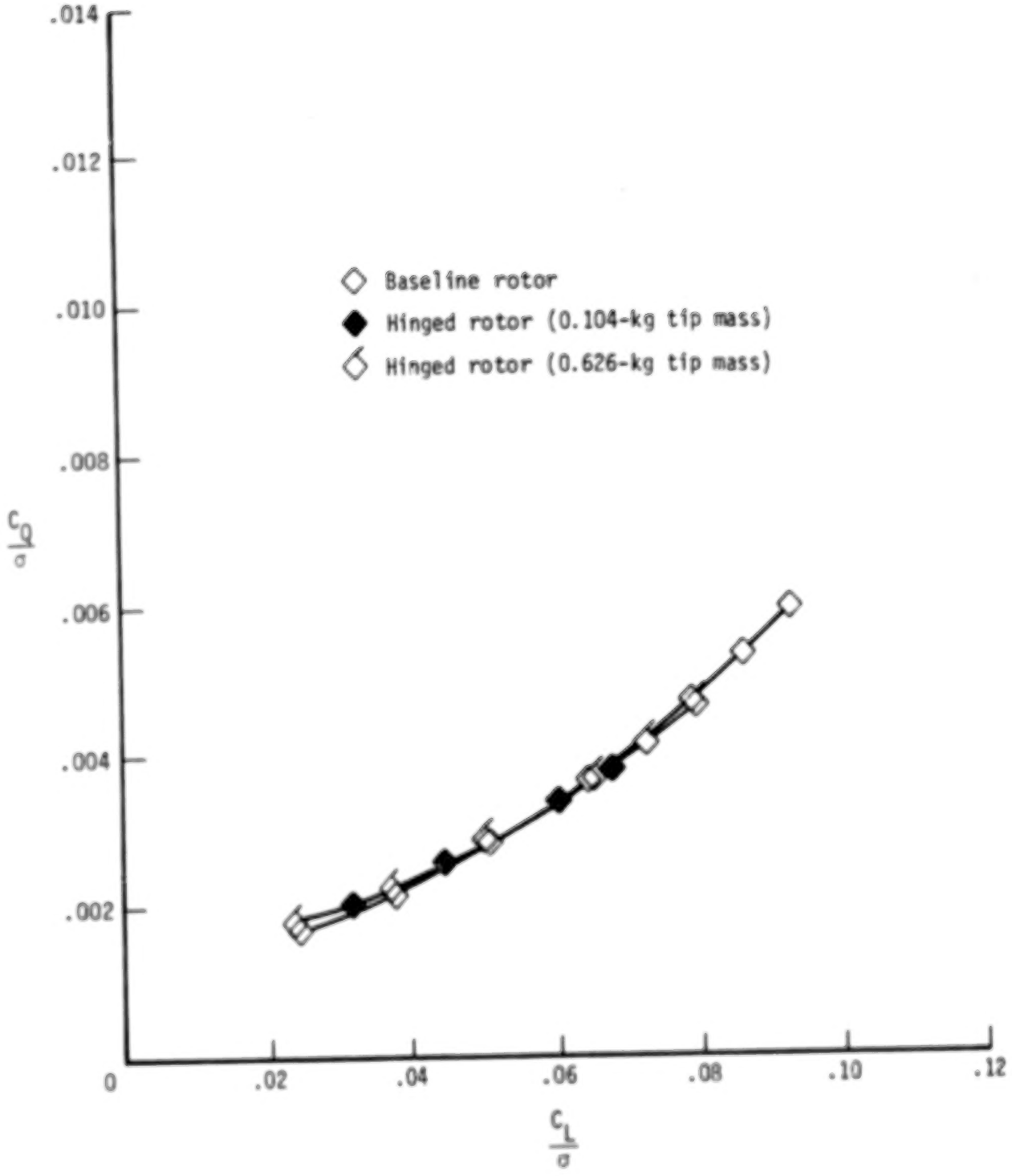

(b) $\mu = 0.25$; $\alpha_s = -4^\circ$.

Figure 18.- Concluded.

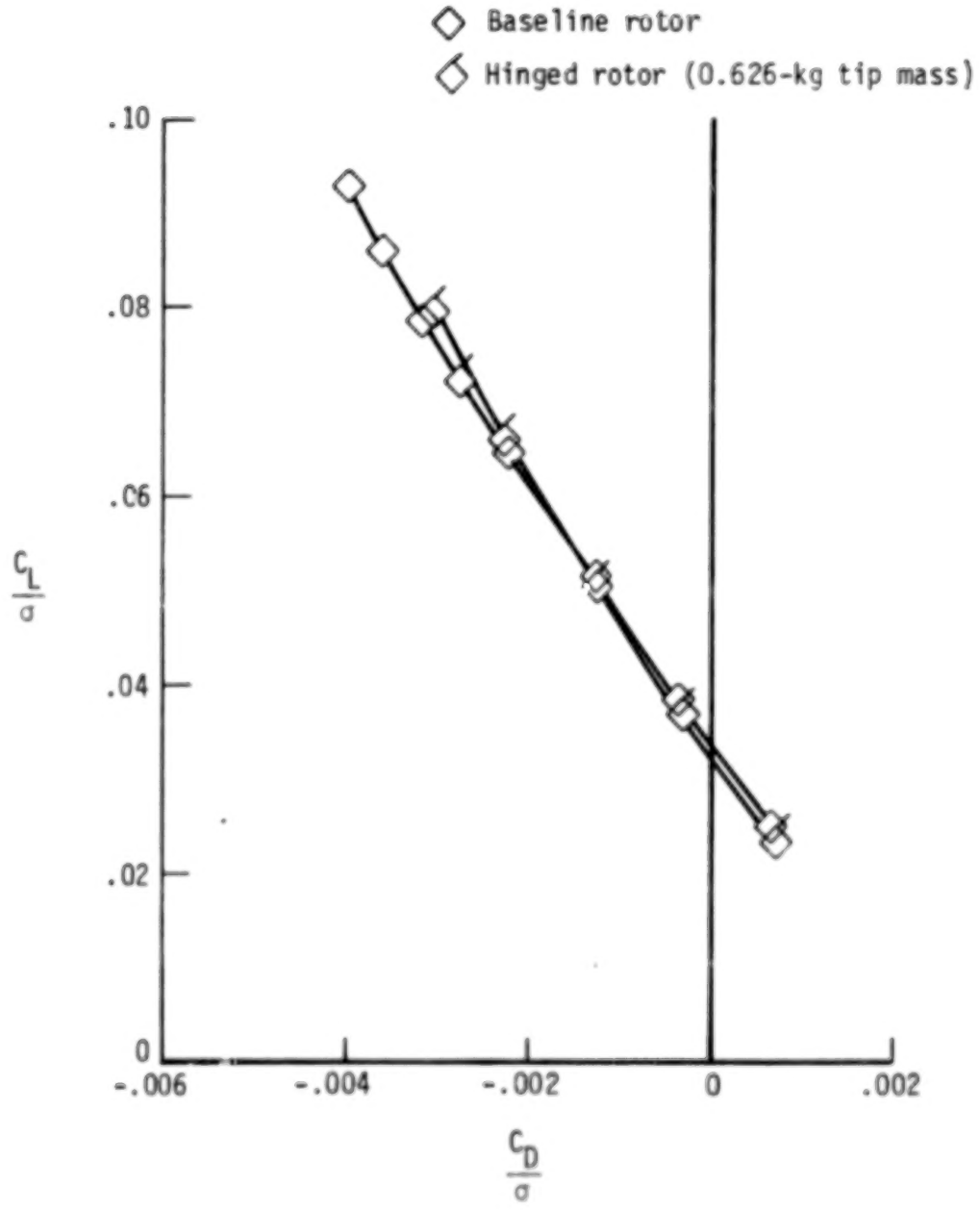

Figure 19.- Variation of rotor lift with drag for baseline and hinged rotors. $\mu = 0.25$; $\alpha_s = -4^\circ$.

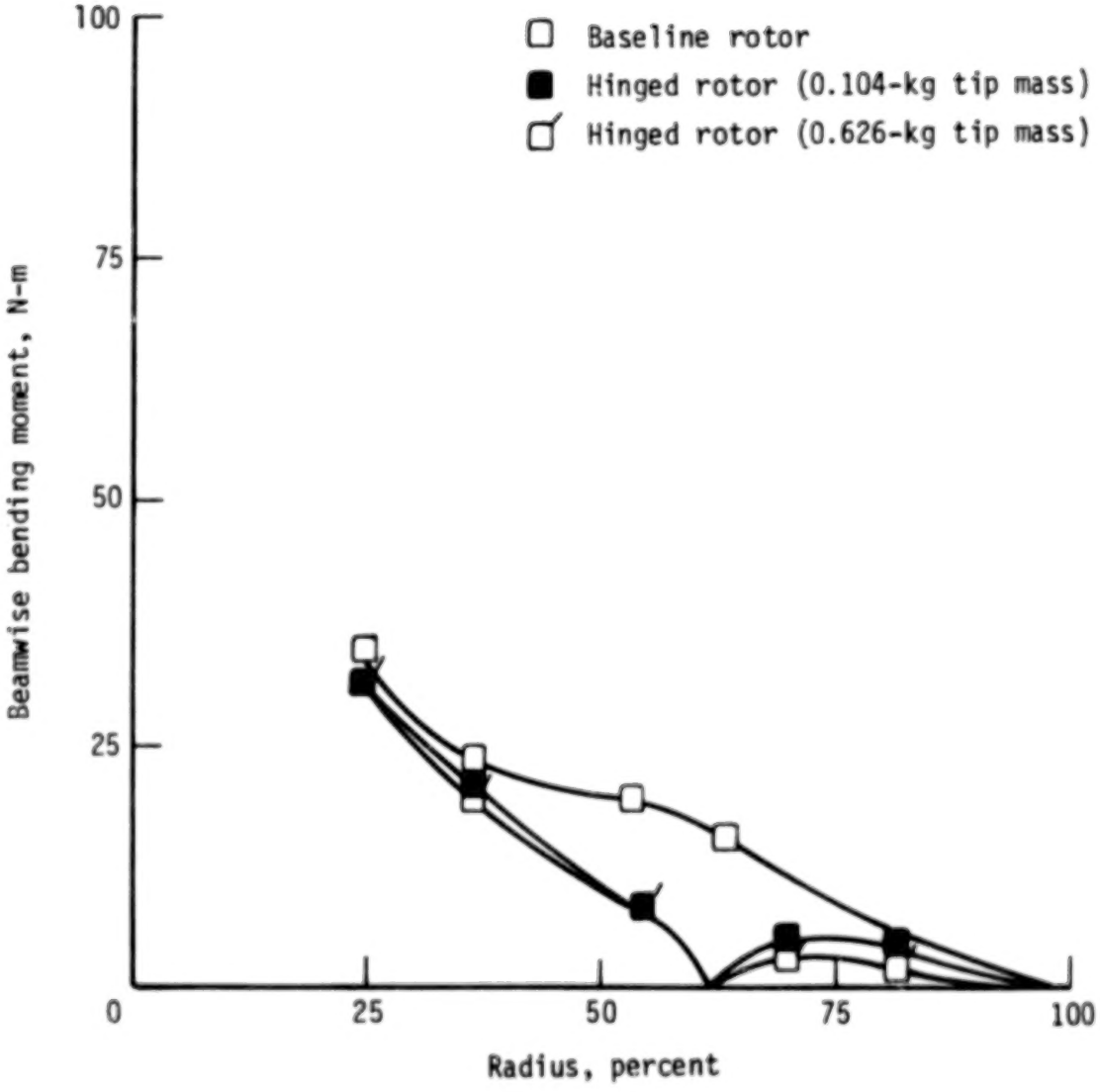

(a) First harmonic moment distribution.

Figure 20.- Beamwise bending moments measured on baseline and hinged rotors. $\mu = 0.25$; $C_L/\sigma = 0.071$; $C_D/\sigma = -0.001$.

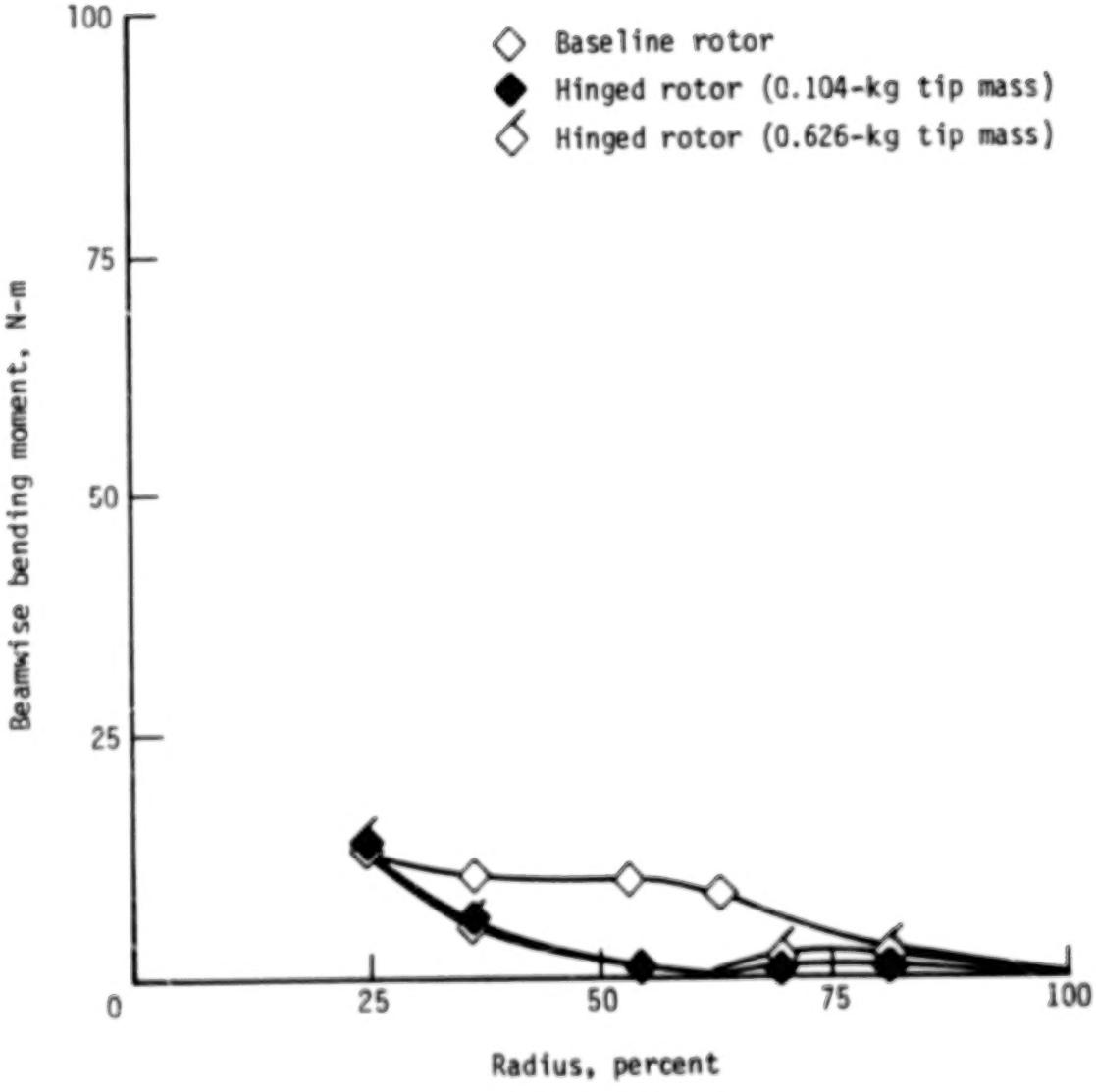

(b) Third harmonic moment distribution.

Figure 20.- Continued.

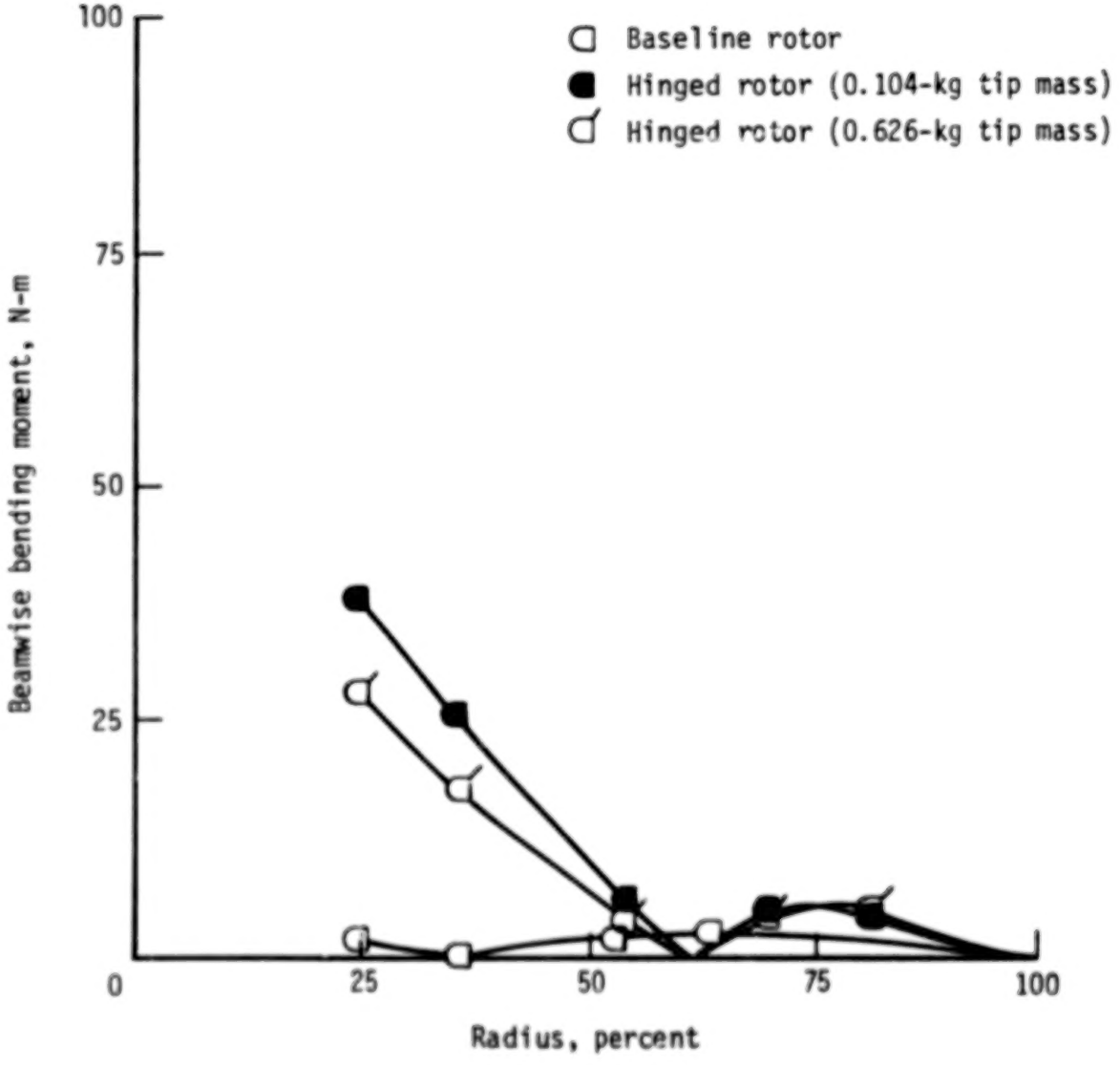

(c) Fifth harmonic moment distribution.

Figure 20.- Continued.

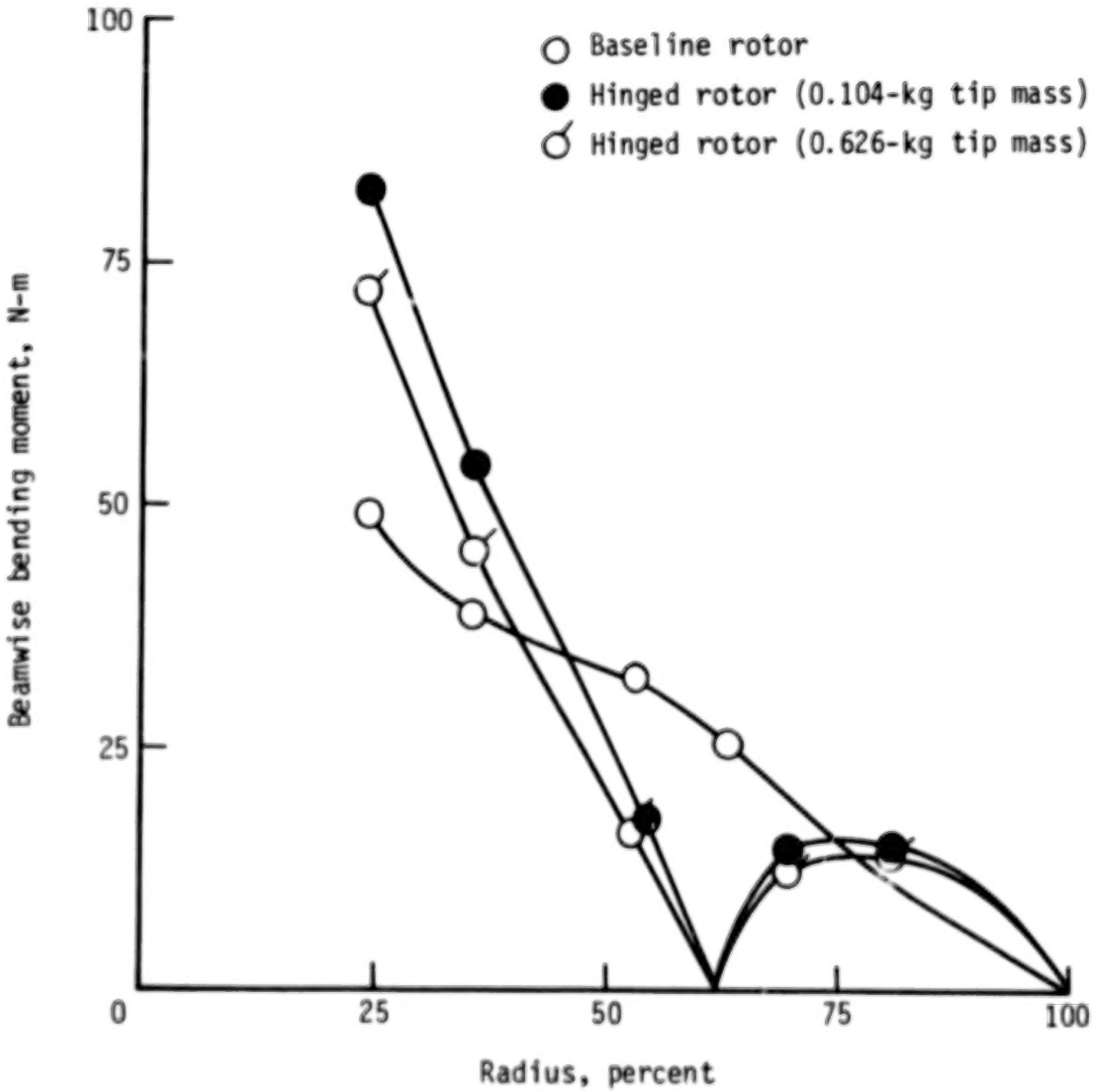

(d) Oscillatory moment distribution.

Figure 20.- Concluded.

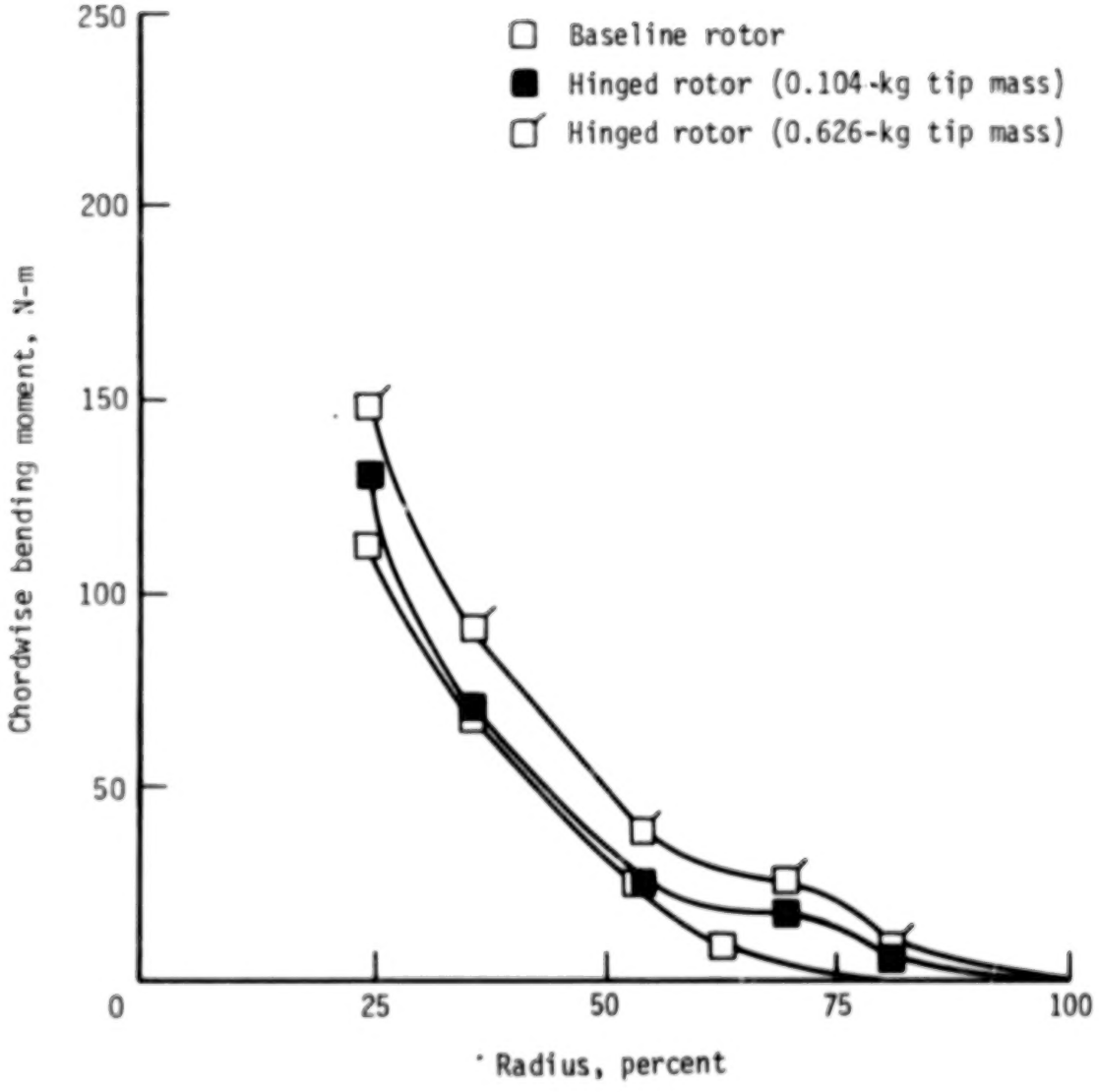

(a) First harmonic moment distribution.

Figure 21.- Chordwise bending moments measured on baseline and hinged rotors. $\mu = 0.25$; $C_L/\sigma = 0.071$; $C_D/\sigma = -0.001$.

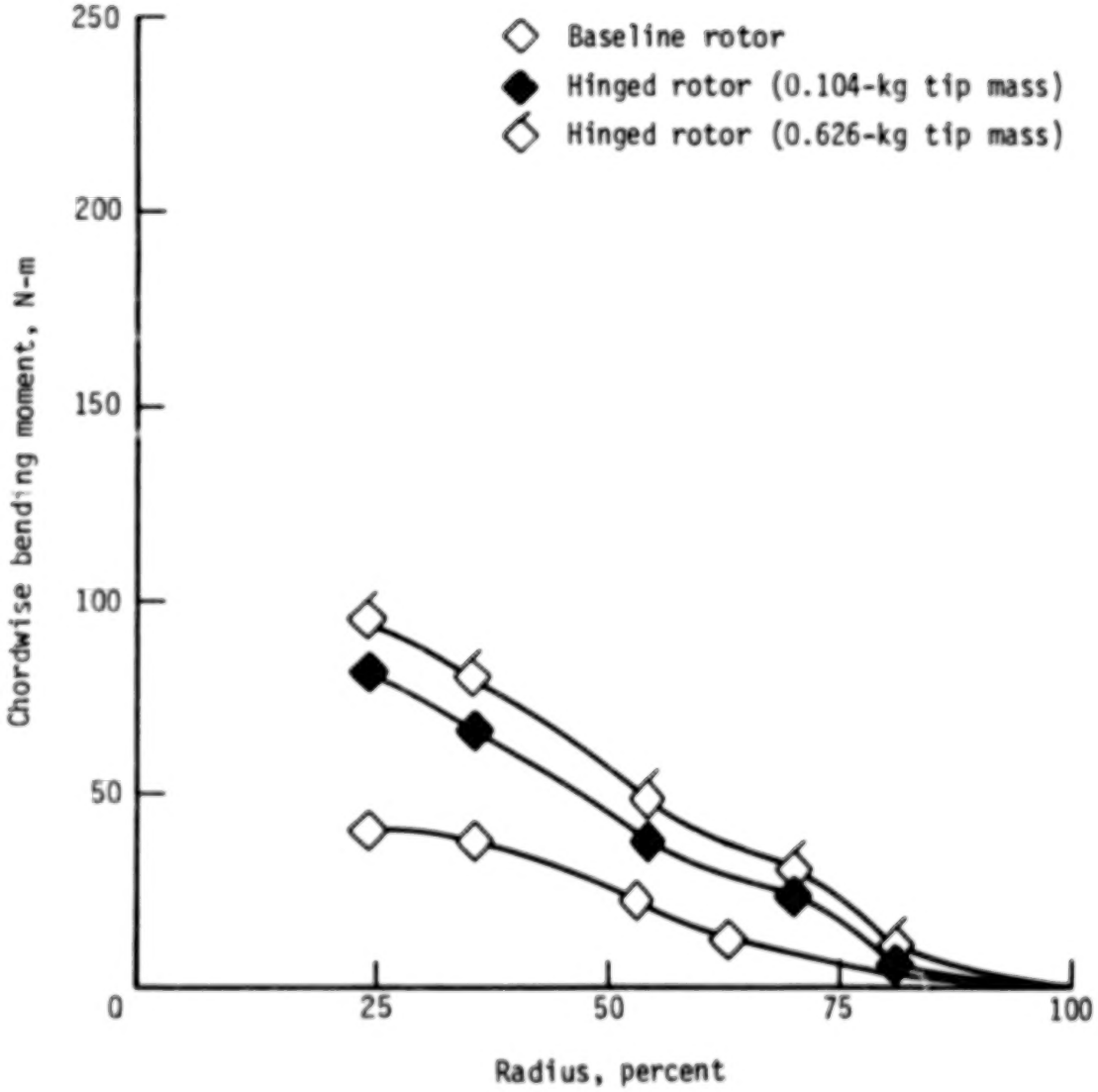

(b) Third harmonic moment distribution.

Figure 21.- Continued.

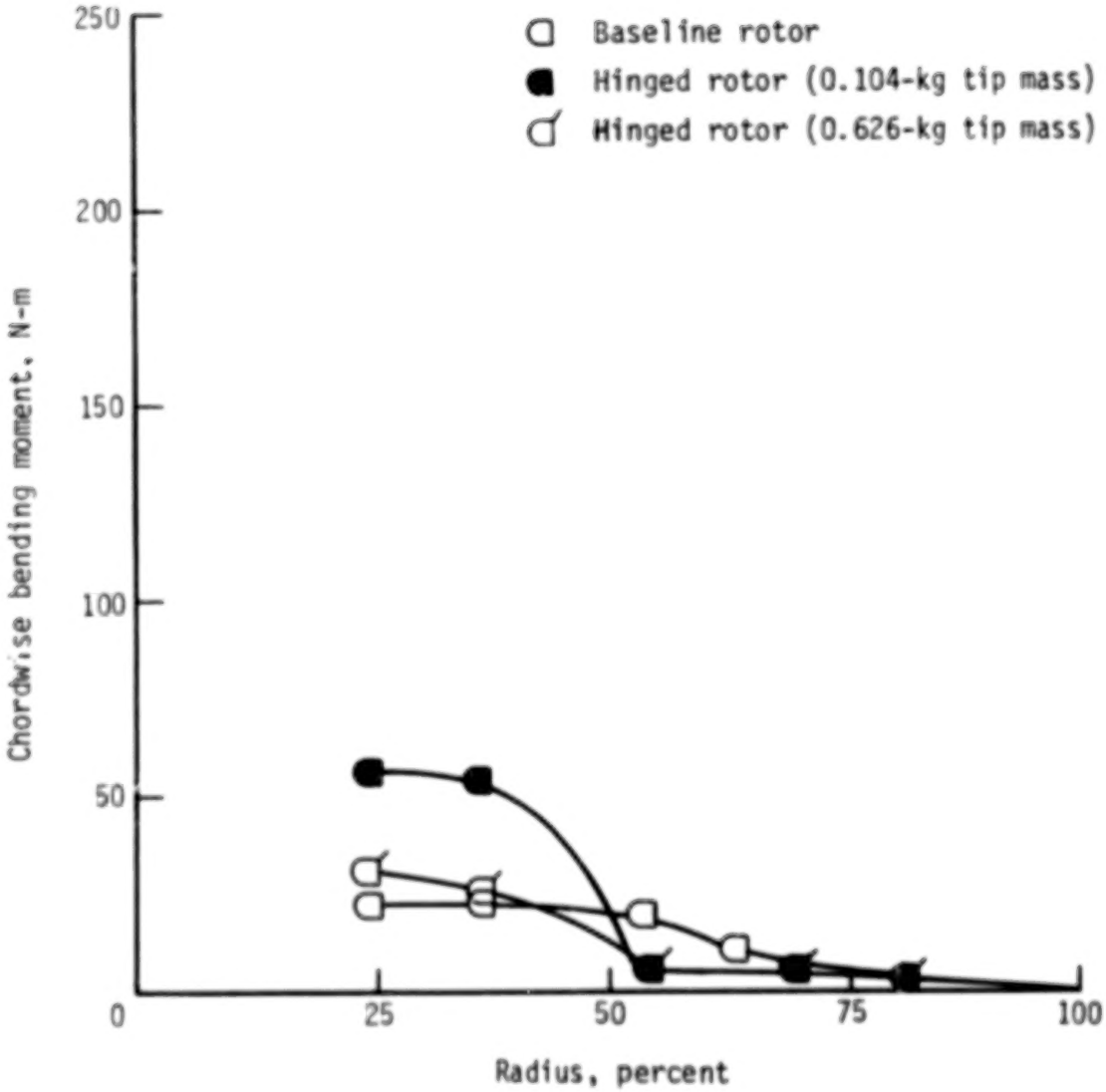

(c) Fifth harmonic moment distribution.

Figure 21.- Continued.

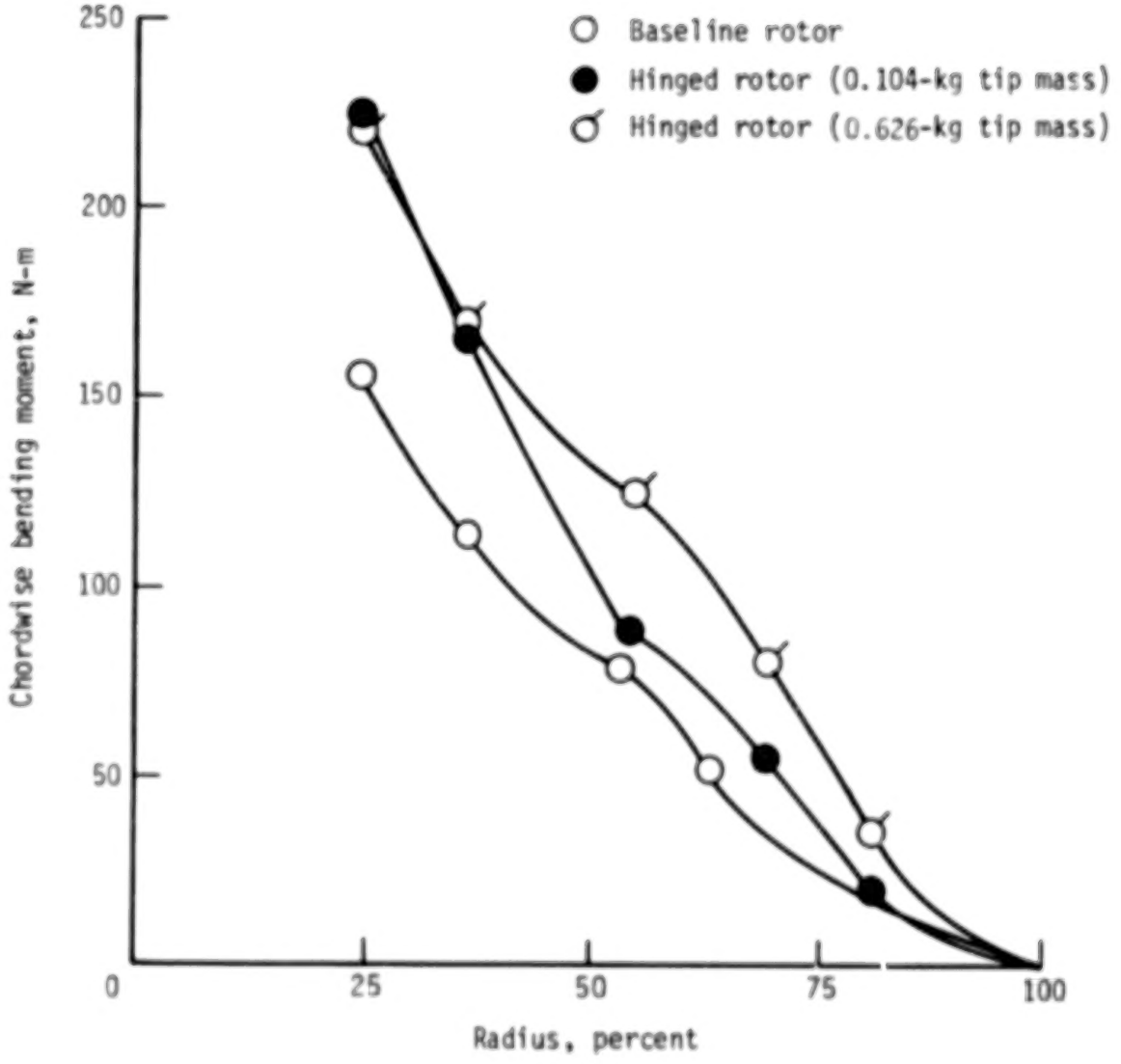

(d) Oscillatory moment distribution.

Figure 21.- Concluded.

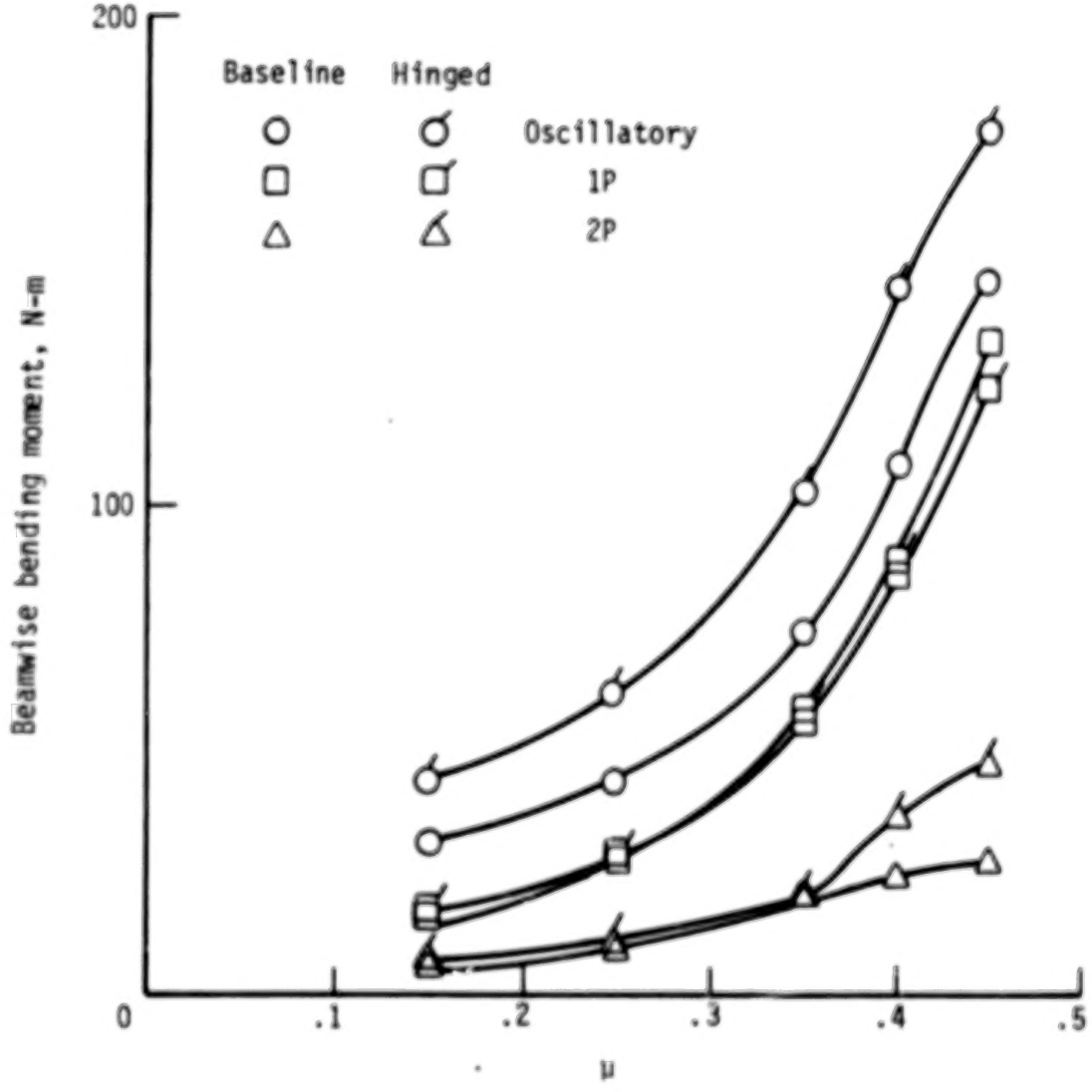

(a) Beamwise bending at x = 0.24.

Figure 22.- Variation of dynamic response with advance ratio for baseline and hinged (0.626-kg tip mass) rotor. $C_L/\sigma = 0.060$.

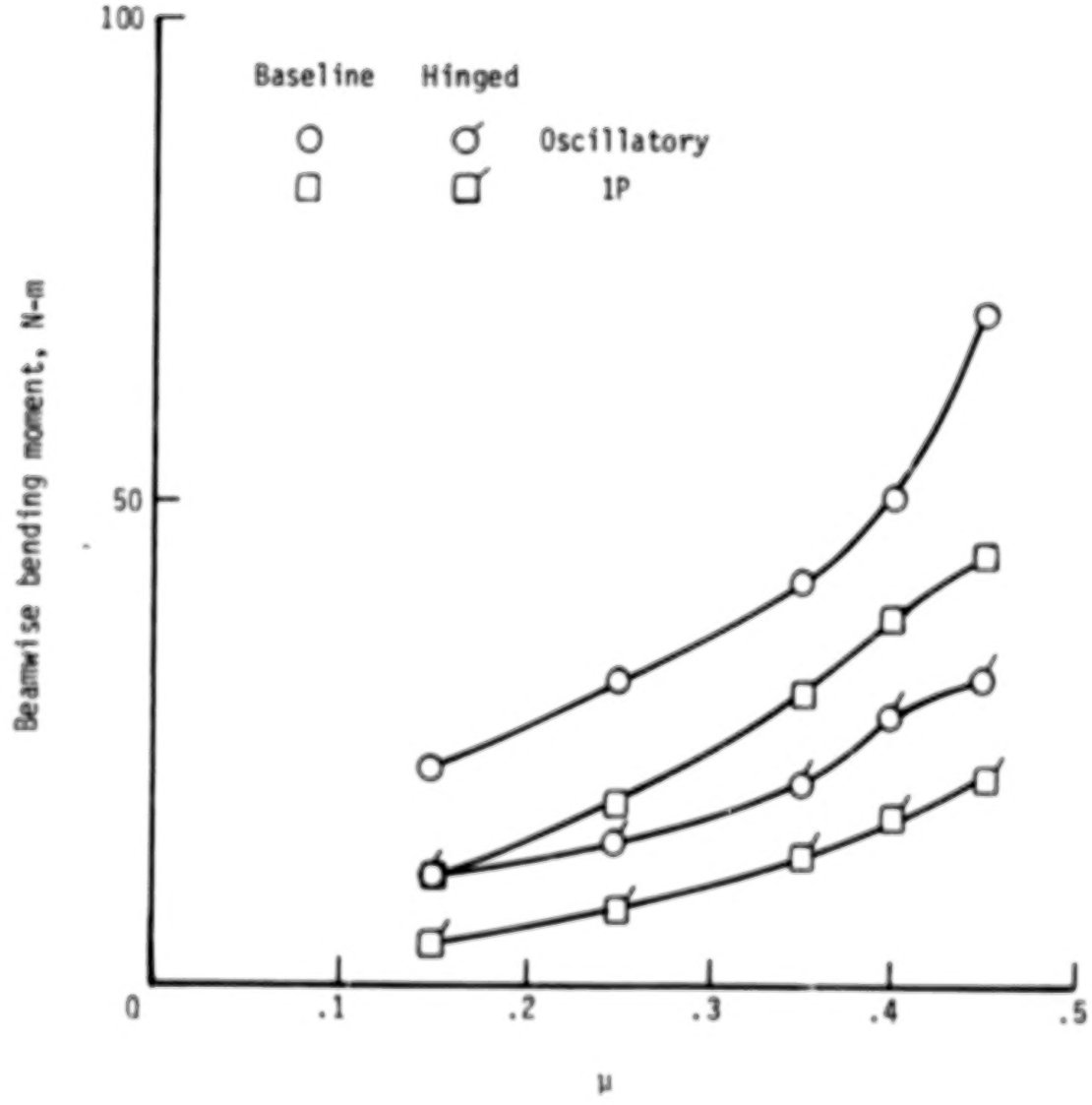

(b) Beamwise bending at x = 0.54.

Figure 22.- Continued.

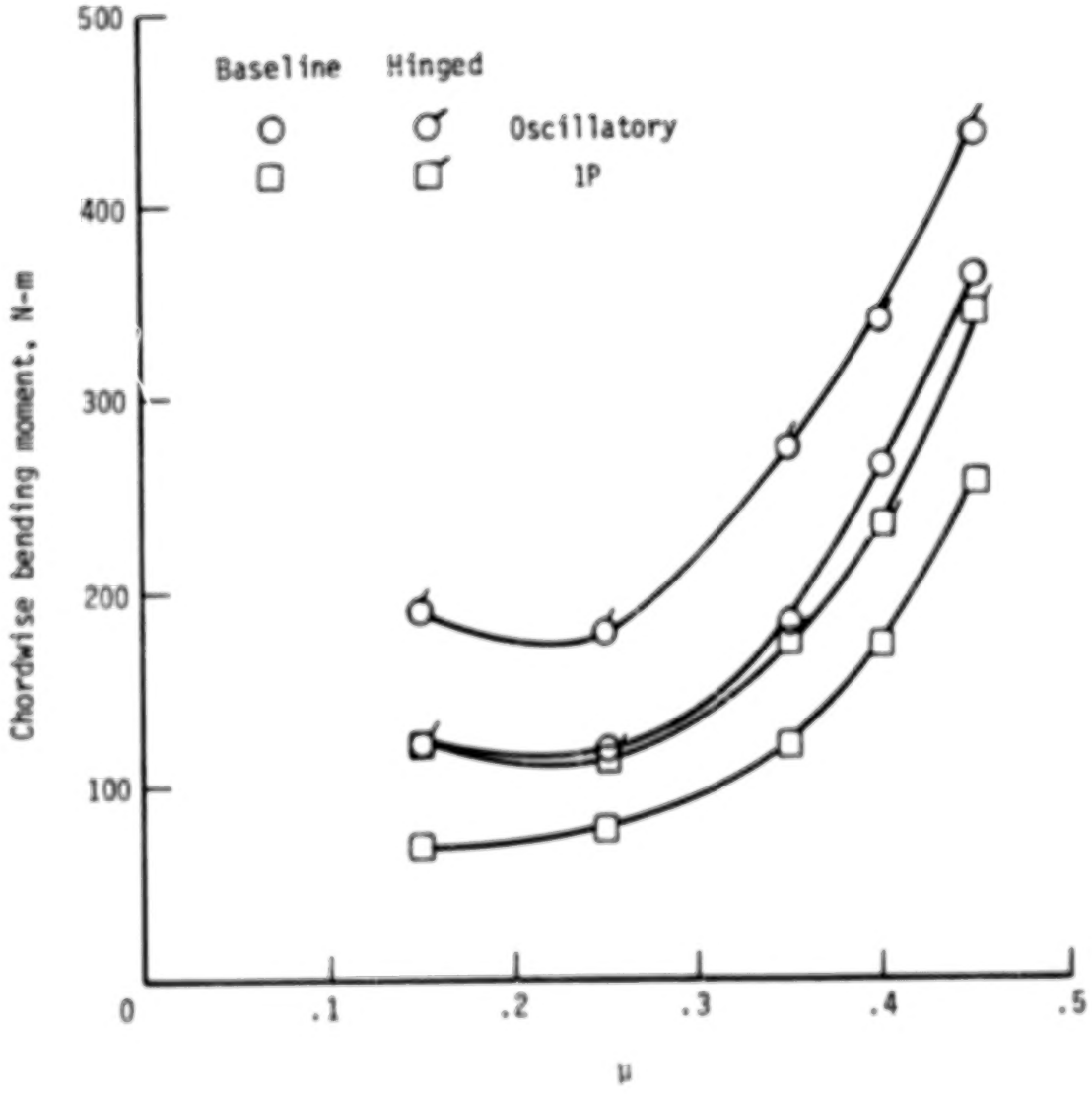

(c) Chordwise bending at x = 0.24.

Figure 22.- Continued.

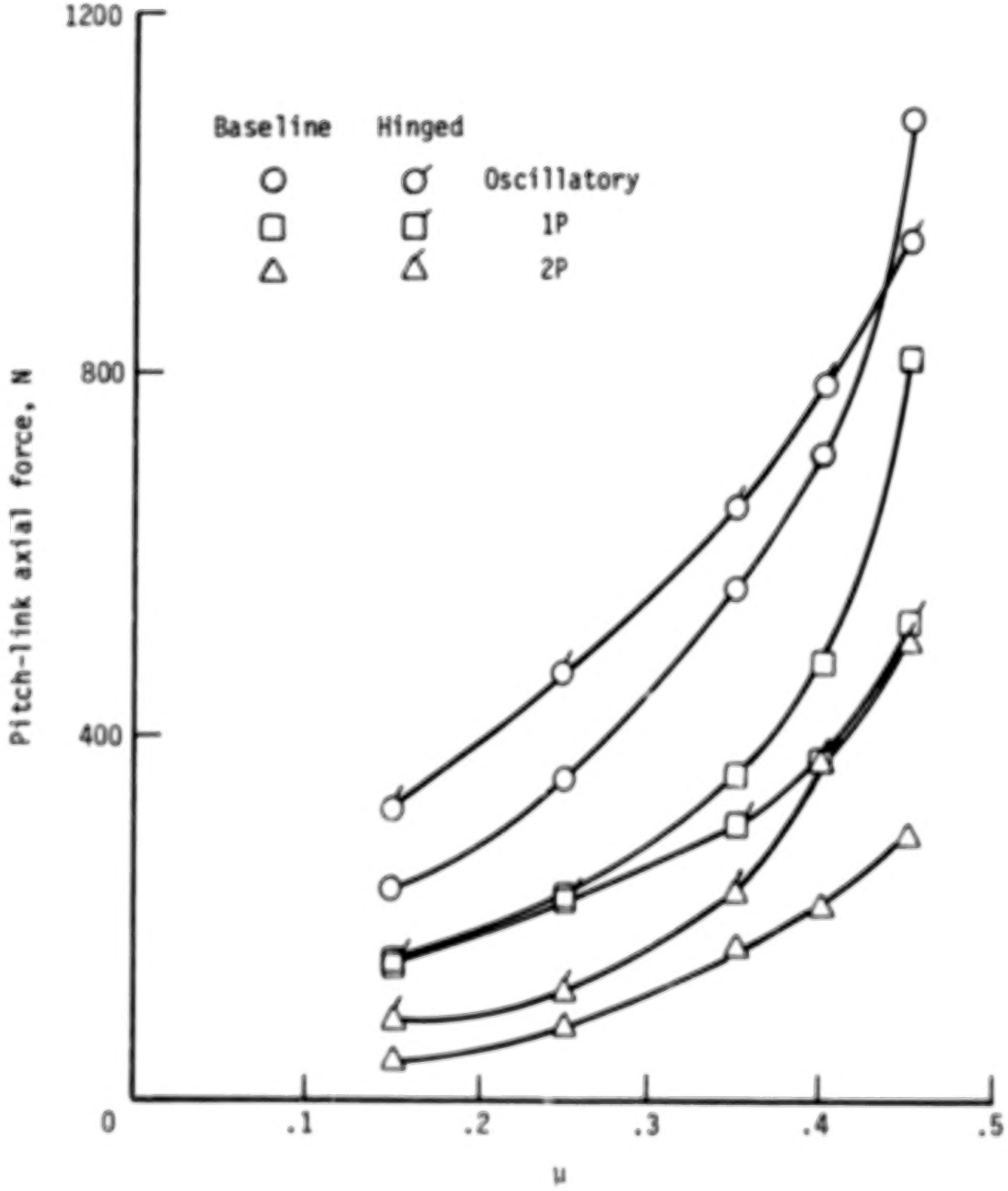

(d) Pitch-link force.

Figure 22.- Concluded.

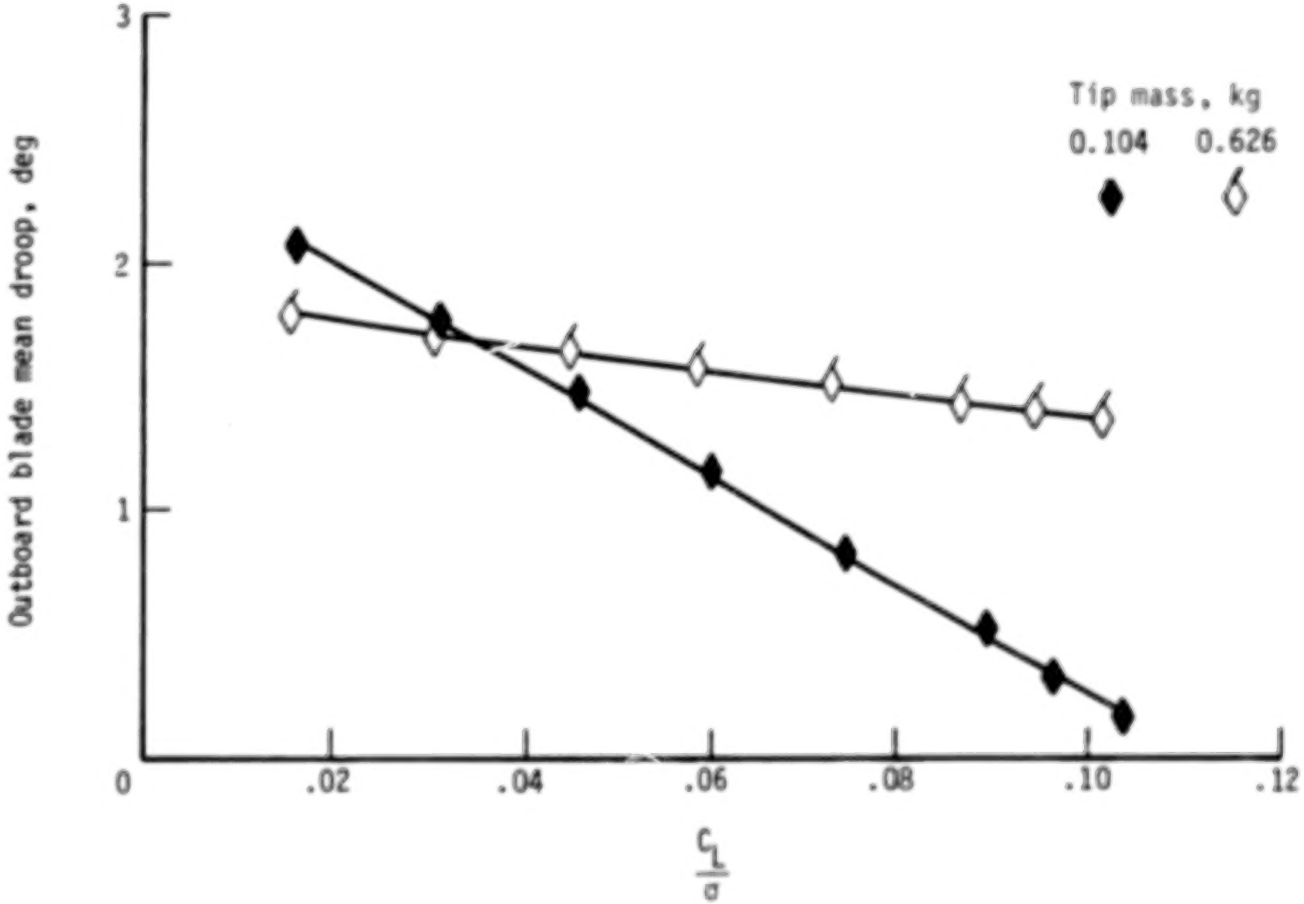

Figure 23.- Variation of outboard blade mean droop angle with lift.
$\mu = 0.15$; $\alpha_s = -2^{\circ}$.

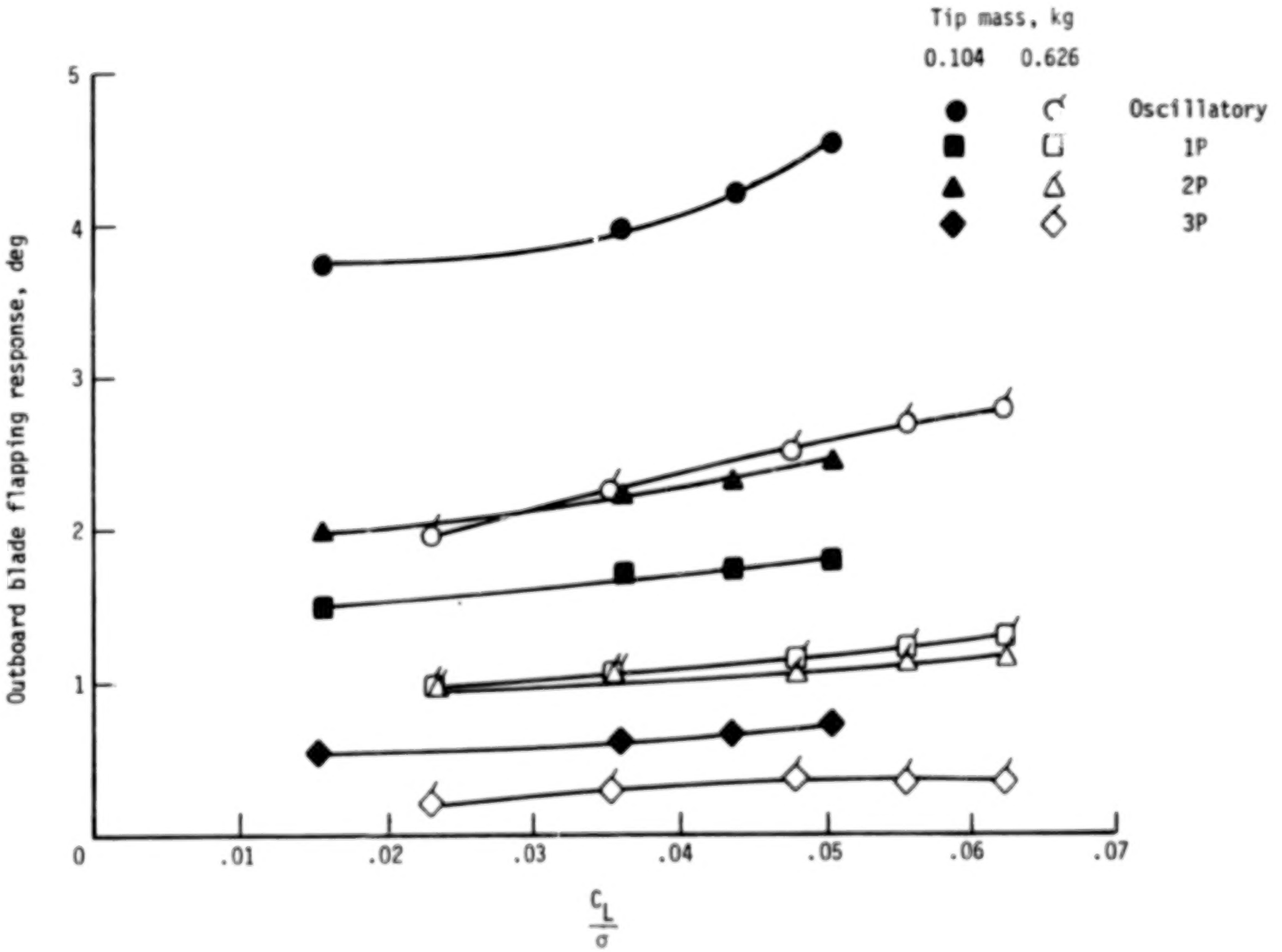

Figure 24.- Variation of outboard blade flapping response with lift.
$\mu = 0.35$; $\alpha_s = -6^\circ$.

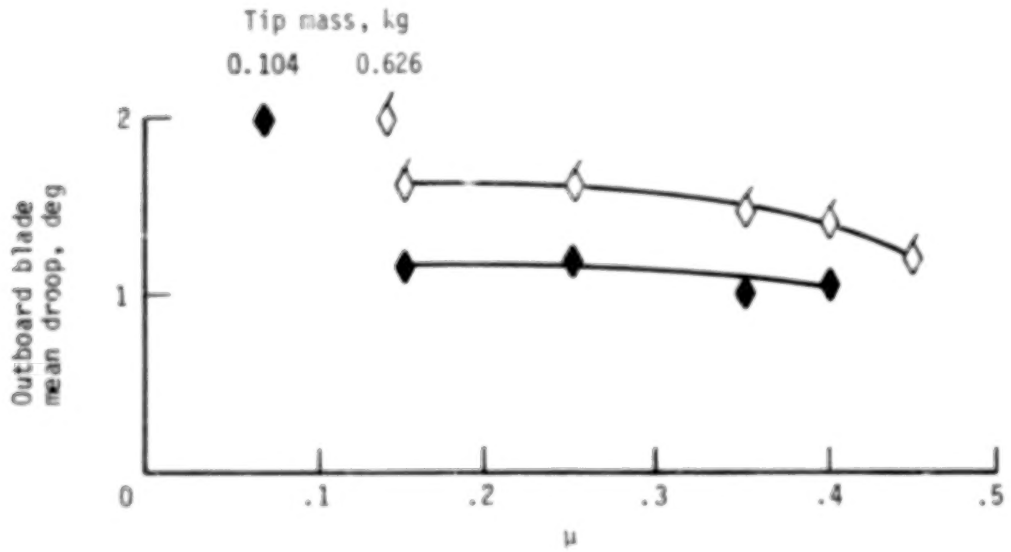

(a) Mean droop angle.

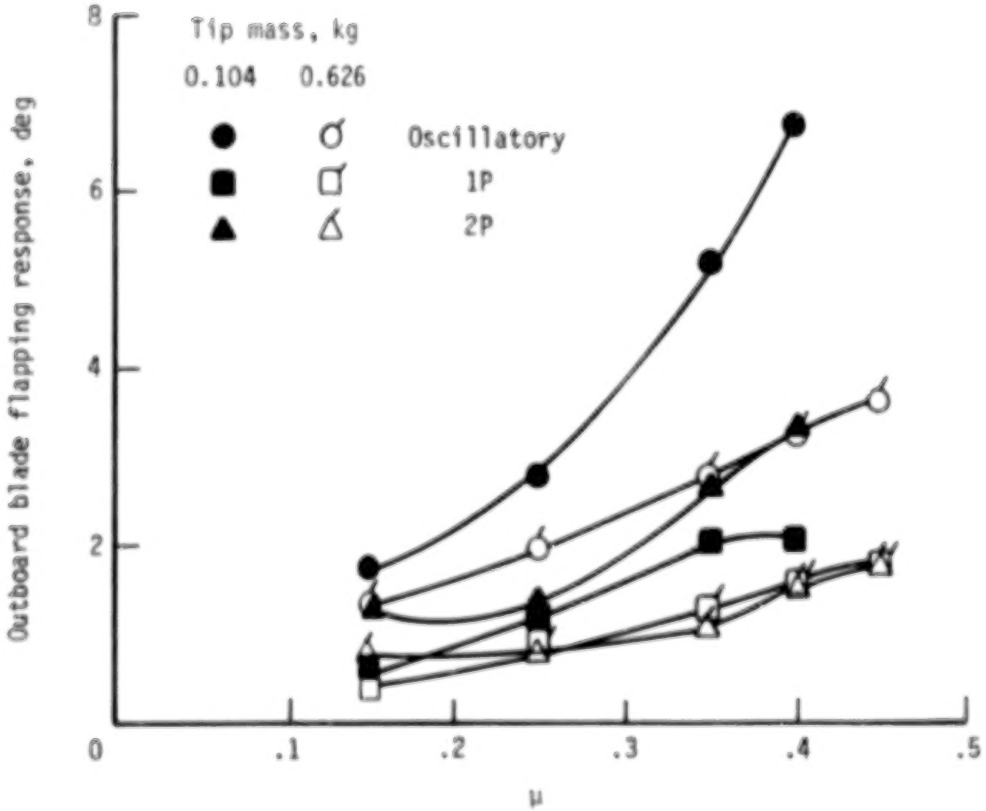

(b) Dynamic response.

Figure 25.- Variation of outboard blade flapping response with advance ratio. $C_L/\sigma = 0.060$.

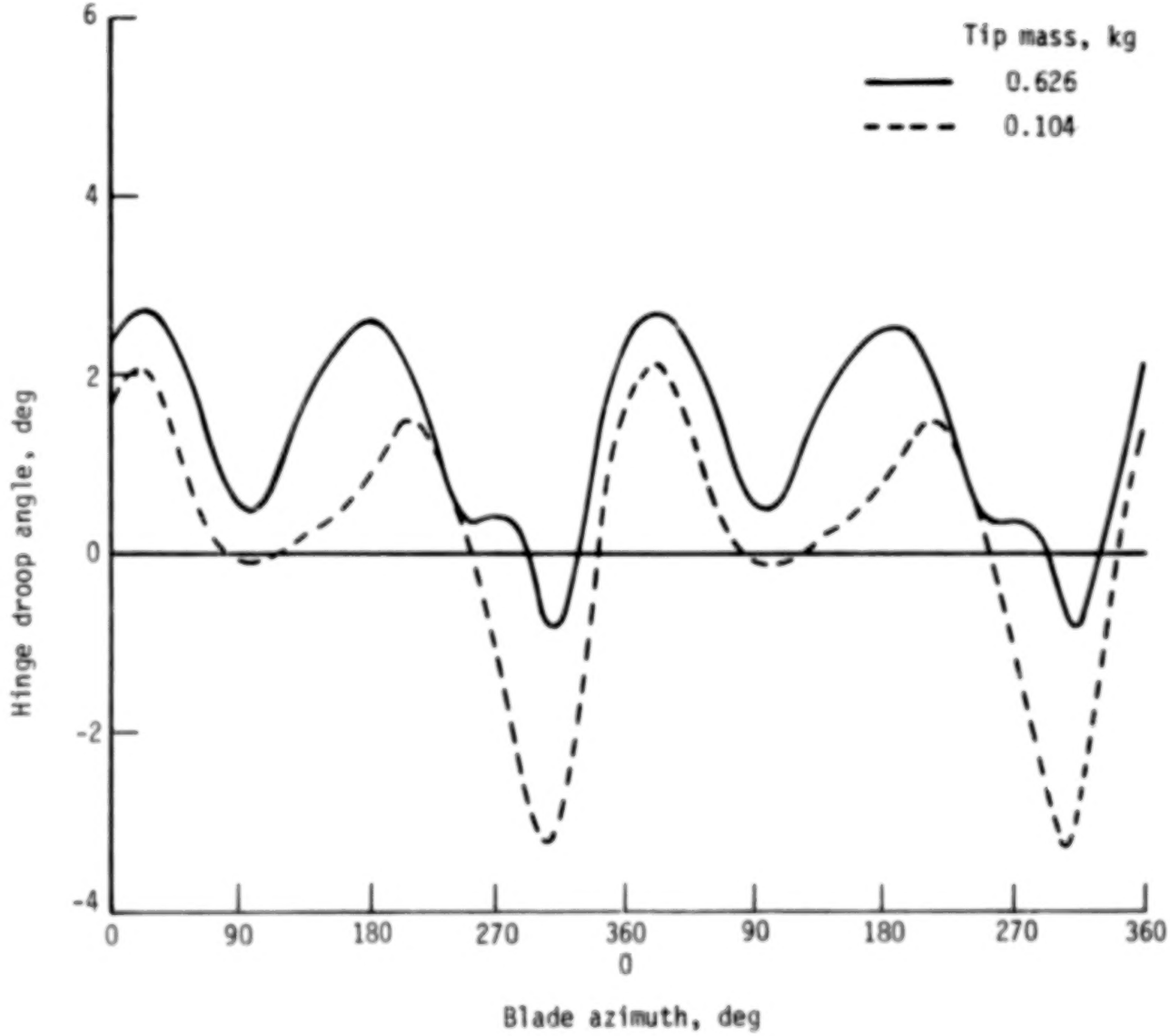

(a) $C_L/\sigma = 0.102$; $\mu = 0.15$; $\alpha_s = -2^\circ$.

Figure 26.- Azimuthal variation of outboard blade flapping angle for two tip masses.

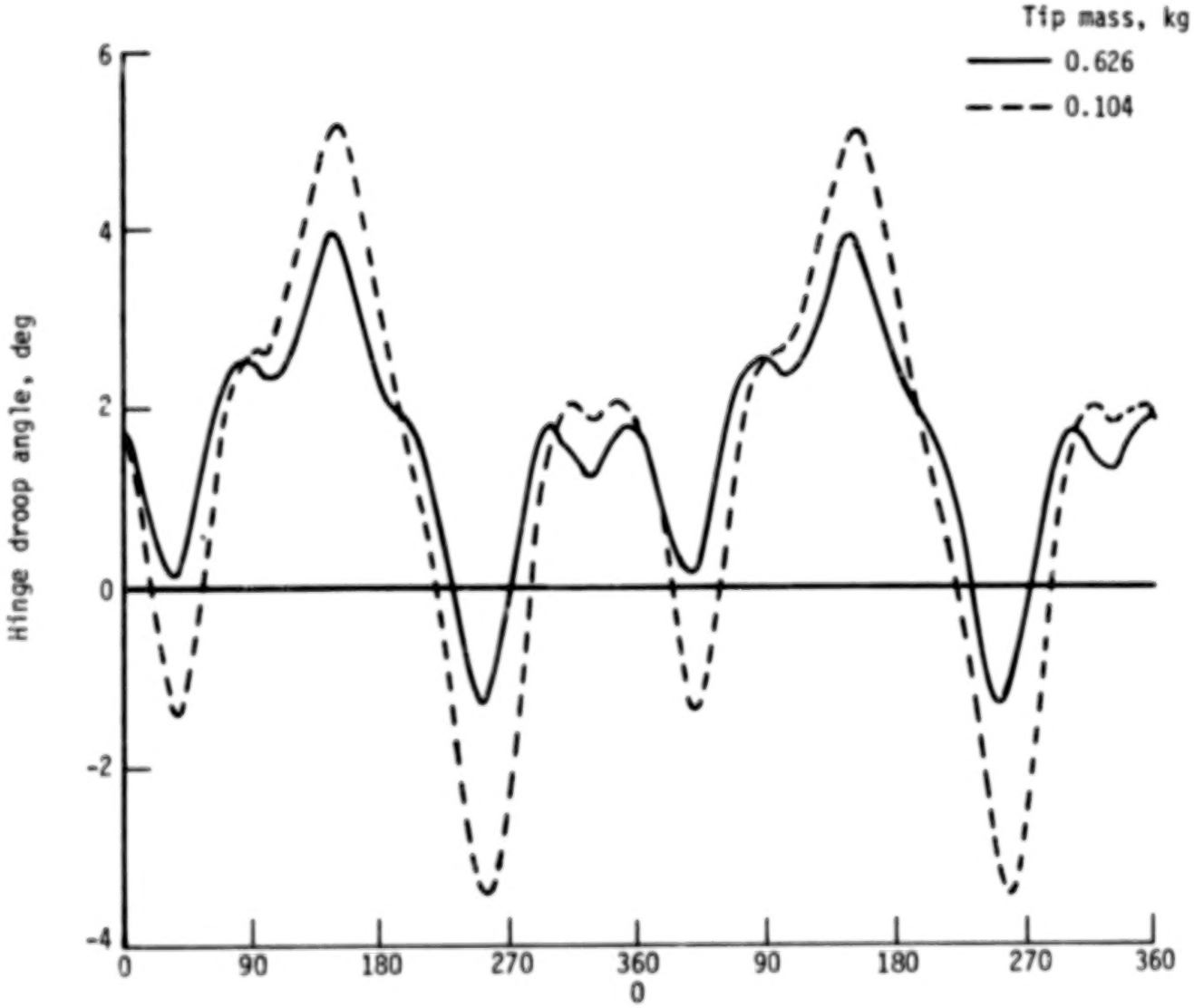

(b) $C_L/\sigma = 0.049$; $\mu = 0.35$; $\alpha_s = -4^\circ$.

Figure 26.- Concluded.

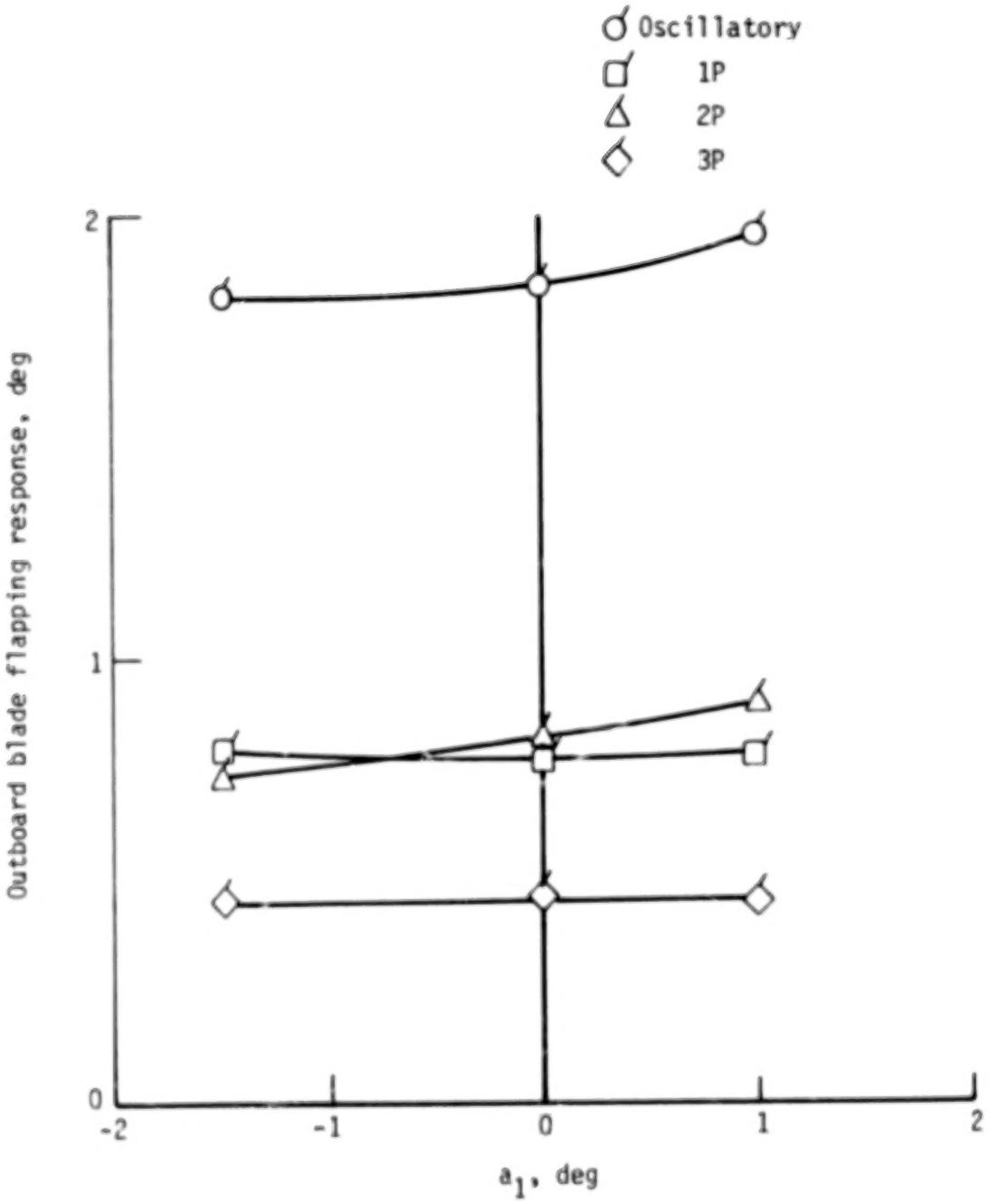

Figure 27.- Variation with rotor longitudinal flapping of outboard blade flapping response of hinged (0.626-kg tip mass) rotor. $\mu = 0.25$; $C_L/\sigma = 0.051$.

1. Report No.	2. Government Accession No.	3. Recipient's Catalog No.
NASA TP-1046		

4. Title and Subtitle	5. Report Date
WIND-TUNNEL TESTS OF WIDE-CHORD TEETERING ROTORS WITH AND WITHOUT OUTBOARD FLAPPING HINGES	November 1977
	6. Performing Organization Code

7. Author(s)	8. Performing Organization Report No.
William H. Weller and Bill L. Lee	L-11749
	10. Work Unit No. 505-10-26-01

9. Performing Organization Name and Address	11. Contract or Grant No.
Structures Laboratory USARTL(AVRADCOM) and NASA Langley Research Center Hampton, VA 23665	

12. Sponsoring Agency Name and Address	13. Type of Report and Period Covered
National Aeronautics and Space Administration Washington, DC 20546 and U.S. Army Aviation R&D Command St. Louis, MO 63166	Technical Paper
	14. Army Project No. 1L262209AH76

15. Supplementary Notes

William H. Weller: Structures Laboratory, U.S. Army R&T Laboratories (AVRADCOM).
Bill L. Lee: Langley Research Center.

16. Abstract

Wind-tunnel tests of aeroelastically designed helicopter rotor models were conducted to obtain rotor aerodynamic performance and dynamic response data pertaining to two-bladed teetering rotors with a wider chord (1.47 m (58 in.)) and lower hover tip speed (195 m/s (640 ft/sec)) than currently employed on production helicopters. The effects of a flapping hinge at 62 percent radius were also studied. Finally, the effects of changing tip mass on operating characteristics of the rotor with the outboard flapping hinge were examined. The models were tested at several shaft angles of attack for five advance ratios, 0.15, 0.25, 0.35, 0.40, and 0.45. For each combination of shaft angle and advance ratio, the rotor lift was varied over a wide range to include simulated maneuver conditions. At each test condition, rotor aerodynamic performance and dynamic response data were obtained. From these tests, it was found that wide-chord rotors may be subject to large control forces. An outboard flapping hinge may be used to reduce beamwise bending moments over a significant part of the blade radius without significantly affecting the chordwise bending moments. Increasing the tip mass was found to be an effective tool in restraining the flapping motions of the blade outboard of the hinge. The criteria for selecting outboard hinge location and tip mass must also include consideration of the effects of these parameters on rotor blade natural frequency. (This study is applicable to the dynamic response of two-bladed rotor configurations.)

17. Key Words (Suggested by Author(s))	18. Distribution Statement
Teetering rotors Rotor dynamic response Rotor performance Model rotor testing	Unclassified - Unlimited Subject Category 05

19. Security Classif. (of this report)	20. Security Classif. (of this page)	21. No. of Pages	22. Price*
Unclassified	Unclassified	73	$4.50

*For sale by the National Technical Information Service, Springfield, Virginia 22161

NASA-Langley, 1977